In vitro and *in vivo* characterization of therapeutic approaches for solid tumors: natural compounds and novel targets

Dissertation

zur Erlangung des Grades

des Doktors der Naturwissenschaften

der Naturwissenschaftlich-Technischen Fakultät

der Universität des Saarlandes

von

Charlotte Dahlem

Saarbrücken

2020

Tag des Kolloquiums:	26. November 2020
Dekan:	Univ.-Prof. Dr. Jörn Walter
Berichterstatter:	Univ.-Prof. Dr. Alexandra K. Kiemer
	Univ.-Prof. Dr. Andriy Luzhetskyy
	Univ.-Prof. Dr. Claus Hellerbrand
Vorsitz:	Univ.-Prof. Dr. Bruce Morgan
Akad. Mitarbeiter:	Dr. Jennifer Herrmann

Contents

Abstract

Cancer represents the second leading cause of death worldwide, and its incidence and mortality are growing. In search for new anti-tumor drugs addressing innovative targets, natural products represent powerful tools in (I) compound-centric, phenotypic and (II) target-centric drug discovery approaches.

This study addresses both strategies, aiming to identify novel therapeutic approaches for solid tumors.

(I) Compounds from various bacterial sources were characterized, elucidating their effects on different hallmarks of cancer in tumor cells and macrophages as key players of the tumor microenvironment.

The compound thioholgamide A stood out for its potent activities against various hallmarks of cancer in tumor cells. Anti-proliferative actions were further confirmed *in vivo*. These anti-tumor effects were accompanied by a modulation of cell metabolism, i.e., the inhibition of oxidative phosphorylation. Furthermore, the metabolic modulation caused repolarization of tumor-promoting human macrophages into a tumor-antagonizing phenotype.

(II) The RNA binding protein IMP2 has been suggested to promote tumorigenesis and tumor progression in several tumor entities. This study revealed a correlation between IMP2 overexpression and tumor progression and poor prognosis in pancreatic cancer. IMP2 was further characterized as a promising anti-cancer target *in vitro* and *in vivo* in colorectal cancer, and potential inhibitors of IMP2 demonstrated their anti-proliferative activity *in vivo*.

Zusammenfassung

Weltweit ist Krebs die zweithäufigste Todesursache und seine Inzidenz und Sterblichkeit sind steigend. In der Wirkstoffentwicklung stellen Naturstoffe vielversprechende Werkzeuge, für (I) naturstofffokussierte, phänotypische und (II) targetfokussierte Strategien dar.

Diese Arbeit adressiert beide Strategien mit dem Ziel der Identifizierung innovativer Targets in der Tumortherapie.

(I) Die Effekte verschiedener bakterieller Naturstoffe wurden in Tumorzellen und Makrophagen als entscheidende Akteure der Tumormikroumgebung charakterisiert.

Thioholgamide A stach dabei durch seine potenten Effekte gegen verschiedene Krebsmerkmale hervor. Seine antiproliferativen Eigenschaften wurden *in vivo* bestätigt. Diese Antitumorwirkungen wurden von einer Hemmung der oxidativen Phosphorylierung begleitet. Darüber hinaus bewirkte diese Modulation des Zellmetabolismus eine Repolarisation tumorfördernder Makrophagen in einen tumorantagonisierenden Phänotyp.

(II) Mehrere Studien weisen auf eine Rolle des RNA-bindenden Proteins IMP2 in der Tumorentstehung und dessen Progression in unterschiedlichen Tumorentitäten hin. Diese Arbeit konnte eine Korrelation zwischen einer IMP2 Überexpression und einer verstärkten Tumorprogression und schlechten Prognose für Pankreaskarzinompatienten aufzeigen. IMP2 wurde ferner als vielversprechendes Target *in vitro* und *in vivo* gegen Kolonkarzinome charakterisiert und potenzielle IMP2 Inhibitoren demonstrierten antiproliferative Aktivitäten *in vivo*.

1 Introduction

1.1 Cancer drug discovery

Cancer represents the second leading cause of death worldwide, and its incidence and mortality are growing (Bray et al., 2018; Roth et al., 2018) (**Figure 1**). In terms of incidence and mortality, lung, breast, prostate, and gastrointestinal cancers rank the lists in varying orders, depending on the observed population (**Figure 2**). Comparing data from 1970-1977 and 2007-2013, the overall five-year cancer survival rates for all cancers increased from 50.3% to 67% in the USA (Jemal et al., 2017). However, certain tumor entities lack effective therapy options, and many current therapeutic agents fail, e.g., due to the development of resistances or severe side effects, indicating the need for new druggable targets.

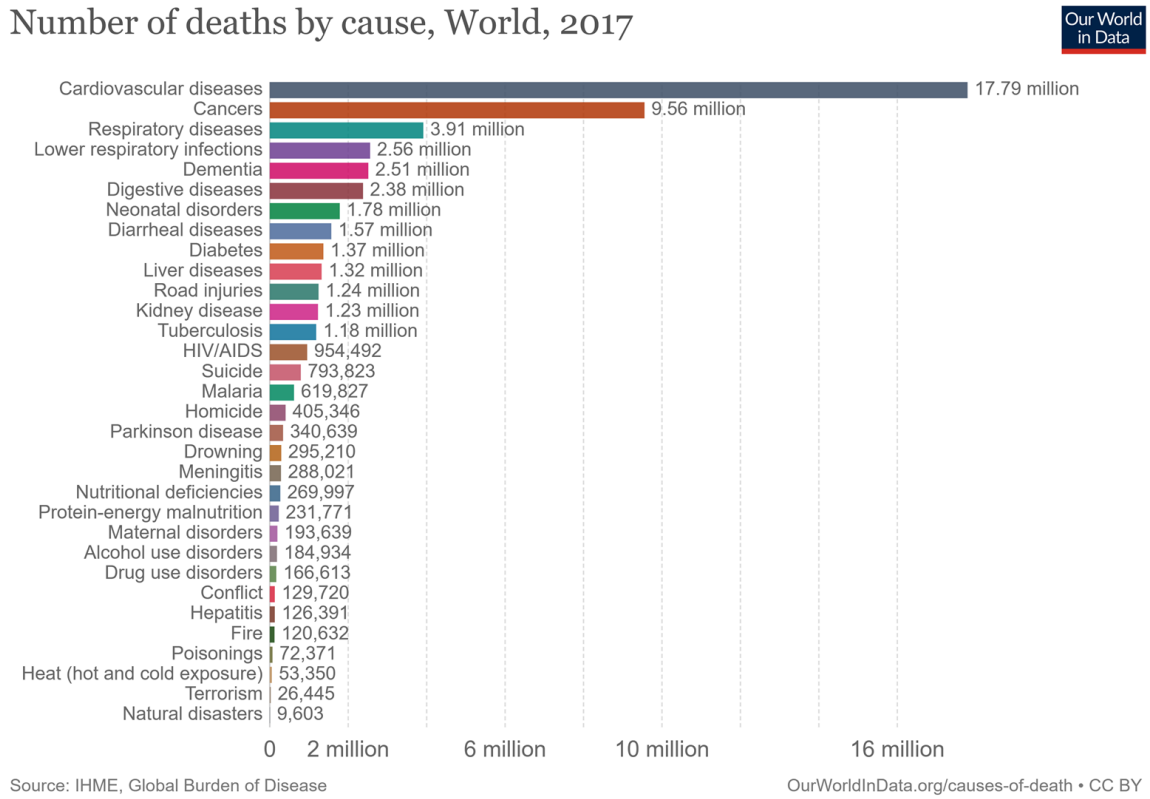

Figure 1. Causes of death worldwide in 2017.
Data from the Global Burden of Disease Study (Roth et al., 2018) was visualized by OurWorldinData.org.

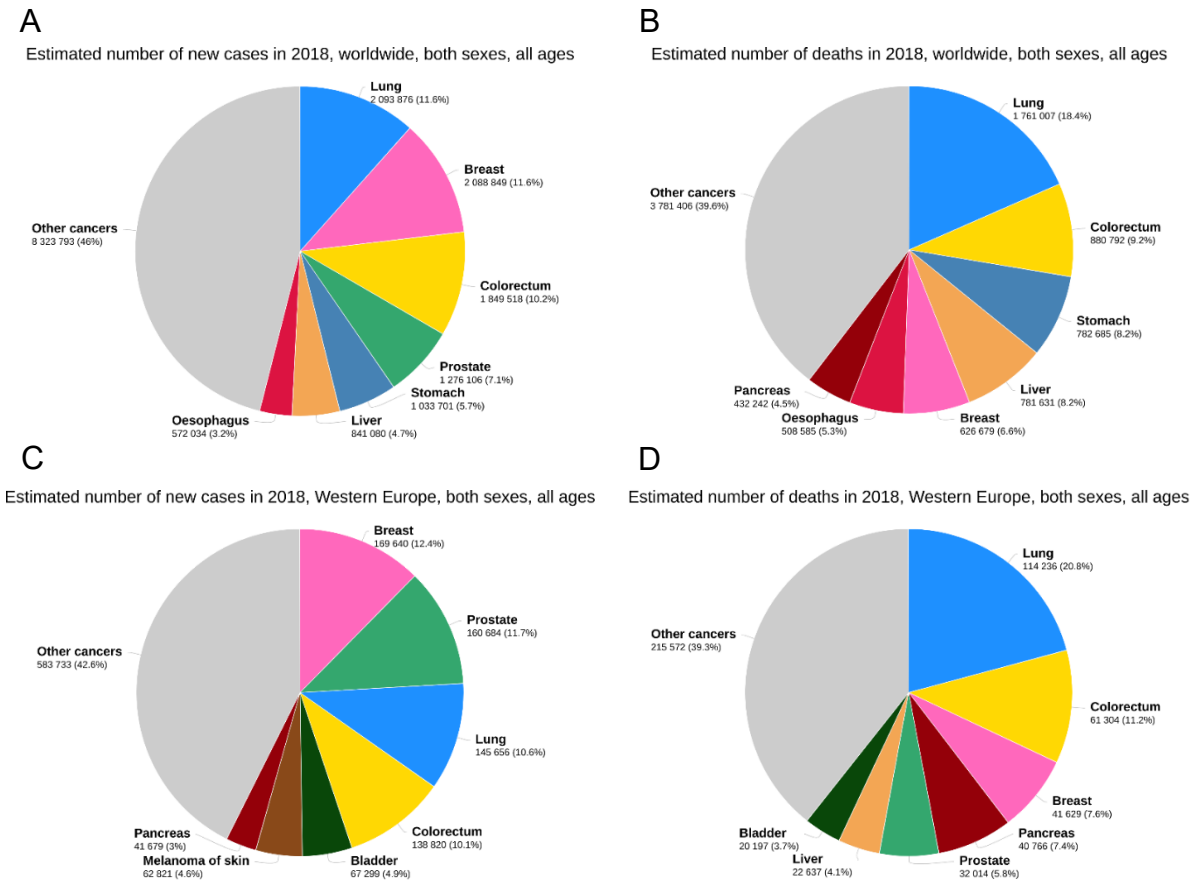

Figure 2. Tumor incidence and mortality in 2018.
Data obtained from the GLOBOCAN 2018 study (Bray et al., 2018) was visualized by Global Cancer Observatory (https://gco.iarc.fr) and demonstrate (**A**, **C**) tumor incidence and (**B**, **D**) mortality, (**A**, **B**) worldwide, and for (**C**, **D**) Western Europe.

1.1.1 Drug discovery strategies

Current drug discovery includes molecular and empirical strategies. The hypothesis-driven, molecular approaches rely on target-centric screenings. In these screenings, compound libraries are screened against a target known to be important for the disease to identify hit compounds that interact with this target. Contrastingly, empirical approaches also referred to as phenotypic screenings, evaluate specific phenotypes and cellular outcomes relevant for a given disease. In this approach, the compounds serve as a starting point for the investigation evaluating their phenotypic effects in the given disease. The molecular mechanisms and targets involved in these effects are determined at a later point (Swinney and Anthony, 2011).

Swinney and Anthony analyzed new molecular entities approved by the FDA between 1999 and 2008 and found that molecules derived from phenotypic screenings mainly provided new first-in-class drugs, while target-based approaches made a greater contribution to best-in-class drugs (Swinney, 2013). This analysis was revised in 2014 by Eder at al. and revealed an

increased contribution of target-based approaches to new first-in-class drugs, highlighting new achievements in high-throughput technologies and target-based assays (Eder et al., 2014).

1.1.2 Natural products in cancer drug discovery

Natural products represent promising tools for both drug discovery strategies. Searching for new anti-tumor drugs addressing innovative targets, natural products contribute to target-based screening libraries and have proven to be powerful tools in phenotypic approaches due to their inherent structures. The widely used natural product-derived chemotherapeutics doxorubicin and taxanes are just two prominent examples.

Between 01/1981 and 09/2019, 247 new chemical entities have been approved as anti-cancer drugs (**Figure 3**). Only 11.7% of these drugs were totally synthetic (Filho, 2018; Newman and Cragg, 2020). Although only a few natural products become clinically relevant drugs in their own right, their structures frequently serve as scaffolds for further drug design, leading to more efficacious analogues (**Figure 3**).

Historically, mainly plant-derived natural products contributed to the structural diversity of new drugs (Baker et al., 2007). However, in the past decades, bacteria have become a promising source for innovative bioactive compounds (Landwehr et al., 2016). Due to growth and upscaling possibilities, they became practical producers of secondary metabolites for drug development. Myxobacteria and Actinobacteria (including *Streptomyces* species) are the top resources of pharmaceutically important compounds, and it is expected that they still hide much potential (Ahmed et al., 2020; Weissman and Müller, 2010).

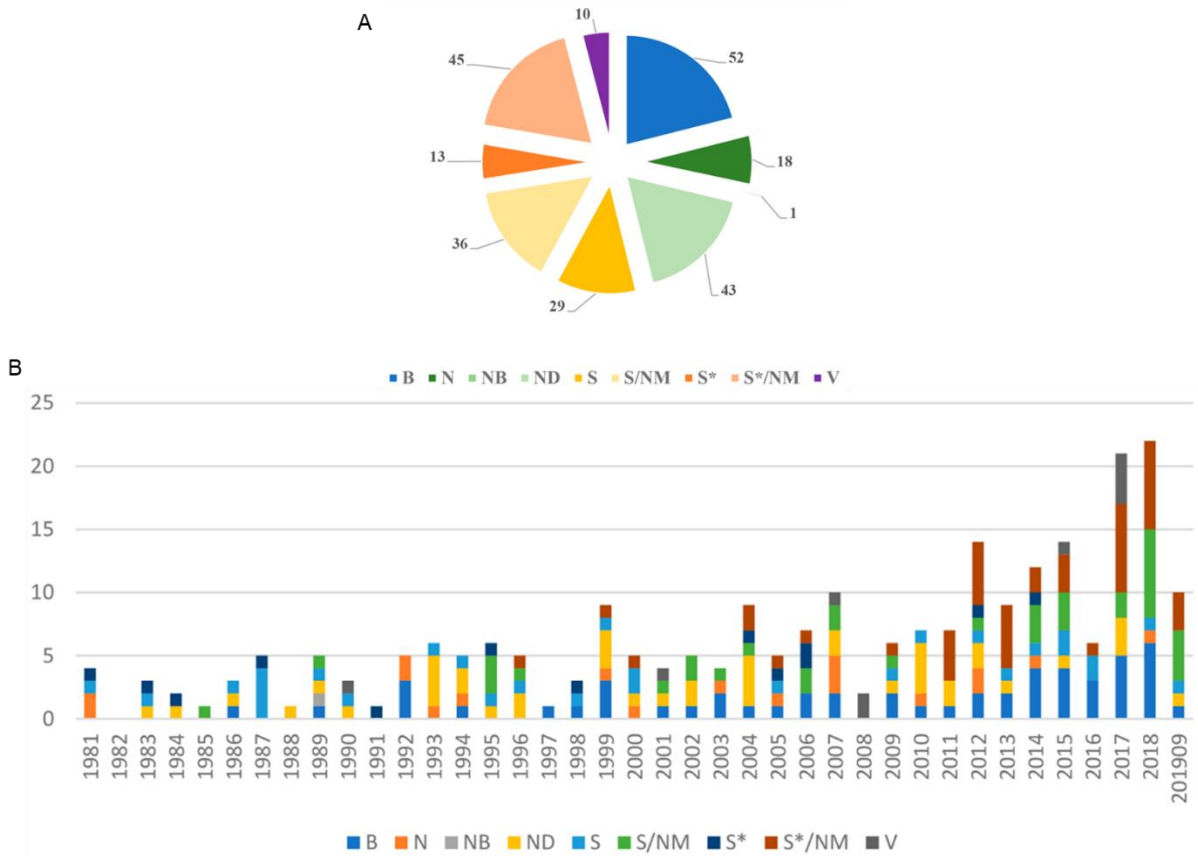

Figure 3. Origin of anti-cancer drugs between 1981 and 2019.
Anti-cancer drugs approved between 01/1981 and 09/2019 (Newman and Cragg, 2020). B (biological macromolecule), N (unaltered natural product), NB (botanical drug, defined mixture), ND (natural product derivative), S (synthetic drug), S* (synthetic drug, natural product pharmacophore), V (vaccine), /NM (mimic of natural product). (**A**) Classification of all 247 drugs approved between 1981 and 2019. (**B**) Annual survey.

1.2 Hallmarks of cancer

Cancer research of the last decades revealed a complex picture of the disease. In the year 2000, Douglas Hanahan and Robert A. Weinberg first described the six "hallmarks of cancer", aiming a simplification of the multiple mechanisms leading to the transformation of healthy cells into malignant cells (Hanahan and Weinberg, 2000). They defined six crucial alterations in cell physiology and suggested them to cover the majority of cancer genotype manifestations dictating malignancy: (I) self-sufficiency in growth signals, (II) evasion of growth suppressors, (III) evasion of programmed cell death, (IV) limitless replicative potential, (V) induced angiogenesis, and (VI) activation of tissue invasion and metastasis. The authors stated that in different tumors, oncogene- and tumor suppressor gene-mutations responsible for the acquisition of these hallmarks could occur at various times during tumor progression. But in the end, these hallmark traits would be shared by all types of tumors.

In 2011, these six hallmarks were revised and complemented with two additional hallmarks. These draw attention to changes in energy metabolism, supporting continued tumor growth and the active evasion of malignant cells from the recognition and subsequent elimination by immune cells (Hanahan and Weinberg, 2011). Additionally, two consequential characteristics, which facilitate the acquisition of hallmark traits, were defined. The so-called "enabling characteristics" comprise genetic instability and mutations, as well as tumor-promoting inflammation. The latter case highlights the dichotomous role of immune cells, which can exert either tumor-suppressive or supporting actions (Fouad and Aanei, 2017). The first- and second-generation hallmarks of cancer, as well as the enabling characteristics, are summarized in **Figure 4**.

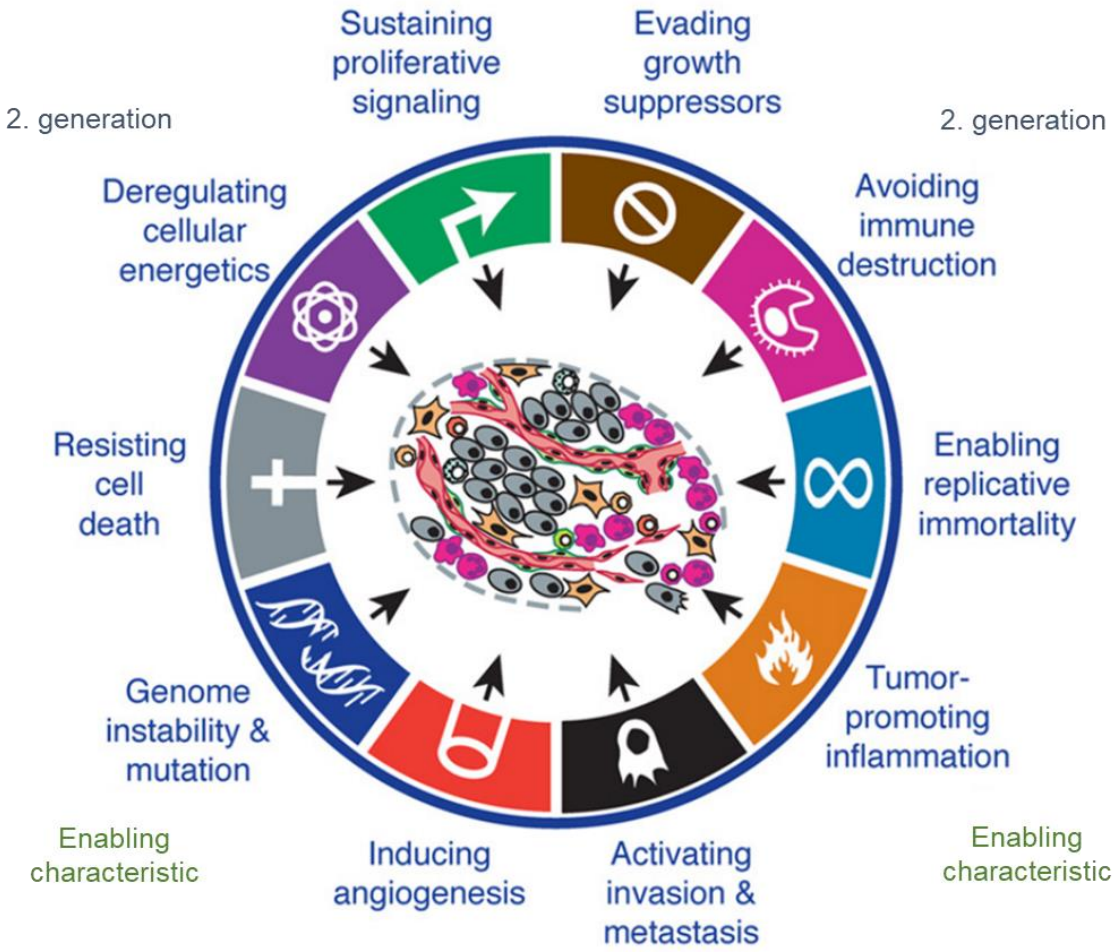

Figure 4. Hallmarks of cancer. Adapted from (Hanahan and Weinberg, 2011).

1.3 Tumor metabolism

The metabolic reprogramming of malignant cells has become an accepted hallmark of cancer (Hanahan and Weinberg, 2011). It has been demonstrated that many cancer cells undergo a phenomenon termed "Warburg effect". The Warburg effect describes the phenomenon of proliferating cells, including cancer cells, using aerobic glycolysis to fulfill their energy demand, while normal differentiated cells rely mainly on mitochondrial oxidative phosphorylation (OXPHOS) (Vander Heiden and DeBerardinis, 2017; Vander Heiden et al., 2009).

Most differentiated cells metabolize glucose to carbon dioxide by oxidation of glycolytic pyruvate in the mitochondrial tricarboxylic acid (TCA) cycle when oxygen is present. This process produces reducing equivalents (NADH and $FADH_2$), which drive OXPHOS as the most efficient ATP production pathway. Hypoxic conditions force these cells into anaerobic glycolysis, producing large quantities of lactate. The phenomenon of aerobic glycolysis

involves the property of proliferating cells to metabolize glucose and secrete the carbon as lactate even when oxygen is present, although the ATP production is much lower compared to OXPHOS (**Figure 5**) (Vander Heiden and DeBerardinis, 2017; Vander Heiden et al., 2009).

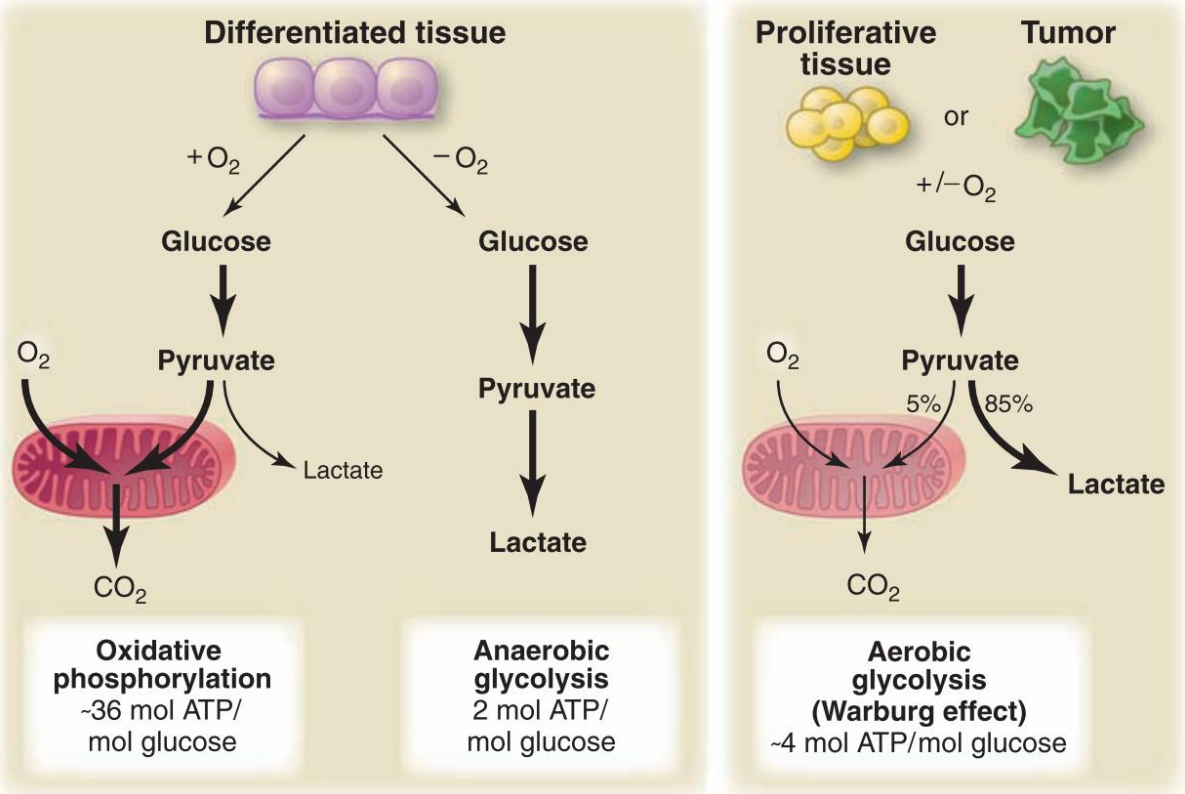

Figure 5. Metabolic pathways in differentiated tissue, proliferative tissue, and tumors (Vander Heiden et al., 2009).

While it was first suggested that the Warburg effect is a result of impaired mitochondria and aerobic respiration, it meanwhile turned out that tumor cells display metabolic plasticity, which allows to switch between metabolic pathways (McGuirk et al., 2020).

This metabolic plasticity enables tumor cells to tailor their high energy demands to changing environmental conditions during cancer progression. During the growth phase, proliferating tumor cells have a high need for rapid ATP production and sources of carbon, nitrogen, and hydrogen, inducing the Warburg effect. As the tumor mass grows, cells experience nutrient deprivation, and hypoxia. Hypoxia, hypoxia-inducible factor 1 (HIF-1), and reactive oxygen species (ROS) further promote anaerobic glycolytic metabolism (Courtnay et al., 2015; Rabinovitch et al., 2017). Mature tumors create gradients of extracellular metabolites and

develop a metabolically diverse microenvironment comprised of stromal and immune cells, which can concur the metabolic coupling of cancer cells (Chang et al., 2015).

Metabolic plasticity demonstrated to play a pivotal role in epithelial-mesenchymal transition (EMT) and metastasis, where metabolic flexibility of tumor cells appears to be advantageous facing different metabolic microenvironments at distinct metastatic niches (Elia et al., 2018; Simões et al., 2015). Moreover, circulating cancer cells demonstrated an enhanced OXPHOS activity (Lebleu et al., 2014). Similarly, tumors displaying higher metabolic heterogeneity also acquire an increased likelihood to develop resistances against therapeutic drugs (Desbats et al., 2020; Matassa et al., 2016).

As a consequence, therapies, combining chemotherapeutic drugs with metabolic modulators to create a metabolic vulnerability are an emerging therapeutic strategy, which is currently under investigation (Ashton et al., 2018; Desbats et al., 2020; Li et al., 2004; McGuirk et al., 2020).

1.4 The tumor microenvironment

First regarded as an agglomeration of malignant cells, tumors have been recognized as complex tissues composed of malignant cells and a variety of other cell types, creating the tumor microenvironment (TME). The TME changes its composition during cancer progression and demonstrated to play a critical role in the evolution of malignancy (Roma-Rodrigues et al., 2019).

Among the cellular compartment, the TME consists of fibroblasts, endothelial, innate, and adaptive immune cells (Chen and Song, 2019; Hinshaw and Shevde, 2019; Maishi and Hida, 2017). Recruited immune cells can form up to 50% of the solid tumor mass (Solinas et al., 2009).

The extracellular matrix of the TME is moreover characterized by low oxygen availability due to rapid tumor proliferation and abnormalities in the structure of surrounding blood vessels (Gilkes et al., 2014).

Supported by the hypoxic environment, tumor cells hijack TME-cells by secreting various cytokines, chemokines, and other molecules. For instance, cancer-derived extracellular metabolites orchestrate an immunocompromised microenvironment by inducing an anti-inflammatory phenotype of macrophages, which promotes tumor growth and interference with the maturation of tumor-toxic T cells (Carmona-Fontaine et al., 2017; Chang et al., 2015).

The ability to co-opt and reprogram neighboring cells demonstrated to support the acquisition of hallmarks of cancer traits. By forcing, e.g., tumor proliferation, invasion, migration, and resistances, the TME plays a detrimental role in tumor progression and thereby also substantially influences the efficacy of anti-cancer therapies (Cassetta and Pollard, 2018; Roma-Rodrigues et al., 2019).

1.5 Macrophages

Macrophages are innate immune cells that can be found in all tissues, taking various roles in development, homeostasis, and tissue repair (Gordon et al., 2014; Murray and Wynn, 2011). It has been shown that most adult tissue-resident macrophages are not derived from bone marrow progenitors, as previously thought, but instead originate from different embryonic sources (yolk sac, fetal liver) and differentiate into tissue-specific macrophages according to their origin (Epelman et al., 2014; Perdiguero and Geissmann, 2016). The contribution of monocyte-derived macrophages to tissue-resident macrophages is still under discussion (Hume et al., 2019).

1.5.1 Macrophage polarization

Macrophages exert a broad range of different physiological functions due to their high plasticity. This plasticity allows the body to tailor their response according to diverse environmental stimuli and adopt multiple phenotypes. Since the stimuli are manifold and temporal, macrophages do not only respond with different functional phenotypes but can also switch between those (Ginhoux et al., 2016). Macrophage phenotypes are characterized by a variety of surface and intracellular receptors, multiple signal transduction pathways, and adaptable arrays of gene expression (Biswas et al., 2012; Mantovani et al., 2013; Xue et al., 2014). This remarkable transcriptional repertoire is described by the macrophage polarization spectrum with its two extreme ends of M1 and M2 polarization states (**Figure 6**).

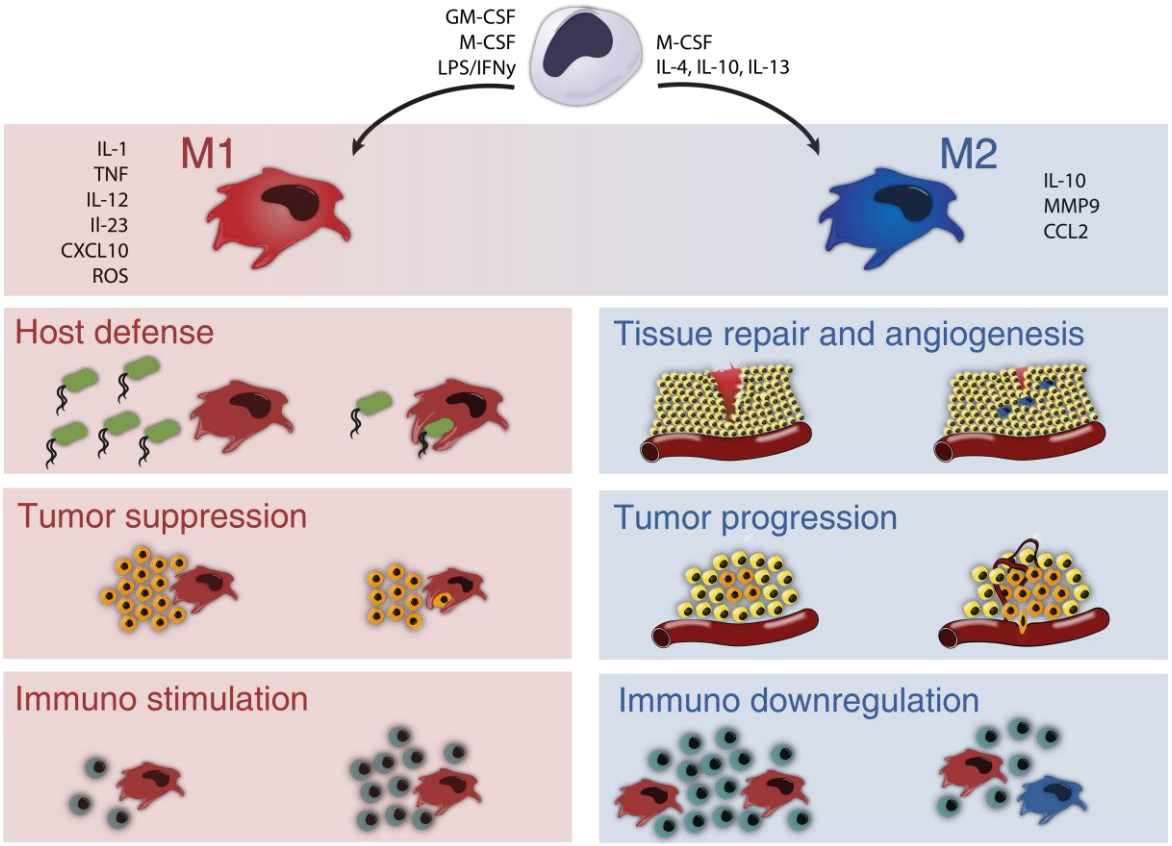

Figure 6. Macrophage polarization and function. Adapted from (Solinas et al., 2009).

The M1/M2 nomenclature is inspired by the T_H1/T_H2 T helper cell response. Therefore, M1 macrophages, also termed "classically activated macrophages", are typically induced by inflammatory stimuli, such as bacterial lipopolysaccharide (LPS), in concert with the T_H1 cytokine interferon-γ (IFN-γ). This inflammatory phenotype promotes host defense effector responses and tumoricidal properties by producing pro-inflammatory cytokines (TNFα, IL1α, IL1β, IL6, IL12, IL23), and cyclooxygenase 2, and low levels of IL10. Moreover, the production of ROS is involved in the effective anti-microbial and anti-tumoral activity of M1 macrophages. The communication with the adaptive immune system is enhanced by upregulation of MHC II and co-stimulatory CD40, CD80, and CD86, and increased production of chemoattractants, such as chemokine (C-X-C motif) ligand 9 (CXCL9), CXCL10, CXCL11, CC chemokine ligand 2 (CCL2), CCL3, and CCL5 (Biswas et al., 2012; Ginhoux et al., 2016; Murray et al., 2014; Shapouri-Moghaddam et al., 2018; Sica and Mantovani, 2012; Takeya and Komohara, 2016).

In contrast, M2 macrophages, or "alternatively activated macrophages" can be found in the resolution phase of inflammations and injured tissues. Their polarization is induced *via* anti-inflammatory cytokines, such as interleukin 4 (IL4), IL10, and IL13. The anti-inflammatory

phenotype is characterized by a decreased ability to produce pro-inflammatory cytokines, while IL10 and TGFβ production are increased. Functionally, M2 macrophages are linked to tissue homeostasis, including tissue remodeling and repair, but also tumor progression. Facilitated by an enhanced expression of scavenger receptors, such as CD204 and CD163, M2 macrophages exert potent phagocytosis capacity. In a cellular process, named efferocytosis, they play a pivotal role in the engulfment and removal of dead cells from tissue (Elliott et al., 2017). M2 macrophages take part in T_H2 responses, clearance of parasites, and display regulatory functions in resolving and chronic inflammation (Biswas et al., 2012; Ginhoux et al., 2016; Murray et al., 2014; Shapouri-Moghaddam et al., 2018; Sica and Mantovani, 2012; Takeya and Komohara, 2016).

However, these two distinct extremes of M1 and M2 polarizations represent a simplification of macrophage phenotypes that can be found *in vivo* in homeostatic and pathological situations (e.g., cancer), where macrophages do not show a clear M1/M2 phenotype (Azizi et al., 2018; Helm et al., 2014).

1.5.2 Tumor-associated macrophages

Tumor-associated macrophages (TAM) are key players in the TME linking cancer progression and inflammation. Being the major population of immune cells in the TME, their origin is still under discussion (Cassetta and Pollard, 2018). Signals originating from malignant cells and other cells of the TME, such as apoptotic cells, influence TAM function and phenotype (Mantovani et al., 2017; Weigert et al., 2016).

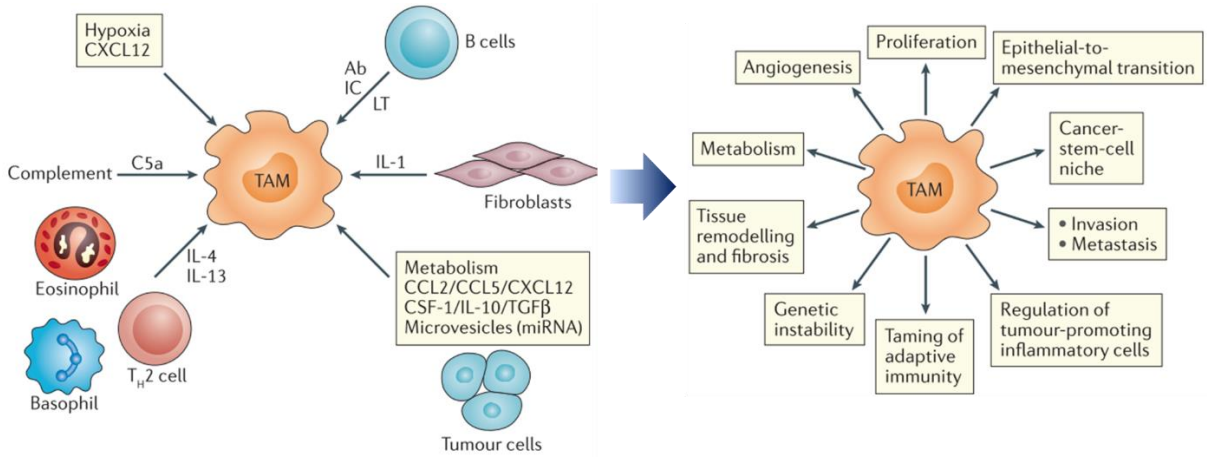

Figure 7. TAM polarization and their role in tumor progression (Mantovani et al., 2017).

Within and across tumors, the TAM compartment is characterized by high dynamics and heterogeneity. Recent findings suggest a mixed phenotype of TAMs depending on their localization in the TME and tumor stage, displaying characteristics of both M1 and M2 macrophages (Azizi et al., 2018; Chevrier et al., 2017; Chung et al., 2017; Cuccarese et al., 2017; Lavin et al., 2017; Müller et al., 2017). This supports the idea that in the initiation stage, TAMs may have pro-inflammatory functions, which can fight malignant cells but can also promote cancer-related inflammation and tumorigenesis. At later stages stimuli from the TME and apoptotic cells educate macrophages and induce an M2-like phenotype. In established tumors, TAMs upregulate anti-inflammatory cytokines (IL4, IL10, and TGFβ) and tumor-promoting factors such as vascular endothelial growth factor (VEGF) or matrix metalloproteinases (MMPs). Thereby TAMs support immunosuppression in the TME and influence various aspects of tumor progression, e.g., tumor growth, invasion, metastasis, or neo-angiogenesis (Biswas et al., 2012; DeNardo and Ruffell, 2019; Shapouri-Moghaddam et al., 2018).

In line with these tumor-promoting functions, a correlation between an increased presence of M2-like TAMs and poor prognosis has been found in various tumor entities (Pathria et al., 2019).

1.5.3 Macrophage energy metabolism

Different macrophage phenotypes have distinct metabolic profiles. Inflammatory macrophages display a Warburg metabolism, including a shift from OXPHOS towards glycolysis. LPS and IFNγ activate the transcription factor nuclear factor-kappa B (NF- kB), which induces the expression of HIF1 (Rius et al., 2008), which is involved in glycolysis promotion (Courtnay et al., 2015). Furthermore, M1 macrophages possess an impaired TCA circle, which has been implicated in their anti-microbial functions, since accumulated citrate can be used for the production of itaconic acid as a metabolite with direct anti-microbial activity (Saha et al., 2017).

M2 macrophages showed to mainly rely on OXPHOS for energy production. To fuel the TCA cycle, IL4-polarized macrophages rely on fatty acid oxidation (FAO) and glutamine metabolism (Geeraerts et al., 2017; Saha et al., 2017). The inhibition of mitochondrial respiration in M1 macrophages demonstrated to prevent repolarization to an M2 stage (Van den Bossche et al., 2016). However, the inhibition of glycolysis in IL4-polarized macrophages using 2-deoxyglucose diminished the expression of M2-associated genes, indicating that glycolysis is not just pro-inflammatory but also crucial for IL4 induced phenotypes (Van den Bossche et al., 2017).

Reflecting different polarization stages of TAMs and their ability to adapt to their environment, their metabolic profile is very dynamic (Netea-Maier et al., 2018; Vitale et al., 2019). TAMs generated *in vitro* by culturing monocyte-derived macrophages in pancreas adenocarcinoma-conditioned medium (Penny et al., 2016), and TAMs from MMTV-PyMT mice incubated with patient-derived breast tumor extract (Liu et al., 2017) exhibit a pronounced glycolytic signature and promote tumor metastasis. On the other hand, hypoxic TAMs showed a shift towards oxidative metabolism. They decreased glucose intake resulting in excessive angiogenic response *via* DNA damage inducible transcript 4 (REDD1) upregulation and subsequent mechanistic target of rapamycin complex 1 (mTORC1) inhibition (Wenes et al., 2016).

1.5.4 Targeting of tumor-associated macrophages

Due to their role in tumor progression to malignancy, TAMs have become an interesting target in tumor therapy. Different targeting strategies are currently under investigation aiming to modulate TAM function to induce anti-tumoral activities, synergize with other anti-cancer therapies, or block resistances to conventional therapies (Cassetta and Pollard, 2018; Kumar et al., 2020; Mantovani et al., 2017; Roma-Rodrigues et al., 2019).

Current targeting strategies involve the inhibition of TAM recruitment, TAM depletion from the TME, and TAM reprogramming.

Since TAM recruitment to the tumor is mediated by the CCL2-CCR2 axis, different approaches were investigated to block this axis and thereby reduce TAM accumulation in tumors. However, clinical trials showed disappointing results, including increased CCL2 serum levels and rebound effects after the withdrawal of anti-CCL2 treatment (Bonapace et al., 2014; Lim et al., 2016). Moreover, antibodies and small molecules targeting colony-stimulating factor 1 receptor (CSF1R) signaling, which controls macrophage differentiation, and encapsulated bisphosphonates were employed for a selective macrophage depletion (Mantovani et al., 2017).

The natural compound Ecteinascidin ET-743 (trabectedin, Yondelis®) has been initially approved as an anti-proliferative agent in cancer therapy (Carter and Keam, 2007). In further studies, the compound demonstrated selective cytotoxicity towards monocytes and macrophages. This depletion is facilitated by activation of caspase 8 through a TNF-related apoptosis-inducing ligand (TRAIL) receptor-dependent mechanism. Selectivity for monocytes is caused by differential TRAIL receptor expression (Germano et al., 2013). Interestingly, TRAIL receptors are upregulated by anti-inflammatory agents and TAMs express functional TRAIL receptors, while this is not the case in tissue-resident macrophages (Liguori et al., 2016), making these receptors interesting TME-targeting candidates.

Besides strategies that focus on a reduced TAM burden in the TME, the repolarization of tumor-supporting to tumor-suppressing macrophages represents a promising strategy. Targeting the inherent plasticity provides the opportunity to rebalance the TME and thereby opening new therapeutic options also in combination therapy with checkpoint inhibitors. Current strategies involve anti-CD40, anti-CD47, and anti-MARCO antibodies, toll-like receptor agonists, metallic nanoparticles, PI3Kγ, and histone deacetylase inhibitors (Cassetta and Pollard, 2018; Kumar et al., 2020).

1.6 The *insulin-like growth factor 2* mRNA binding protein 2 (IMP2)

Insulin-like growth factor (*IGF2*) mRNA binding proteins (IGF2BPs/IMPs/VICKZs) are members of the group of RNA binding proteins (RBPs) (Degrauwe et al., 2016), which play a pivotal role in diverse physiological functions and are involved in mRNA maturation, stability, localization, and translation of mRNA targets (Mohibi et al., 2019).

IMPs are highly conserved RBPs, and three mammalian IMP paralogs have been identified (IMP1-3). The IMP family shares structural similarity, comprising two RNA recognition motifs (RRM) in the N-terminal region and four hnRNP K homology (KH) domains in their C-terminal region (Degrauwe et al., 2016; Nielsen et al., 1999).

IMPs are oncofetal proteins, and their physiological expression occurs primarily during fetal development and tissue maturation. In most adult tissues, IMPs are eighter absent or expressed at low levels (Czepukojc et al., 2019; Dai et al., 2011; Degrauwe et al., 2016). However, re- and over-expression have been associated with malignant transformations (Degrauwe et al., 2016).

p62 represents a shortened splice variant of IMP2 (lacking exon 10) but harbors the identical RNA-binding domains. p62 was initially identified as a 62 kDa autoantigen from an hepatocellular carcinoma (HCC) patient and was found to be overexpressed in HCC tissues (Kessler et al., 2015a; Lu et al., 2001; Zhang et al., 1999). Its expression was further shown to correlate with *IGF2* expression in HCC, which is involved in the IGF pathway, as one common oncogenic signaling pathway disturbed in many cancers (Kessler et al., 2016, 2013).

IMP2 showed to bind thousands of different transcripts in a PAR-CLIP approach (Hafner et al., 2010), and several genes encoding mitochondrial components (Cao et al., 2018; Dai et al.,

2015). Having multiple targets, IMP2 correlates with a broad range of (patho)-physiological functions in embryonic development, muscle cell motility, and lipid metabolism (Boudoukha et al., 2010; Laggai et al., 2014; Liu et al., 2019).

In a pathophysiological context, IMP2 is associated with insulin resistance (Christiansen et al., 2009) and its overexpression has been correlated to poor patient outcome in human HCC, esophageal adenocarcinoma, breast, gallbladder, and colorectal cancer (Barghash et al., 2015, 2016; Kessler et al., 2013, 2015b, 2017; Liu et al., 2013; Ye et al., 2016). Moreover, IMP2 enhances different hallmarks of cancer, i.e., genomic instability, cancer cell proliferation and migration, and maintenance of cancer stemness (Degrauwe et al., 2016; Kessler et al., 2015a; Xing et al., 2019). IMP2 overexpression further induces an aggressive HCC phenotype, linked to inflammatory and oxidant actions (Kessler et al., 2015a). Therefore, IMP2 is suggested to play a distinct role in cancer progression and responsiveness to chemotherapy (Kessler et al., 2013, 2017).

Hepatic IMP2 transgenic mice displayed steatosis and improved glucose tolerance, associated with an induction of fatty acid elongation (Laggai et al., 2014; Tybl et al., 2011). Moreover, these mice demonstrated a more pronounced manifestation of fibrosis on methionine-choline-deficient (MCD) diet, which models non-alcoholic fatty liver disease (NAFLD), one of the main HCC risk factors (Czepukojc et al., 2019; Simon et al., 2014). They also show a higher tumor incidence associated with increased inflammation after diethylnitrosamine (DEN) treatment (Kessler et al., 2015a).

By its role in the regulation of cell metabolism, IMP2 exerts further functions implicated in cancer development and progression. Janiszewska and colleagues described a role of IMP2 in OXPHOS regulation in glioblastoma spheres by binding several mRNAs encoding mitochondrial respiratory chain complex subunits I and IV. The depletion of IMP2 decreased the oxygen consumption rate and complex I and complex IV activity in glioblastoma spheres and resulted in impaired clonogenicity as a mean of cancer stemness (Janiszewska et al., 2012).

Moreover, IMP2 stabilizes *GLUT1* and *HK2* mRNA in colorectal cancer and *GLUT1* in pancreatic ductal adenocarcinoma and thereby increases glycolysis (Huang et al., 2019; Shen et al., 2020).

1.7 Objectives

This work aimed to identify and validate new targets for cancer therapy by pursuing two different strategies:

(I) The first part of this study focuses on the characterization of newly identified natural compounds from different sources. This phenotypic approach addresses the identification of innovative anti-tumor strategies, targeting not only tumor cells but also shaping the tumor microenvironment by affecting tumor-associated macrophages.

(II) The second part of this study focuses on the *in vitro* and *in vivo* target validation of IMP2 as a novel anti-cancer target in colon cancer and the *in vivo* validation of potential inhibitors.

2 Materials and methods

2.1 Cell culture

2.1.1 Cultivation of cell lines

Tumor cell lines were cultured in RMPI-1640 (A549, HeLa, Huh7, PLC/PRF5, Sk-Mel5) or DMEM (HCT116, CCSW, MCF7, RIL175, SW620) medium, supplemented with 10% FCS, 100 U/mL penicillin, 100 mg/mL streptomycin, and 2 mM glutamine, if not indicated otherwise. Media and supplement were purchased from Sigma-Aldrich (#R0883, #D6546, #F7524, #P433, #G7513). Cells were maintained at 37 °C in a humidified atmosphere of 5% CO_2. Subculturing was performed according to the ATCC recommendations: Cells were washed with PBS buffer (2.7 mM KCl, 1.8 mM KH_2PO_4, 137 mM NaCl, and 10 mM Na_2HPO_4 in distilled water; adjusted pH 7.4, autoclaved) and detached with trypsin-EDTA (Sigma-Aldrich #T3924). The reaction was stopped with culture medium, the cell suspensions were centrifuged for 5 min at 250 x *g* and resuspended in full growth media. Cell suspensions were used for cell seeding and further passaging.

2.1.2 Cell freezing and thawing

After splitting, cell suspensions were centrifuged for 5 minutes at 250 x *g* and resuspended in FCS supplemented with 10% DMSO (Sigma-Aldrich). Cells were aliquoted into cryovials, frozen at -80 °C, and transferred to a liquid nitrogen tank for storage.

To thaw cells, vials were warmed up quickly in a 37 °C water bath. Cell suspensions were transferred into growth media and centrifuged for 5 min at 250 x *g*. Cells were resuspended in full growth media and cultured as described above.

2.1.3 3D cell culture

For spheroid formation, 3,000 HCT116 cells were seeded into low attachment U-bottom plates (Band #781900) or into 96 well plates, that had been coated with 50 µl 1.5% agar (Biozym #840004). Plates were centrifuged for 3 min at 200 x *g*. 3-day old spheroids were used for further experiments.

2.1.4 Stably EGFP-expressing Huh7

To generate stably EGFP-expressing Huh7 cells, cells were transfected with the empty backbone mEGFP-C1 plasmid (Addgene plasmid #54759) using lipofectamine 3,000 (Thermo Fisher Scientific #L3000008) according to the manufacturer's protocol (2.5 µg plasmid for 3 x

10^5 cells). 48 h after transfection medium was changed, and the selection antibiotic geneticin (Thermo Fisher Scientific #11811023) was added in a concentration of 1 mg/ml for further cultivation. Cells were used for xenograft injections after at least 3 sub-culturing steps, and stable EGFP expression was controlled by flow cytometry. Culturing without geneticin up to 3 days did not change EGFP expression.

2.1.5 Cultivation of resistant cells

Doxorubicin -resistant cells, generated as described previously (Schultheiss et al., 2017), were cultured permanently in RPMI-1640 medium containing 2 µM doxorubicin (Alfa Aesar #J-64000). For experiments, cells were seeded in medium without doxorubicin.

2.1.6 Differentiation of Huh7

For differentiation, 3,000 Huh7 cells were seeded into 96 well plates in RPMI-1640 full growth medium. The next day, medium was changed to RPMI-1640 supplemented with 2% human serum (PAN biotech #P40-2701) instead of FCS (El-Shamy et al., 2015). Medium was changed twice a week, for 3 weeks.

2.1.7 Isolation and cultivation of primary human endothelial cells

Primary human umbilical vein endothelial cells (HUVECs) were isolated and cultured by Theo Ranßweiler as described previously (Astanina et al., 2015). Umbilical cords were provided by the Klinikum Saarbrücken (Saarbrücken, Germany; ethics committee permission no. 131/08). For all experimental procedures HUVECs were used in passage three. Cells were detached by trypsin-EDTA and seeded at a density of 10,000 cells per well in 96 well plates.

HUVEC medium: Endothelial Cell Growth Medium (# C-22010, PromoCell, Heidelberg, Germany) with supplement mix (# C-39215, PromoCell), penicillin 100 U/ml, streptomycin 100 mg/ml, kanamycin 50 mg/ml, and 10% FCS.

2.1.8 Isolation and cultivation of human monocyte-derived macrophages

Buffy coats were obtained from healthy donors (Blood Donation Center, Saarbruecken, Germany), authorized by the local ethics committee (Saarland, Germany; ethics committee permission no. 173/18). Peripheral blood mononuclear cells (PBMC) were isolated by density gradient centrifugation using Lymphocyte Separation Medium 1077 (PromoCell #C-44010) in Leucosep tubes (Greiner #227290). CD14 positive cells were selected from PBMCs by positive selection using CD14 magnetic beads (Miltenyi #130-050-201). Sorted monocytes were seeded at a density of 5 x 10^5 cells/ml and differentiated in full growth RPMI-1640 media

supplemented with 20 ng/ml recombinant human macrophage colony-stimulating factor (M-CSF, Miltenyi #130-096-492) for 6 days.

2.1.9 Polarization of human monocyte-derived macrophages

To polarize human monocyte-derived macrophages (HMDMs) *in vitro*, the differentiation media was supplemented with 20 ng/ml recombinant IFNγ (Miltenyi #130-096-484) and 100 ng/ml LPS (Ultrapure LPS from *E. coli* K12 #tlrl-peklps) for M1 polarization; either 20 ng/ml IL4 (Miltenyi #130-093-921) or IL10 (Miltenyi #130-093-948) for M2 polarization; or left without further supplementation for M0 macrophages. TAM-like macrophages were generated with tumor conditioned media (TCM) supplemented with 20 ng/ml M-CSF. For TCM production, 20 ml media were incubated with a confluent cell layer of A549 cells in a T75 cell culture flask for 48 h, following sterile filtration to remove cell debris. In all experiments comparing macrophage subsets, cells were differentiated and polarized from monocytes obtained from the same donor.

2.1.10 Differentiation and polarization of THP-1-derived macrophages

Cells of the human monocyte cell line THP-1 were grown in RPMI-1640 medium fully supplemented as described above. For differentiation, 50,000 cells per well were cultured in 96 well plates in the presence of 30 ng/ml phorbol 12-myristate 13-acetate (PMA, Calbiochem #524400) for 48 hours. For polarization, PMA-differentiated cells were stimulated as described in section 2.1.9.

2.1.11 Macrophage tumor cell co-culture

HMDMs were isolated and differentiated as described above in cell culture flasks. On day 5, differentiated macrophages were harvested by accutase solution (Sigma-Aldrich #A6964) and stained with cell tracker deep red (Thermo Fisher Scientific #C34565) using 500 nM dye dissolved in RPMI-1640 for 30 min at culturing conditions. HeLa cells were harvested by trypsin digestion and stained with 5 µM cell tracker violet BMQC (Thermo Fisher Scientific #C10094) for 30 min. Stained cells were washed twice with PBS and resuspended in RPMI-1640. HeLa cells and macrophages were co-cultured in a 1:1 ratio (2.5×10^5 cells each, seeded into six-well plates) for 24 h before experiments were performed.

2.2 Bacterial culture

2.2.1 Transformation

TOP10 chemically competent *E.coli* (Invitrogen #C4040-03) were mixed with 100 ng plasmid solution and incubated on ice for 20 min. Bacteria were heat-shocked for 40 sec at 42 °C, and incubated on ice for further 2 min. Bacteria were resuspended in 900 µl prewarmed LB_{amp} medium (Roth #X968.1; autoclaved and supplemented with 100 µg/ml ampicillin, Sigma #A0166) and incubated at 37°C and 250 rpm for 1.5 h. Afterwards, 100-500 µl suspension was plated on LB_{amp} plates (1.5% agar in LB_{amp} medium) and incubated overnight.

2.2.2 Plasmid isolation

Single colonies were picked from agar plates for the preparation of liquid overnight cultures. Plasmids were isolated from overnight cultures using the High Pure Plasmid Isolation Kit (Roche #11754777001) according to manufacturer`s protocol.

2.3 Endotoxin measurements

Thioholgamide A and auratryptanon were tested for the absence of endotoxins using the Endozyme II assay kit (Biomérieux #890030) according to manufacturer`s instructions.

2.4 Cell viability measurements

2.4.1 MTT assay

For viability assays based on MTT reduction, cells were seeded in appropriate numbers to reach confluency the next day. They were treated with the compounds in increasing concentrations for 48 h. The stock solutions were prepared in DMSO, and solvent controls were tested concurrently. The viability of adherent cells was determined by replacing the supernatants with 0.5 mg/ml MTT (3-(4,5-dimethylthiazole-2-yl)-2,5 diphenyltetrazolium bromide, Sigma-Aldrich #M5655) solution in respective culture media. After incubation, cells were lysed in DMSO, and the absorbance was measured at 560 nm using a microplate reader (GloMax™). IC_{50} values were calculated by non-linear regression using OriginPro®.

2.4.2 APH assay

The viability of HCT116 cells forming tumor spheroids was analyzed in an acid phosphatase (APH) assay, measuring phosphatase activity. 3-day old spheroids (generated on agar-coated 96 well plates) were treated for 48 h with the compounds or vehicle control before the supernatant was replaced by 100 µl assay buffer (0.1 M sodium acetate (pH 5.2), 0.1% (V/V) Triton X-100 in H_2O), supplemented freshly with 4 mg/ml p-nitrophenyl phosphate (final pH 4.8, Thermo Fisher Scientific # 34045). Spheroids were incubated for 1.5 h at 37°C before 10 µl 1 M NaOH were added, and absorption was measured at 405 nm on a microplate reader (GloMax™).

2.4.3 Time-dependent cell death measurement

For the time-dependent analysis of cell death, cells were analyzed in an IncuCyte® S3 System (Sartorius). The day after seeding, supernatant was replaced by the respective media containing IncuCyte® Cytotox Red (Sartorius #4632) and Caspase-3/7 Green (Sartorius #4440) reagents according to the manufacturer's instructions. Cells were treated with different concentrations of the respective compounds, or DMSO vehicle control, and cell confluency as well as apoptotic and necrotic events were monitored for 3 days. Apoptotic and cytotoxic IC_{50} values were calculated based on Cytotox Red or Caspase-3/7 Green positive cells by non-linear regression using OriginPro®.

2.5 *In vitro* proliferation measurements

2.5.1 2D proliferation measurement - Automated microscopy

For the kinetic, automated microscopy-based proliferation analysis, cells were seeded to reach 10% confluency the next day. Cells were treated with increasing concentrations of compounds or vehicle control, and their proliferation was observed in an IncuCyte® S3 system. Proliferation was quantified by the IncuCyte basic analyzer software based on cell confluency. Proliferation inhibitory IC_{50} values were calculated by non-linear regression using OriginPro®.

2.5.2 2D proliferation measurement - ECIS

For the kinetic, impedance-based proliferation analysis, the electric cell-substrate impedance sensing (ECIS®) system was used. The day before seeding, the arrays were preincubated with the respective cell culture medium at 37°C. 8,000 A549 cells were seeded into 96-well ECIS arrays (96W10E+, with 10 electrodes per well) and impedance measurements (every 15 min

for 100 h, 16,000 Hz) was started immediately after cell seeding. 5 h after seeding, cells were treated with the respective compounds or vehicle control. Impedance was normalized to 7 h after seeding.

2.5.3 3D proliferation measurement

The growth of HCT116 spheroids was monitored in an IncuCyte® S3 system. 3-day old spheroids, generated in U-bottom plated as described above, were treated with the respective compound or vehicle control, and the spheroid area was determined over 6 days. Spheroids were analyzed using the IncuCyte spheroid analyzer software.

2.6 Migration measurements

Migration was analyzed in an IncuCyte® S3 system by seeding 80,000 HCT116 cells per well in an ImageLock 96 well plate to reach 90-100% confluency next day. Scratches were conducted using the Woundmaker® tool (IncuCyte Migration Kit). Afterwards, cells were washed twice with media containing 2% FCS, which was also used for further cultivation. Cells were treated with compounds or vehicle control, and the migration was monitored for 48 h. The cell covered wound area was analyzed and quantified using the IncuCyte migration software.

2.7 Seahorse measurements

The cellular glycolysis stress and mito stress tests were performed using an Agilent Seahorse® 96XF device and respective kits. The assays were performed as recommended in the manufacturer's protocol (#103020-400, #103015-100). In brief, the cells were seeded and pre-treated with thioA if indicated. The medium was replaced by Seahorse medium one hour prior to measuring. For the glycolysis stress test, 20,000 RIl175 cells were seeded and treated with 10 mM glucose, 1 µM oligomycin, and 50 mM 2-desoxyglucose. Macrophages were analyzed using the mito stress test. Macrophages were differentiated for 6 days, and 120,000 cells were seeded per well. Macrophages were polarized for 24 h prior to measurements and treated with either 1 µM oligomycin or 1 µM thioA, 2 µM carbonyl cyanide-p-trifluoromethoxy-phenylhydrazone (FCPP), and 0.5 µM rotenon/antimycin A. The data were analyzed by the Seahorse Wave Software (Agilent Technologies).

After Seahorse measurements, cells were stained with Hoechst dye, and fluorescence intensity was analyzed in a plate reader to ensure an equal cell distribution also after different treatment

steps. Since no significant changes were observed upon different treatments, ORC and ECAR values were analyzed without further normalization. Seahorse measurements in RIL175 tumor cells were performed by Siow Wei Xiong (Pharmaceutical Biology, Ludwig Maximilian University of Munich).

2.8 ROS measurement

To detect reactive oxygen species in the supernatant of tumor cells, the homovanillic acid (HVA) oxidation assay was performed. Cells were seeded into 96 cell plates to reach 90-100% confluency the next day. Cells were treated with the compounds or vehicle control for the indicated time periods. Cells were washed with PBS, 150 µl 1x HVA assay buffer in PBS were added (10x HVA assay buffer: horseradish peroxidase (HRP, Sigma # P8250) 40 unit/ml, HVA (Sigma #H1252) 1 mM in PBS), and cells were incubated for 1 h at 37 °C. Afterwards, 100 µl supernatant were transferred into a white 96 well plate, and 15 µl stop solution (0.1 M glycine, 25 mM EDTA, 0.1 M NaOH, pH 12 in H_2O bidest.**)** were added per well. Plates were covered from light and fluorescence was measured at 312 nm excitation and 420 nm emission in a Spectramax Plate reader. Fluorescence readings were normalized to the protein amount per well.

2.9 Determination of protein concentrations

Protein concentrations were determined using the Pierce BCA protein assay kit (Thermo Fisher Scientific #23225) according to the manufacturer's instructions.

2.10 RNA isolation, reverse transcription, and quantitative PCR

Total RNA was isolated using the High Pure RNA Isolation Kit (Roche #11828665001). Concentration of isolated RNA was quantified by NanoDrop™ (Thermo Fisher Scientific), and RNA with an A_{260}/A_{280} ratio higher than 1.8 was used for further experiments. Equal amounts of RNA were transcribed using the High Capacity cDNA Reverse Transcription Kit (Thermo Fisher Scientific #4368813) in the presence of an RNase inhibitor (Invitrogen #10777-019) according to the manufacturer's instructions. cDNA was analyzed by qPCR using a

5xHotFirePol EvaGreen qPCR Mix (Solis BioDyne #08-24-00020) and the primers listed in **Table 1**. The PCR was performed in a CFX96 touch™ Real-Time PCR detection system (BioRad). Data were normalized to the housekeeping gene *RNA18S* (macrophages) or *ACTB* (tumor cells).

Table 1. Primer sequences used for qPCR.

Gene	Accession number	Primer forward sequence	Primer reverse sequence
ACTB	NM_001101.5	TGCGTGACATTAAGGAGAAG	GTCAGGCAGCTCGTAGCTCT
AFT4	NM_001675.4	CAACTGCCCTGTTCCCGATT	GAAGGCATCCTCCTTGCTGTT
CHOP	NM_001195053.1	GGAACCTGAGGAGAGAGTGTTC	CTGCCATCTCTGCAGTTGGA
IL10	NM_000572	CAACAGAAGCTTCCATTCCA	AGCAGTTAGGAAGCCCCAAG
MMP9	NM_004994.3	CTTTGAGTCCGGTGGACGAT	TCGCCAGTACTTCCCATCCT
TNF	NM_000594.4	CTCCACCCATGTGCTCCTCA	CTCTGGCAGGGGCTCTTGAT
IP10	NM_001565.4	GAGCCTACAGCAGAGGAACC	AAGGCAGCAAATCAGAATCG
RNA18S	NR_003286.4	AGGTCTGTGATGCCCTTAGA	GAATGGGGTTCAACGGGTTA

2.11 Fluorescence microscopy

Cells were seeded on µ-Slide 8 Well for 24 h and treated as indicated. The cells were rinsed with PBS and incubated with MitoTracker™ Green FM (100 nM, Thermo Fisher Scientific #M7514) for 30 min. The nuclei were stained by Hoechst 33342 (2.5 µg/ml) for 30 min. The slides were mounted with mounting buffer prior to the insertion of the coverslip. All images were observed by fluorescence microscopy (Leica SP8 Inverted Scanning Confocal Microscope). Fluorescence microscopy was performed by Siow Wei Xiong (Pharmaceutical Biology, Ludwig Maximilian University of Munich).

2.12 Western blot

Cells were harvested and lysed in RIPA lysis buffer containing a protease inhibitor mix (Roche #4693159001). Lysates were centrifuged at 10,000 x g for 10 min and 4 °C. Protein amounts were assessed by Bradford assay, and an equal amount of protein was separated by SDS-PAGE and transferred to nitrocellulose membranes (Hybond-ECLTM, Amersham Bioscience). 5% BSA in PBS with 0.1% Tween 20 were used as a blocking buffer for 1 h, and membranes were

incubated with anti-PARP (1:1,000, Cell Signaling #9542), anti-caspase 3 (1:1,000, Santa Cruz #sc-7148), or anti-active caspase 3 (1:1,000, Sigma Aldrich #C8487), OPA1 (1:1,000, Cell Signaling #80471) or DRP1 (1:1,000, Cell Signaling #8570) primary antibodies at 4°C overnight. Secondary antibodies were incubated accordingly and subsequently conjugated with horseradish peroxidase and freshly prepared ECL solution, which contained 2.5 mM luminol. Conjugated proteins were detected by the ChemiDoc™ Touch Imaging System (Bio-Rad) and quantified by ImageLab software. For quantification, protein amount was normalized to total protein loading, detected by 2,2,2-trichloroethanol activation as described previously (Chopra et al., 2019; Gürtler et al., 2013). Western blot was performed by Siow Wei Xiong (Pharmaceutical Biology, Ludwig Maximilian University of Munich).

2.13 Mitochondrial mass

Cells were treated as indicated for 24 h and incubated with Mito-Tracker™Green FM (100 nM, Thermo Fisher Scientific #M7514) for 30 min. Cells were harvested and mean fluorescence intensity of Mito-Tracker™ staining was analyzed by flow cytometry (Canto II, Beckton Dickinson, Heidelberg, Germany). The number of 30,000 events was collected for each sample. The analysis of mitochondrial mass was performed by Siow Wei Xiong (Pharmaceutical Biology, Ludwig Maximilian University of Munich).

2.14 Flow cytometry measurements

2.14.1 Macrophage surface marker expression

HMDMs were isolated, differentiated, and polarized as described above for 24 h. Polarized cells were treated with 50 nM thioholgamide A for 7 h. Cells were detached using accutase solution (Sigma-Aldrich #A6964), washed, and resuspended in FACS wash (PBS, 2.5% FCS, 0.1% sodium azide). Cells were blocked in human Fc Block (BD, #564220) for 15 min, and stained for 30 min on ice with anti-CD14-APC (BD #555399), anti-CD163-PE-CF594 (BD #562670), anti-CD80-BB515 (BD #565008), and anti-HLA-DR-PerCP-CY5.5 (BD #560652) antibodies. After washing, stained cells were resuspended in 1% paraformaldehyde in PBS prior to flow cytometric analysis on a BD LSRFortessa. Data were analyzed using BD FACSDiva software (BD Biosciences). Median fluorescence intensity of singlet cells was used to quantify surface marker expression.

Isotype controls: APC mouse IgG2a, κ (BD #555576), PE-CF594 mouse IgG1 κ (BD #562292), BB515 mouse IgG1 κ (BD #564416), PerCP-Cy5.5 mouse IgG2a, κ (BD #550927).

2.14.2 Macrophage phagocytosis assay

HMDMs were isolated, differentiated, and polarized as described above for 24 h. Polarized cells were treated with 1 µM thioholgamide A for 30 min. After incubation for 15 min with fluorescent latex beads (50 beads/cell, Fluoresbrite carboxylated YG microspheres, 1.75 µm, Polyscience #17687), macrophages were washed four times with cold PBS and detached from plates using PBS containing 5 mM EDTA. Cells were resuspended in FACS wash and 10,000 singlet cells were examined on a BD LSRFortessa using BD FACSDiva software (BD Biosciences).

2.14.3 Yeast and nanoparticle uptake

Stained yeast loaded with nanoparticles and plain nanoparticles were provided by Ruth Kiefer as described in Kiefer et al. (Kiefer et al., 2019). In brief, *S. cerevisiae* (BY4742) were stained with 2.5 µM carboxyfluorescein diacetate succinimidyl ester (CFSE; Life Technology # C34554) for 30 min at 37°C. CFSE-stained yeast cells were washed twice with PBS and opsonized using 25% human serum for 30 min at 37°C. Rhodamine-labeled PLGA nanoparticles (NP) were used plain or were complexed with CFSE-stained yeast for 1 h at 20 °C following centrifugation to remove residual free NPs.

For uptake studies, plain or complexed NPs were added to the tumor cell/macrophage co-culture at culturing conditions for 0.5 or 4 h. Yeast cells were added at an MOI of 5 (multiplicity of infection), and plain NPs in the corresponding amount that was loaded to yeast (which equals 38 µg). Plates were centrifuged at 200 x *g* for 3 min to ensure that yeast and co-culture were in close contact. After incubation, supernatants were collected, and cells were harvested using PBS containing 5 mM EDTA. Supernatants combined with harvested cells were centrifuged at 500 x *g* for 5 min, resuspended in 1% formaldehyde in PBS, and 10,000 singlet cells were examined *via* flow cytometry on a BD LSRFortessa using BD FACSDiva software (BD Biosciences).

2.15 Macrophage morphology analysis

HMDMs were isolated, differentiated, and polarized as described above for 24 h. Polarized cells were treated with 50 nM thioholgamide A for 7 h. Cells were imaged at the beginning and at the end of treatment in an IncuCyte® S3 system. Afterward, cells were analyzed for their morphology with the IncuCyte Cell-by-Cell analysis software and grouped in a round and elongated phenotype based on their eccentricity.

2.16 *In vivo* experiments

2.16.1 Zebrafish husbandry and viability monitoring

AB wild-type zebrafish embryos were used for experiments. Zebrafish husbandry and all experiments were performed in accordance with the European Union Directive on the protection of animals used for scientific purpose (Directive 2010/63/EU) and the German Animal Welfare Act (§11 Abs. 1 TierSchG) and maintained using standard methods (Westerfield, 2000). Adult zebrafish were kept in the automated aquatic ecosystem (PENTAIR, Apopka, UK) and monitored regularly: temperature (27 ± 0.5°C); pH (7.0 ± 0.1); conductivity (800 ± 50 µS); light-dark cycle (14 h-10 h). Fish were fed twice a day with dry small granulate food and freshly hatched live *Artemia Cysts* once a day. Embryos were euthanized not later than 5 days post fertilization (dpf).

The effects of thioholgamide A on zebrafish embryo development and viability was assessed in 24 hours post fertilization (hpf) embryos. 48 hpf embryos were used for the toxicity assessment of IMP2 inhibitors. Embryos were treated with the compounds or vehicle control in the fish water. Eye, heart, and body axis formation, heartbeat, and pigmentation were observed microscopically during 3 days of treatment.

2.16.2 Zebrafish xenograft model and in vivo proliferation measurement

During experiments, embryos were kept at 28°C in 0.3 x Danieau's solution (17 mM NaCl, 2 mM KCl, 1.5 mM HEPES, 1.8 mM $Ca(NO_3)_2$, 0.12 mM $MgSO_4$). At 48 hpf, embryos were dechorionized manually, anesthetized using 168 µg/ml tricaine (Sigma-Aldrich #A5040), and tumor cell suspension was injected into the yolk sac using a FemtoJet microinjector (Eppendorf). After injection, single embryos were placed into 96 well plates. On the next day, embryos were sorted for tumor formation and monitored with a Leica M205 FCA fluorescence

stereomicroscope. Tumor growth was determined by imaging 3 days post-injection (dpi). The growth rate was calculated as follows: (tumor area 3 dpi – tumor area 1 dpi) / tumor area 1 dpi.

For the Huh7 xenograft model, followed by thioholgamide A treatment, 2 x 10^6 stably EGFP-expressing cells were suspended in 1 µl 0.1% BSA/PBS, and approximately 1 nl was injected per embryo. Embryos were incubated with 0.3 x Danieau's solution containing solvent control or 5 µM thioholgamide A after injection.

For the HCT116 xenograft model, parental and IMP2 knockout cells were used. Prior to injection, tumor cells were stained with cell tracker orange (#C34551, Thermo Fisher Scientific) according to the manufacturer´s protocol. 2 x 10^6 cells were suspended in 1 µl 0.1% BSA/PBS. For analysis of compound-induced effects on tumor growth, tumor cells were suspended in 0.1% BSA/PBS containing the compounds in the indicated concentrations just prior to injection.

2.17 Analysis of human gene omnibus (GEO) datasets

Preprocessed and normalized data from the RNA microarray GEO datasets GSE28735 (Schetter et al., 2012; Zhang et al., 2013a), GSE43288 (Crnogorac-Jurcevic et al., 2013), and GDS4329 (Sergeant et al., 2012) were analyzed. In GSE28735 differential gene expression was analyzed between PDAC and non-tumor tissues (n = 45 each). Pearson correlation was applied to detect possible co-expressions between genes of interest and other genes in the dataset (threshold: $R^2 \geq 0.75$ or ≤ -0.75, respectively).

2.18 Tissue microarray and immunohistochemistry

Formalin-fixed, paraffin-embedded pancreatic tissue samples and the corresponding clinical data were provided by the Biobank Graz under the permission of the ethics commission (Ethikkommission Medizinische Universität Graz, 12/2013, EK number 25-259 ex 12/13). A total of 200 patients (operated between 1991 and 2005) with a median age of 64 (range 31–81) years were retrospectively evaluated. The series included 184 ductal, 5 glandular, 3 intraductal papillary mucinous neoplasms (IPMN), and 2 endocrine tumors. For 25 patients survival data were missing. Immunohistochemical stainings against IMP2 were performed as previously described (Kessler et al., 2017) using the Dako Envision AEC Kit (#K4009, Dako, Germany) for antibody detection according to the manufacturer's instructions. TMAs contained three

tissue spots per tumor. Stainings were evaluated for cytoplasmatic intensity by two independent, blinded investigators. Intensity was scored using the following scoring system: score 0 = no staining, score 1 = weak staining, score 2 = moderate staining, score 3 = strong staining. If the replicates of the same tumor differed in staining intensity median score was used for further analysis. The tissue microarray and immunohistochemistry were performed by Sonja Kessler (Pharmaceutical Biology, Saarland University), Philip Puchas and Johannes Haybaeck (Institute of Pathology, Medical University of Graz).

2.19 Statistical analysis

The data are expressed as mean ± SEM (standard error of the mean) of at least 3 independent experiments performed in replicates, if not indicated otherwise. Statistical differences between two groups were calculated using a two-tailed Student's t-test; one-way Analysis of Variance (ANOVA) analysis followed by Tukey's or Bonferroni's analysis was used for statistical comparison of more than two groups. Differential expression analysis was based on the Kolmogorov–Smirnov test. Pearson correlation was applied to detect correlations between genes of interest. All tests are two-sided, and differences were considered statistically significant when p-values were less than 0.05. Calculations were performed using the OriginPro® 2020 software.

3 **Part I:** Characterization of natural compounds targeting tumor cells and shaping the tumor microenvironment

3.1 **Chapter 1.** Thioholgamide A, a new anti-proliferative anti-tumor agent, modulates macrophage polarization and metabolism

3.1.1 Introduction

The recently described natural product thioholgamide A (thioA) belongs to the family of ribosomally synthesized and post-translationally modified peptides (RiPPs), a group of compounds that feature a high structural diversity and that achieve a variety of biological activities (Zhang et al., 2018). ThioA was identified as a product of *Streptomyces sp. MUSC 136T* by genome mining and has been reported to exhibit cytotoxic activities (Kjaerulff et al., 2017).

Increasing evidence indicates that the tumor microenvironment (TME) contributes to the acquisition of hallmarks of cancer traits. These comprise, e.g., sustaining proliferative signaling, evading growth suppressors, resisting cell death, enabling metastasis, reprogramming of energy metabolism, and evading immune destruction (Hanahan and Weinberg, 2011). The TME can also substantially influences the efficacy of anti-cancer therapies (Roma-Rodrigues et al., 2019). Innate immune cells are highly represented in the TME, with tumor-associated macrophages (TAMs) being the major population (Cassetta and Pollard, 2018). Signals originating from malignant cells and cells of the TME influence the function and phenotype of TAMs. On one end of the multifaceted spectrum of macrophage plasticity, M1 macrophages exhibit a tumor-suppressing response and are usually found in the early phase of tumor formation. During tumor progression, the macrophage population is predominantly skewed towards an M2-like phenotype. This polarization state orchestrates cancer-related inflammation, supports angiogenesis, extracellular matrix remodeling, and tumor cell proliferation. Thereby macrophages promote tumor growth and metastasis (Mantovani et al., 2017; Ostuni et al., 2015). A correlation between an increased presence of M2-like TAMs and poor prognosis has been found in various tumor entities, highlighting TAMs as an interesting target in tumor therapy (Pathria et al., 2019).

In this work, the effects of thioA on different hallmarks of cancer were evaluated in 2D and 3D *in vitro* models and a zebrafish embryo *in vivo* model. Moreover, its influence on macrophage phenotypes was investigated.

3.1.2 Results

3.1.2.1 Thioholgamide A impairs tumor cell viability and proliferation

The natural product thioA has been shown to reduce tumor cell viability in a set of different tumor cell lines upon a 5-day treatment (Kjaerulff et al., 2017). We confirmed reduced viability in cancer cell lines from the most abundant and most deadly tumor entities, i.e., breast, liver, colon, and lung (Bray et al., 2018). Tumor cell viability was determined after 48 h treatment by MTT assay, leading to IC_{50} values in the nano- to low micromolar range (**Table 2**, **Figure 8 A**). In a 3D-spheroid model, thioA attenuated cell viability as determined by the activity of acid phosphatases) APH (**Figure 8 B**).

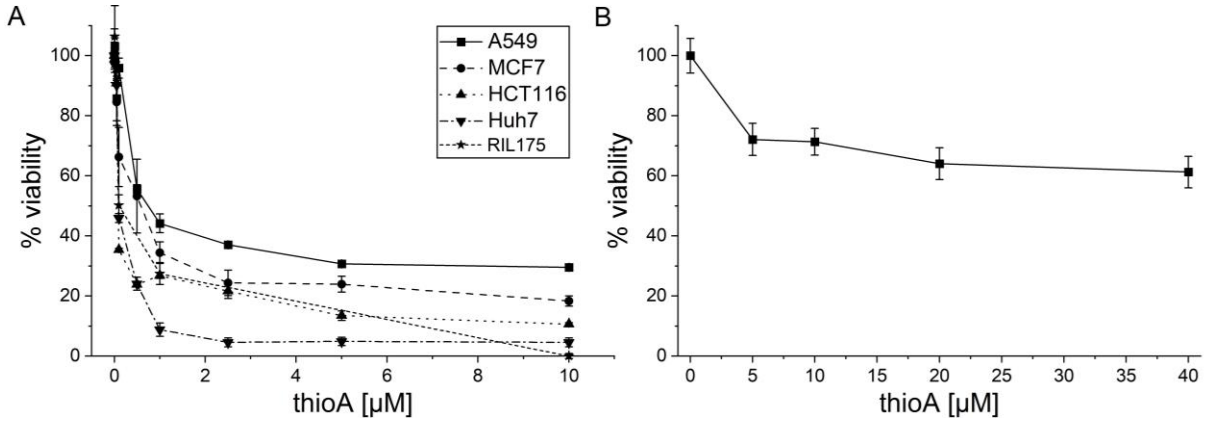

Figure 8. ThioA-induced effects on tumor cell viability.
(**A**) A set of tumor cells was treated with increasing concentrations of the compound, and cell viability was determined after 48 h treatment in an MTT assay.
(**B**) 3-day old HCT116 spheroids were treated with thioA for 48 h, followed by an APH assay to assess viability. Vehicle control-treated cells were used for data normalization; n=3 (triplicates).

Table 2. Metabolic viability assay-based IC_{50} values of thioA.
IC_{50} values of thioA against a panel of tumor cell lines measured in the MTT assay after 48 h treatment.

cell line	*IC_{50}*
HCT116	176 nM
Huh7	141 nM
MCF7	480 nM
A549	1.16 µM
RIL175	157 nM

Since MTT-based assays make use of the metabolic activity as an indirect parameter of cell viability, we further assessed the fractions of cells exhibiting actual markers of cell death in a comprehensive time-dependent live-cell microscopic analysis. We used combined staining for active caspase 3/7 as an indicator of apoptosis and membrane permeability as an indicator of necrosis (**Figure 9 A-F**). Interestingly, in comparison to the low IC_{50} values from MTT measurements, only rather high thioA concentrations and long treatment times provoked the appearance of apoptotic and necrotic markers (for comparison of IC_{50} values see **Table 3**). Still, apoptosis was induced in concentrations comparable to other apoptosis inducers, such as staurosporine (**Figure 10**). When comparing IC_{50} values, caspase 3/7 activity- and membrane permeability-based values were several-fold higher than the MTT-based values.

Since thioA induced cell death only at high concentrations, we tested a potential anti-proliferative effect by monitoring cell confluency during treatment using automated microscopy. Notably, the anti-proliferative activity of thioA resulted in the by far lowest IC_{50} values (**Figure 9 G-I**, **Table 3**). MCF7 cells, devoid of caspase 3 (Jänicke et al., 1998), showed a reduced proliferation but no detectable induction of cell death in thioA concentrations up to 1 µM.

Due to the discrepancy between the cytotoxicity expected based on MTT results and that ultimately confirmed by apoptotic and necrotic events as well as the fact that the MTT assay is a metabolic assay, we suggested an influence of thioA treatment on metabolism.

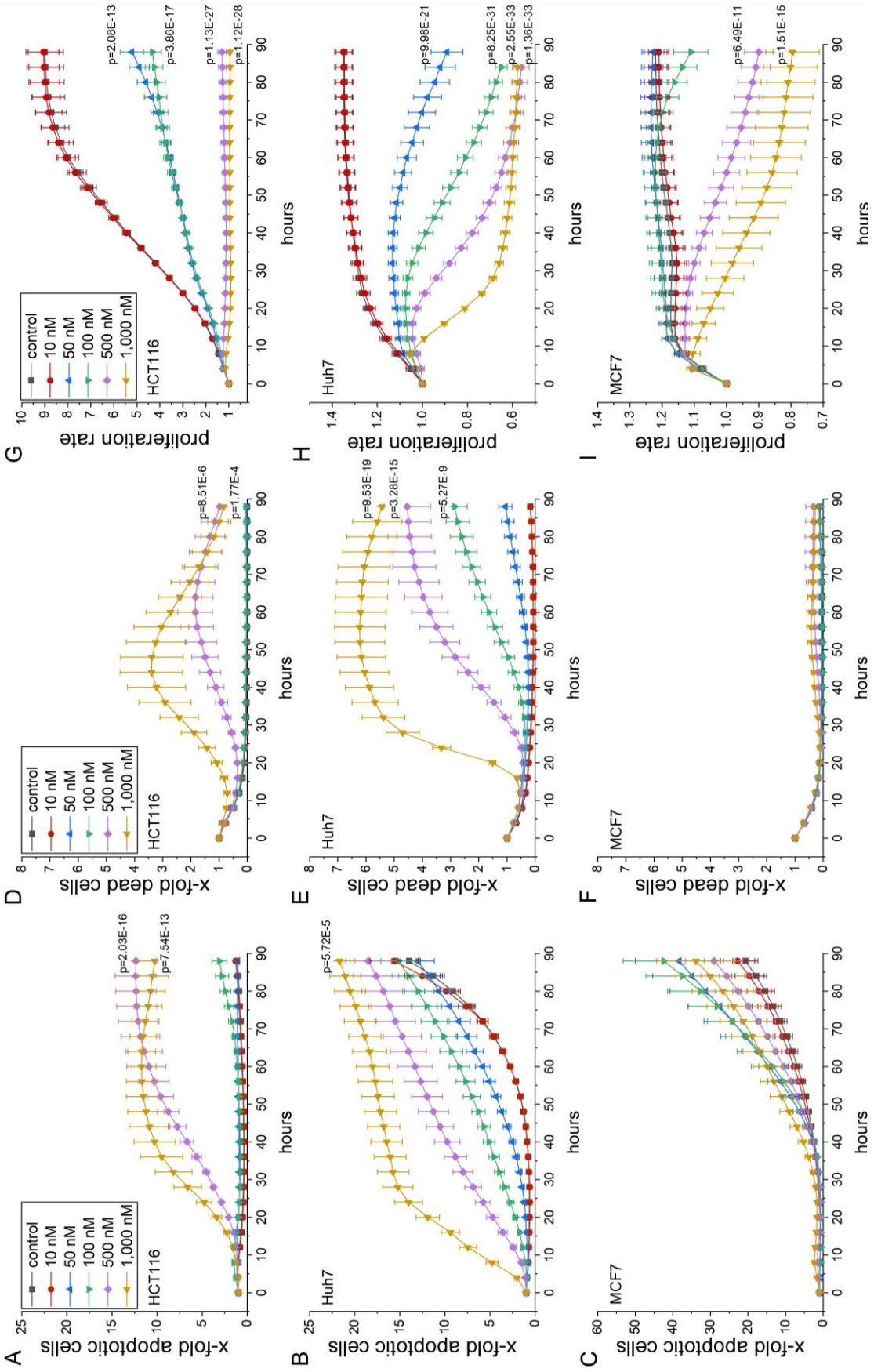

Figure 9. Live cell microscopy-based analysis of thioA-induced cell death and anti-proliferative activity. Continued.

Figure 9 continued.
(**A-C**) HCT116, Huh7, and MCF7 cells were stained for caspase 3/7 activity and (**D-F**) cell membrane permeability and monitored in an IncuCyte® S3 system during thioA or vehicle control treatment over 88 h.
(**G-I**) Cell confluency was monitored in parallel. Cell confluency was normalized to time point 0 h.
(**A-F**) Fluorescent signals from apoptotic and dead cells were normalized to cell confluency. Statistical analysis was performed for the last acquired time point using one-way ANOVA followed by Bonferroni's post-hoc analysis; n=3 (quadruplicates).

Table 3. Apoptosis-, necrosis-, and proliferation-based IC_{50} values of thioA.
IC_{50} values [nM] ± SEM of thioA against HCT116, Huh7, and MCF7 tumor cell lines based on caspase 3/7 activity, membrane permeability, and cell confluency measured by automated microscopy; calculated for 48 h treatment.

cell line	*caspase 3/7 activity*	*membrane permeability*	*proliferation*
HCT116	412.7 ± 27.5	840.8 ± 163.6	90.8 ± 5.5
Huh7	197.2 ± 44.8	578.8 ± 55.8	52.1 ± 5.7
MCF7	n.d.	n.d.	489.9 ± 9.3

n.d. (not detectable, in concentrations up to 1 µM thioA)

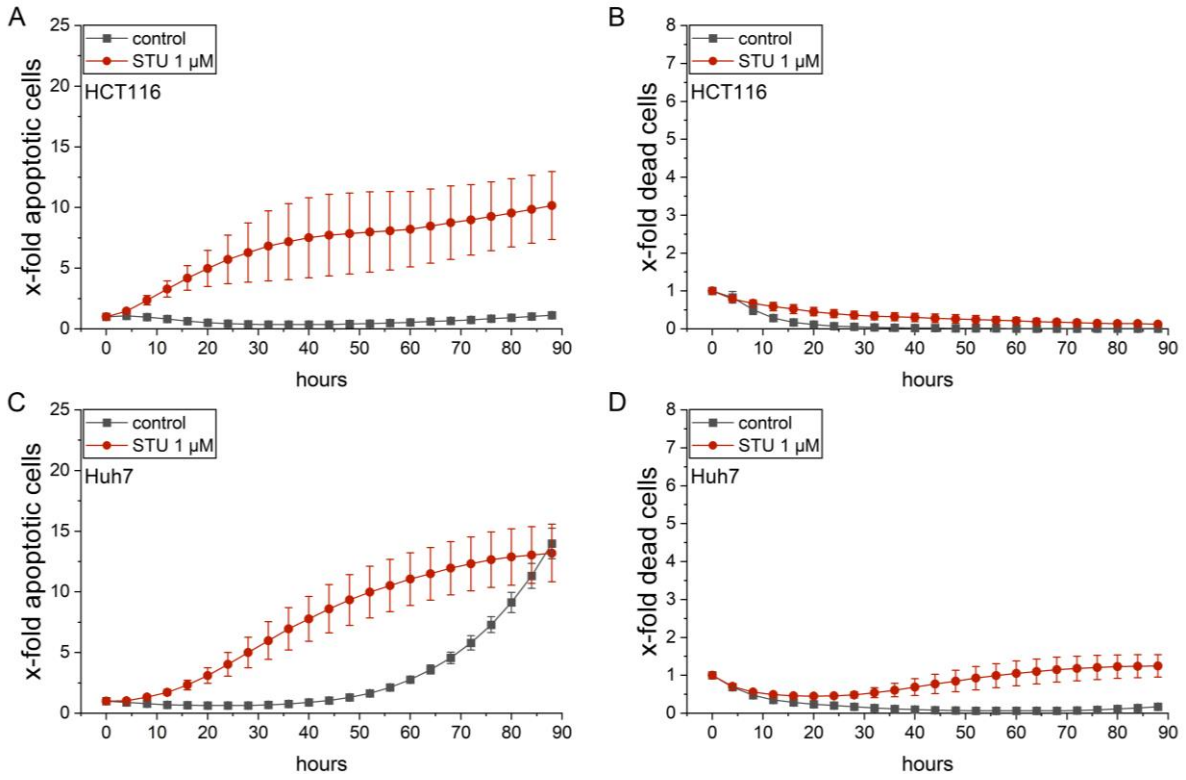

Figure 10. Live cell microscopy-based analysis of staurosporine-induced cell death.
Live cell microscopy-based analysis of staurosporine-induced cell death. HCT116 and Huh7 cells were stained for (**A, C**) caspase 3/7 activity and (**B, D**) cell membrane permeability, and monitored in an IncuCyte® S3 system during STU (staurosporine) or vehicle control treatment over 88 h. Fluorescent signals from apoptotic and dead cells were normalized to cell confluency; n=3 (triplicates).

3.1.2.2 Thioholgamide A inhibits oxidative phosphorylation and affects mitochondrial mass and morphology

The Warburg effect represents a well-known metabolic hallmark of cancer cells, i.e., their dependency on glycolysis rather than on oxidative phosphorylation to sustain proliferation, even in the presence of enough oxygen supply. We, therefore, analyzed the bioenergetic profile of thioA treated tumor cells using a seahorse glycolytic stress test. Pretreatment with thioA resulted in reduced responsiveness towards the ATP synthase inhibitor oligomycin (**Figure 11 A**), but no significant change in the ECAR ratio upon glucose addition as compared to the DMSO control. Hence, we suggested that there is no change in glucose uptake capacity but a shutdown of oxidative phosphorylation (OXPHOS) in a dose-dependent manner (**Figure 11 B**). These actions occurred already in concentrations that do not induce cell death and could not be amplified by the ATP synthase inhibitor oligomycin. Since Takase et al., identified the ATP synthase as a target of the RiPP prethioviramide (Takase et al., 2019), we hypothesized that thioA shares this mode of action. Therefore, we replaced oligomycin injection by thioA. Indeed, thioA injection resulted in similar profile curves (**Figure 11 C**) and reduced the oxygen consumption rate (OCR) within the first 20 min of treatment (**Figure 11 D**). The inhibition of oxygen consumption was comparable to the effect induced by the ATP synthase inhibitor oligomycin, indicating that thioA inhibits mitochondrial function Analysis of mitochondrial structure by Mitotracker Green staining further demonstrated a morphological change in the mitochondrial network (**Figure 11 E**), indicating a mitochondrial impairment. Along this line, analysis of mitochondrial mass revealed a similar phenotype of thioA and oligomycin. At low concentrations, mitochondrial mass was not significantly changed, yet was increased in higher concentrations. The latter is most likely a compensatory mechanism to account for dysfunctional mitochondria (**Figure 11 F**). Additionally, western blot analysis of prominent mitochondrial fission regulators OPA1 and DRP1 showed alterations in their cleavage, indicating deregulation in mitochondrial fusion-fission-dynamics (**Figure 11 G-K**).

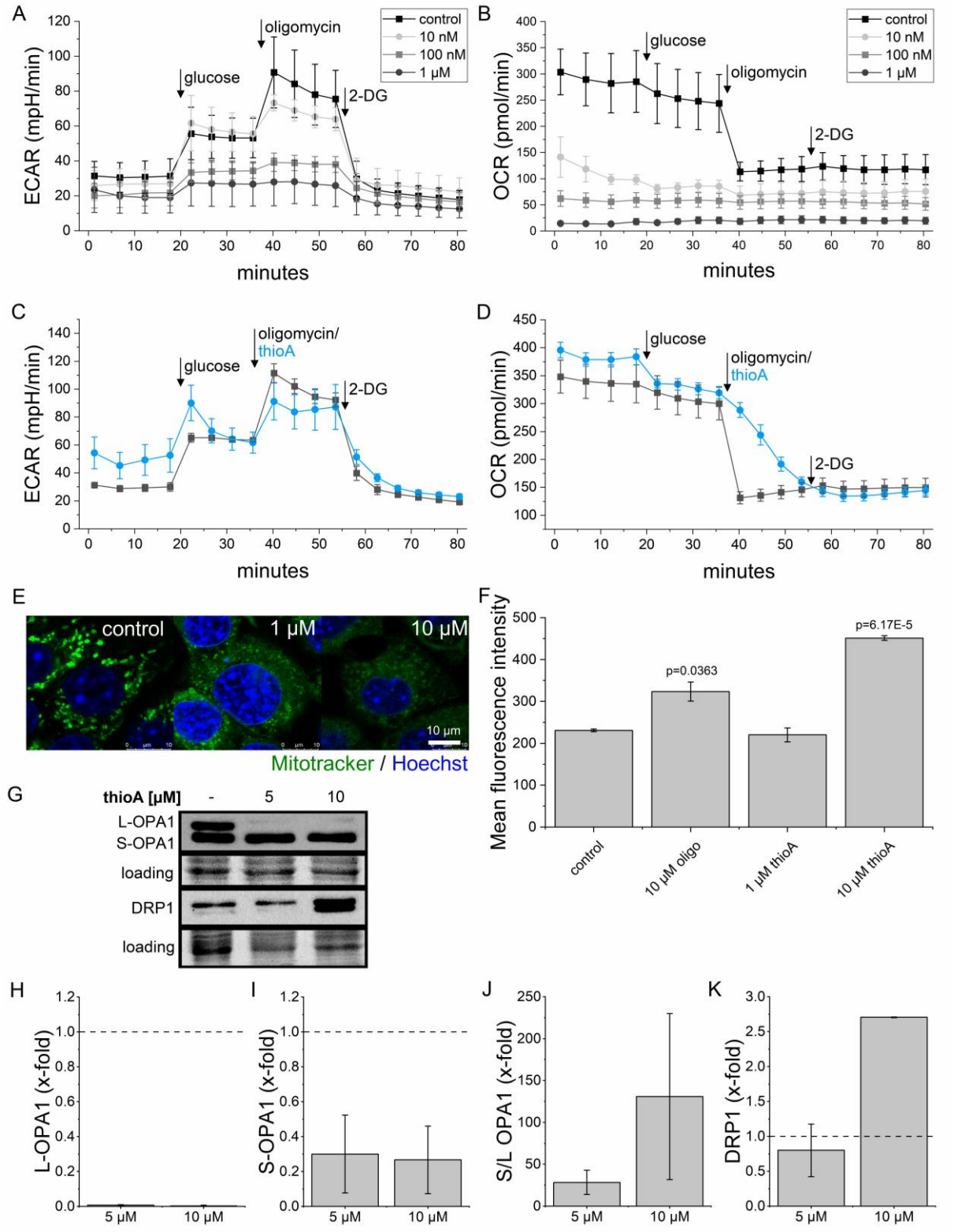

Figure 11. ThioA effects on tumor cell metabolism and mitochondria.
(**A-D**) Extracellular acidification rate (ECAR) and Oxygen consumption rate (OCR) were measured in RIL175 cells in a glycolysis stress test using a Seahorse 96XF instrument. (**A, B**) Cells were either pre-treated for 24 h with 10 nM, 100 nM, (**C, D**) or 1 µM thioA, or the injection of the ATP synthase inhibitor oligomycin (1 µM) was replaced by an injection of 1 µM thioA. Continued.

Figure 11 continued.
(**E**) The mitochondrial morphology of RIL175 cells treated for 24 h with thioA was visualized by Mitotracker Green (mitochondria) and Hoechst (nuclei) co-staining followed by confocal live cell imaging. Microscopy revealed a diffuse staining.
(**F**) Mitochondrial mass of RIL175 cells was analyzed *via* flow cytometry after 24 h treatment with vehicle control, thioA or oligomycin (oligo), respectively.
(**G-K**) Expression of the mitochondrial fission markers OPA1 and DRP1 were analyzed by immunoblotting in RIL175 cells after 24 h thioA treatment. ThioA increased the (**H-J**) S/L OPA1 ratio and (**K**) DRP1 levels. One representative western blot is shown, including a loading control for total protein. Vehicle control-treated cells were used for data normalization.
Statistical analysis was performed using one-way ANOVA and Dunnett post-test; $p < 0.05$ (*), $p < 0.01$ (**), $p < 0.001$ (***); n=3 (triplicates), n=2 for DRP1 quantification. Data were generated by Siow Wei Xiong (Pharmaceutical Biology, Ludwig Maximilian University of Munich).

3.1.2.3 ThioA induces ISR-associated ATF4 and CHOP

Takase et al. observed an activated integrated stress response (ISR) *via* the GCN2-ATF4 pathway upon treatment with prethioviridamide and suggested that this process induced cell death (Takase et al., 2019). They further demonstrated that the higher sensitivity to prethioviridamide of E1A-3Y1 cells compared to 3Y1 cells was accompanied by increased basal mRNA levels of the ISR-mediators *GCN2* and *eIF2*. In E1A-3Y1 cells, prethioviridamide further showed an increased ISR-induction compared to the less sensitive 3Y1 cells, as demonstrated by elevated levels of the ISR-effector ATF4.

In order to investigate whether the ISR is also induced upon treatment with thioA, we assessed mRNA expression of the ISR effectors *ATF4* and *CHOP* (Pakos-zebrucka et al., 2016) after treatment of HCT116, Huh7, and MCF7 cells in toxic concentrations of thioA (**Figure 12 A, B**). There was a significant induction of both mRNAs in all three cell lines suggesting that thioA, as prethioviridamide, induces ISR.

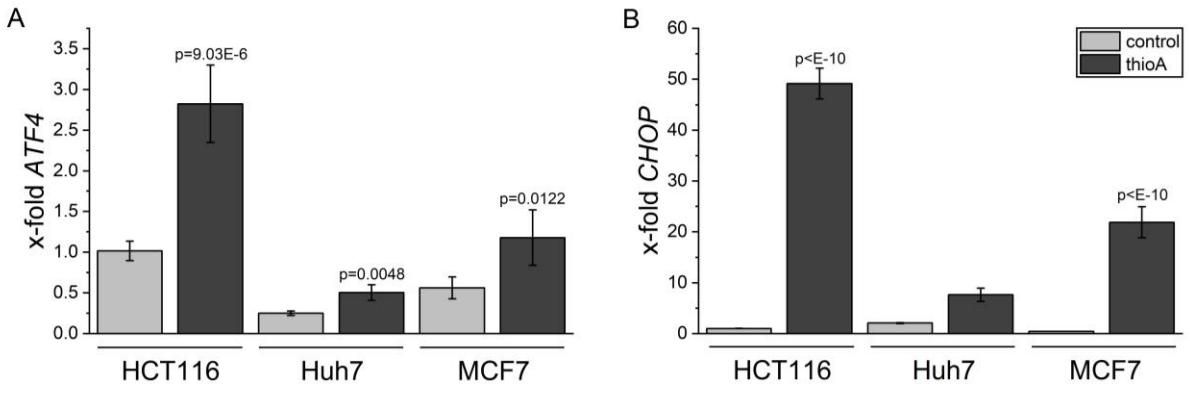

Figure 12. ThioA induces ISR-associated genes.
Continued.

Figure 12 continued.
Tumor cells were treated for 8 h with 1 µM thioA. Gene expression of (**A**) *ATF4* and (**B**) *CHOP* was measured after treatment by qPCR. Expression values were normalized to β-actin as a housekeeping gene following normalization to vehicle control-treated HCT116 cells using the ΔΔCt method. Statistical analysis was performed using one-way ANOVA followed by Tukey´s post-hoc analysis. n=3 (triplicates).

3.1.2.4 Thioholgamide A inhibits tumor cell proliferation in vitro, in tumor spheroids, and in vivo

Our data suggested that attenuated viability in cancer cells upon thioA treatment is due to its actions on tumor cell metabolism (**Figure 11**) and proliferation (**Figure 9**) while only to a lower extent on the induction of cell death. To investigate the *in vitro* anti-proliferative activity more extensively, we made use of a 3D tumor spheroid model. ThioA reduced the growth of spheroids accompanied by a loosened spheroid structure and a detachment of outer cells from the spheroid core (**Figure 13**), which was not observed for the control treatment with the apoptosis inducer staurosporine (**Figure 14**).

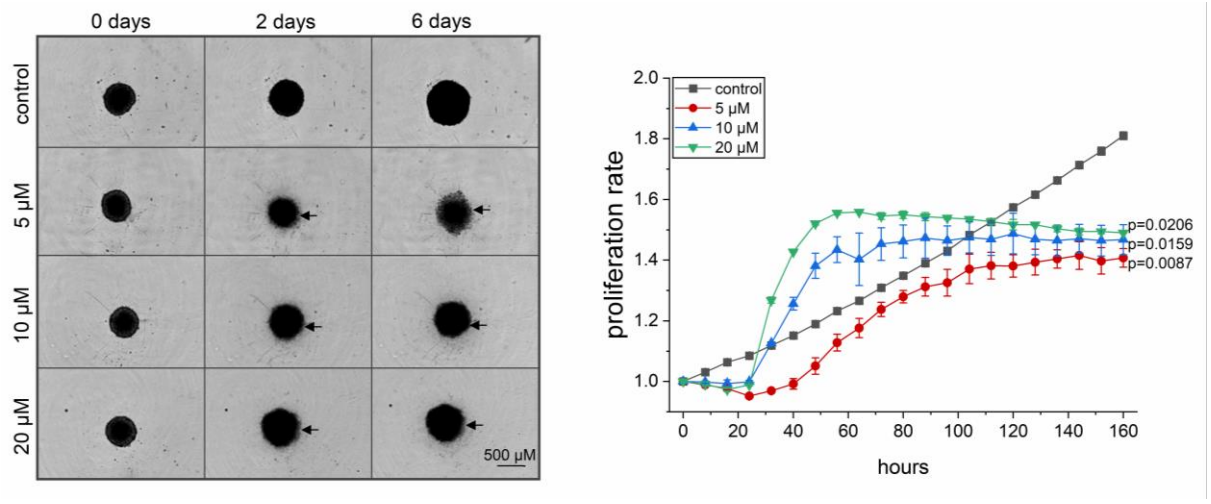

Figure 13. ThioA inhibits proliferation in 3D cell culture.
3-day old HCT116 tumor spheroids were treated with thioA, and the spheroid area was analyzed by automated microscopy (right panel). Treatment with thioA led to a disrupted spheroid structure, as seen by a detachment of cells from the core (arrows, left panel), causing an initial spheroid area increase. Spheroids are shown in representative pictures at the starting point and the time points 2 days and 6 days after treatment (left panel). Statistical analysis was performed for the last acquired time point using one-way ANOVA followed by Bonferroni's post-hoc analysis; n=2 (quadruplicates).

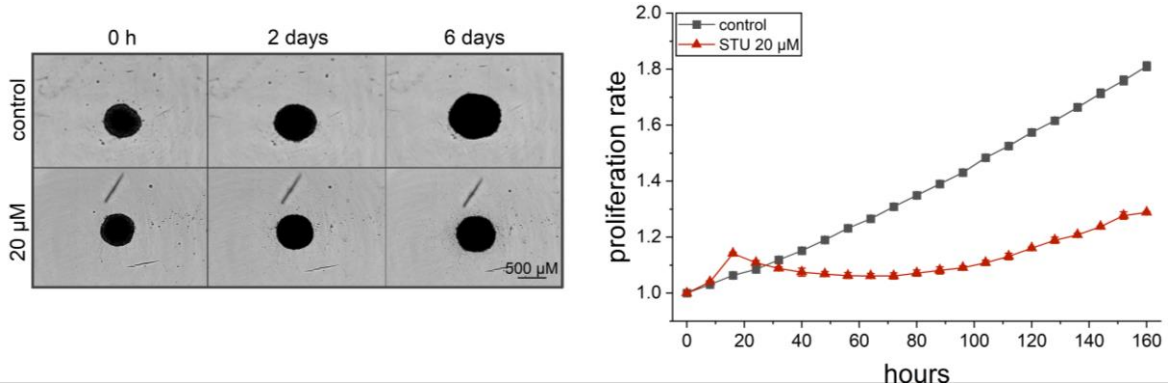

Figure 14. Staurosporine-induced effects on proliferation in 3D cell culture.
3-day old HCT116 tumor spheroids were treated with 20 µM staurosporine or vehicle control, and the spheroid area was analyzed by automated microscopy (right panel). Spheroids are shown in representative pictures at the starting point and the time points 2 days and 6 days after treatment (left panel); n=2 (quadruplicates).

As a next step, we used a xenograft zebrafish embryo model to further study the anti-proliferative effects of thioA *in vivo*. The zebrafish (*Danio rerio*) represents a favorable alternative model for tumor xenograft experiments in accordance with the 3R rules. In addition to immunosuppressed mouse models, it offers advantages, such as the straightforward monitoring of tumor growth in living embryos or the easy application of comparatively small amounts of drugs (Kirchberger et al., 2017). In this model, thioA treatment of the tumor cell-injected embryos resulted in significant inhibition of tumor growth (**Figure 15**). ThioA showed no toxic effects on zebrafish embryos in concentrations up to 10 µM for 72 h, and up to 20 µM for 48 h, as assessed by the observation of eye, heart, and body axis formation, heartbeat, and pigmentation (**Figure 16**).

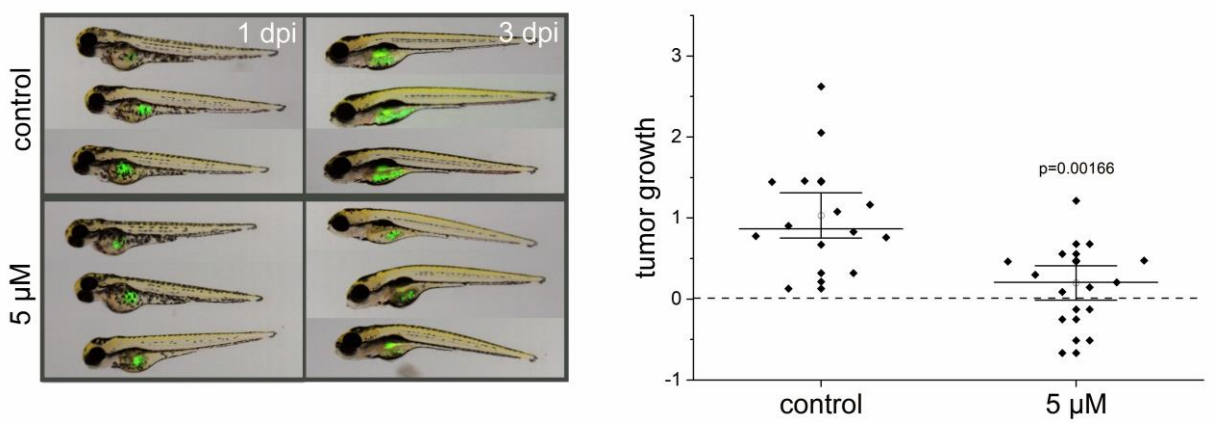

Figure 15. ThioA inhibits proliferation *in vivo*.
Stably EGFP-expressing Huh7 cells were injected into the yolk sac of zebrafish embryos 48 hpf (hours post fertilization), followed by treatment with 5 µM thioA or vehicle control in the fish water. Tumor growth was monitored 3 dpi (days post-injection) (left panel) *via* fluorescence imaging, and the tumor area was determined using ImageJ (right panel). Continued.

Figure 15 continued.
Representative pictures are shown. The plot includes individual values and the median line ± 1.5 SEM. Statistical analysis was performed using a two-tailed student's t-test.

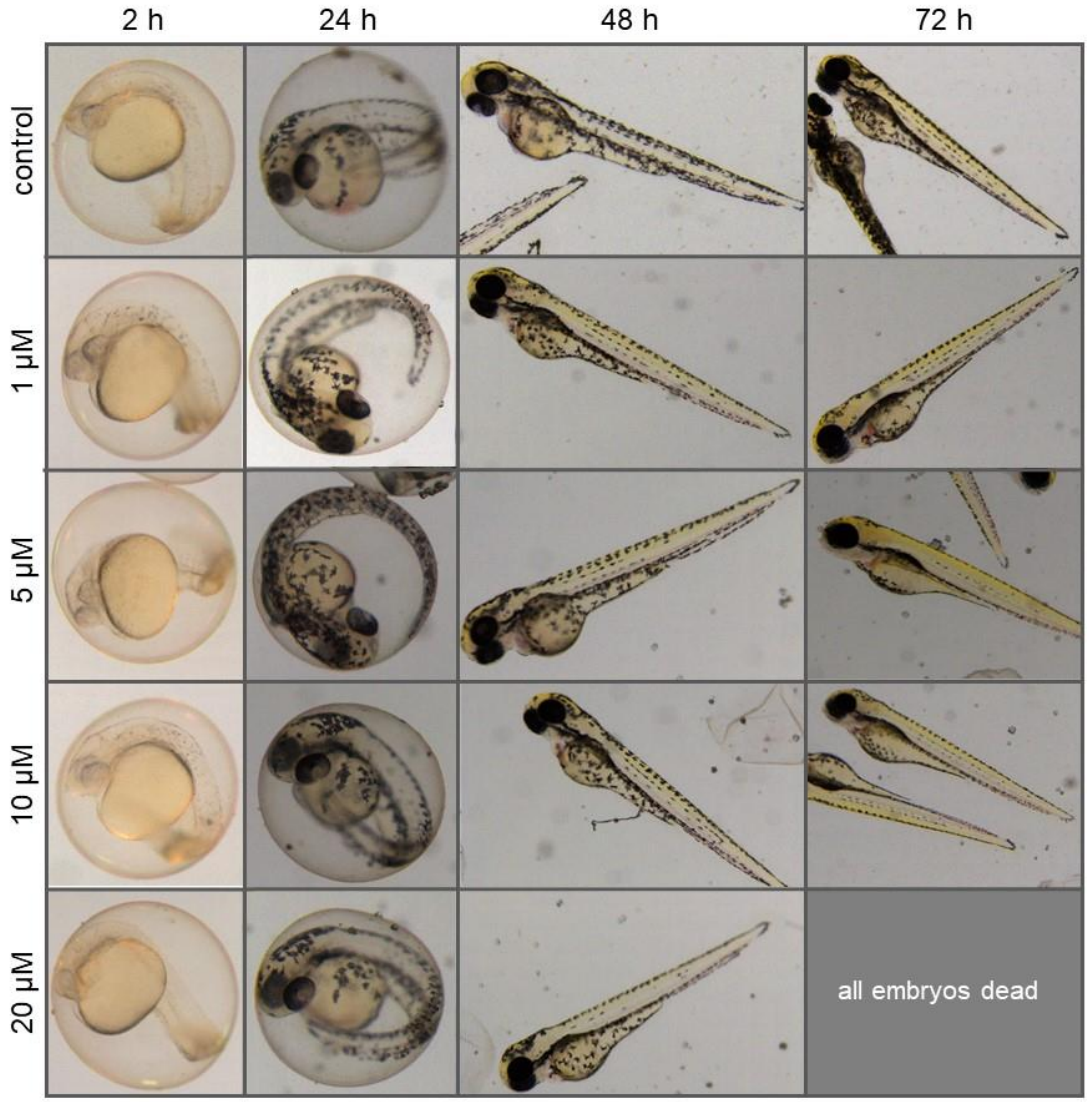

Figure 16. ThioA effects on zebrafish embryo development and viability.
Embryos at 24 hpf were treated with thioA or vehicle control in the fish water. Eye, heart, and body axis formation, heartbeat, and pigmentation were observed during 72 h treatment. Representative pictures are shown.

We further evaluated the toxicity of thioA towards non-tumorigenic human cells using two different *in vitro* models. Both, primary human umbilical vein endothelial cells (HUVECs) and human serum-differentiated Huh7.5 cells that feature a cell phenotype exhibiting a metabolism similar to normal cells (El-Shamy et al., 2015), demonstrated to be less affected by thioA compared to tumor cells (**Figure 17**). For instance, at 5 µM thioA, which is several-fold higher than the tumor IC_{50} values, over 40% were still alive in primary human endothelial cells.

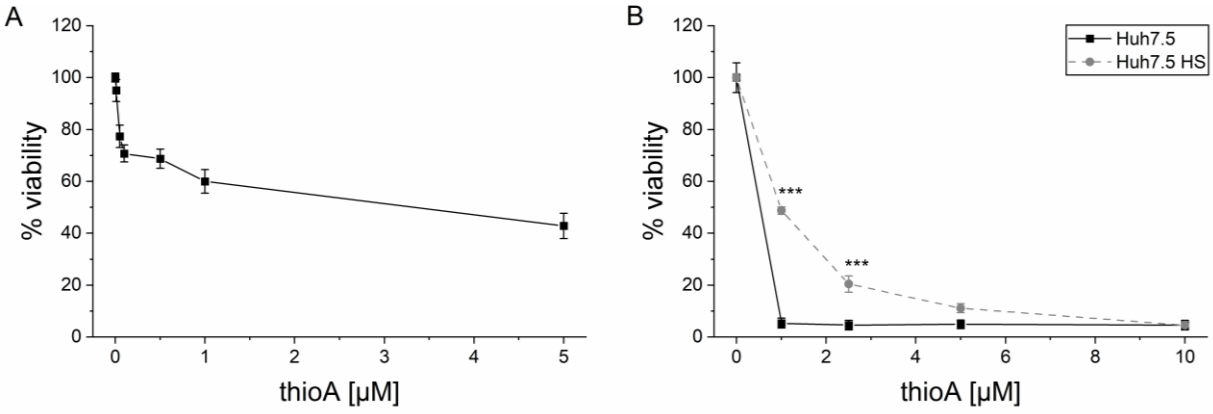

Figure 17. ThioA-induced effects on normal cell viability.
(**A**) HUVECs and (**B**) human serum-differentiated (HS) Huh7.5 cells were treated with increasing concentrations of the compound, and cell viability was determined after 48 h treatment in an MTT assay. Vehicle control-treated cells were used for data normalization. Statistical analysis was performed for the respective concentrations using one-way ANOVA followed by Bonferroni's post-hoc analysis; n=3 (quadruplicates).

3.1.2.5 Thioholgamide A inhibits tumor cell migration

In order to test whether thioA affects other hallmarks of cancer, we evaluated the metastatic capacity of tumor cells as modeled by cell migration in a scratch wound assay. Even the very low dose of 10 nM thioA, which showed neither an effect on cell viability nor on proliferation, significantly reduced cell migration of serum-starved tumor cells (**Figure 18**).

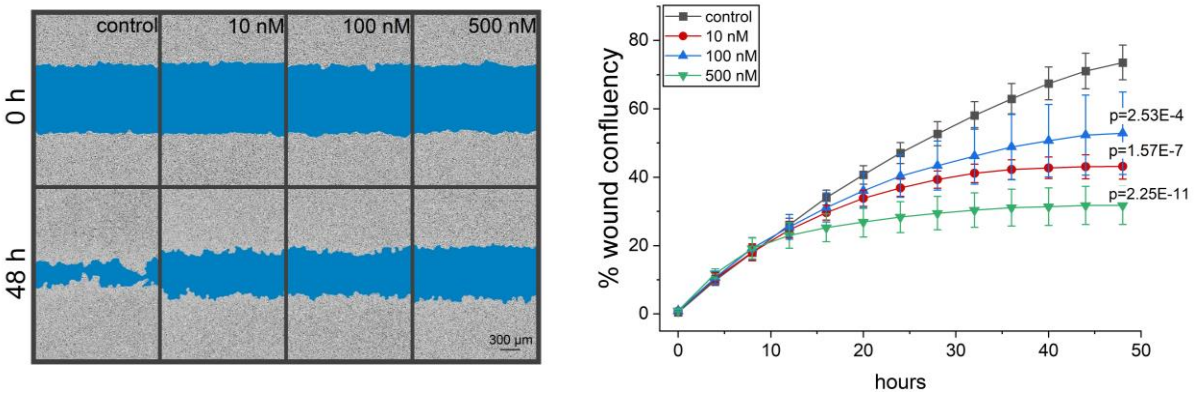

Figure 18. ThioA inhibits cancer cell migration in a scratch wound assay.
HCT116 cells were treated with thioA, and wound closure was analyzed in an IncuCyte® S3 system over 48 h (right panel). Representative pictures are shown (left panel). Statistical analysis was performed for the last acquired time point using one-way ANOVA followed by Bonferroni's post-hoc analysis; n=3 (quadruplicates).

3.1.2.6 Thioholgamide A inhibits OXPHOS-dependent ATP production in macrophages

Our data showed effective anti-tumor actions of thioA by affecting tumor cell metabolism. With the importance of macrophages in tumor progression, we analyzed the effects of thioA on the bioenergetic profile of *in vitro* differentiated and polarized human monocyte-derived macrophages (HMDMs). We investigated five different polarization states of macrophages. Macrophages were generated by either polarizing them in the presence of the M2 cytokines IL4 (M2(IL4)) or IL10 (M2(IL10)) or in the presence of tumor-cell conditioned medium (TAM-like). As a comparison, M0 and classically activated M1 macrophages (LPS/IFNγ) were investigated.

On a basal level, M2(IL10) and TAM-like macrophages showed the lowest OCR in Seahorse measurements, while M2(IL4) macrophages had the highest consumption of oxygen (**Figure 19 A, E**). A similar pattern was observed for the subsets in terms of spare respiratory capacity (SRC, **Figure 19 G**), considered as an indicator of how efficiently cells can adapt to changing energy demands (Divakaruni et al., 2014). The extracellular acidification rate as an indirect measurement of glycolysis revealed the highest basal levels in M1 and M2(IL4) macrophages (**Figure 19 C, F**). ThioA injection reduced OXPHOS-dependent ATP production (**Figure 19 B**). In comparison to oligomycin, this effect was achieved more slowly, leading to higher minimal OCR values after injection (**Figure 19 H**). Due to donor-specific differences in the bioenergetic profile of *in vitro* polarized macrophage subsets, individual graphs are shown in **Figure 20**.

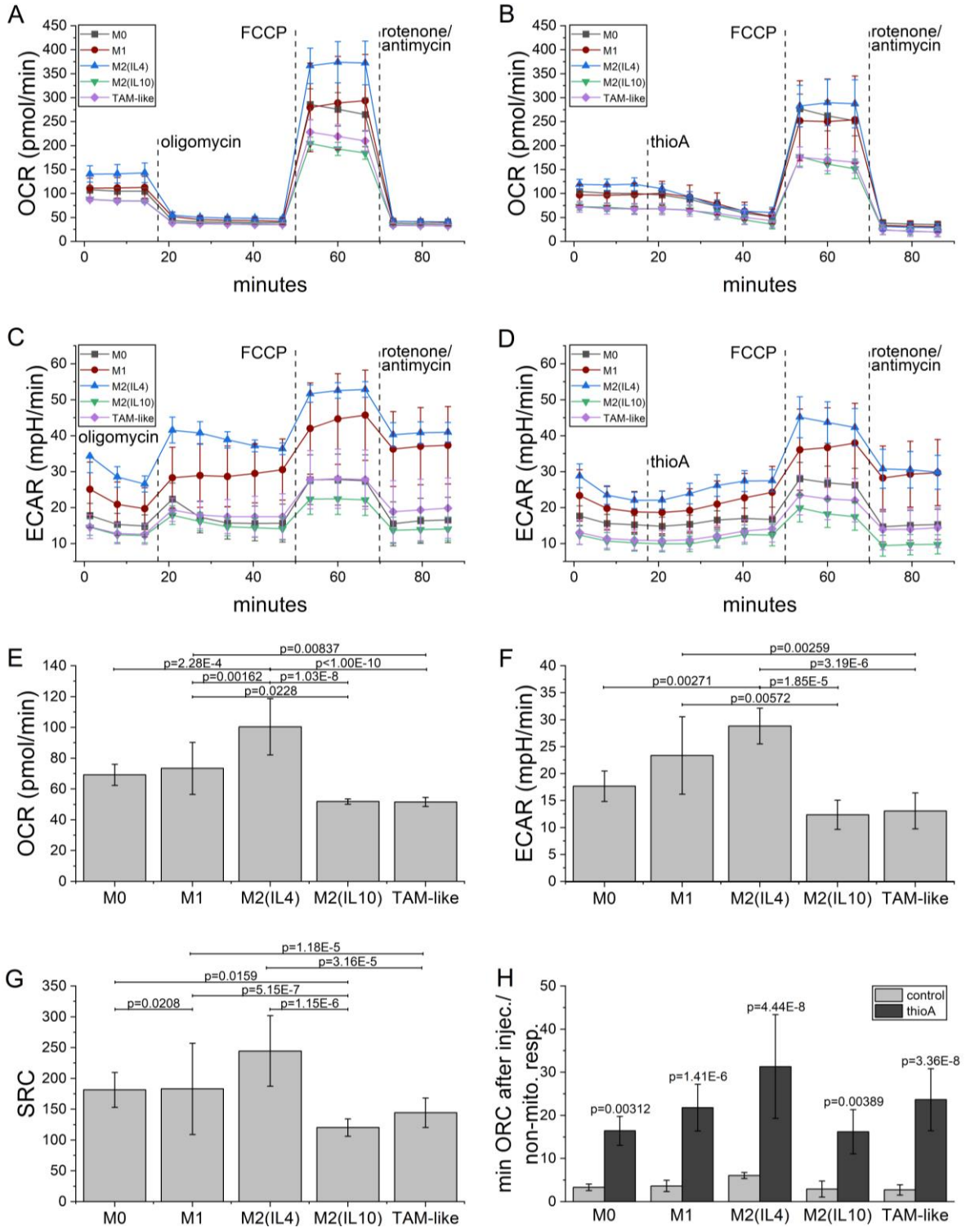

Figure 19. ThioA affects the metabolism of *in vitro* differentiated and polarized macrophages. HMDMs were polarized into M0, M1, M2(IL4), M2(IL10), and TAM-like macrophages for 24 h. OCR and ECAR were measured in a mito stress test using a Seahorse 96XF instrument. Either (**A, C**) 1 µM oligomycin was injected to shut down OXPHOS-dependent ATP production, or (**B, D**) 1 µM thioA was injected instead. (**E**) Basal OCR, (**F**) ECAR, and (**G**) SRC were analyzed for the different macrophage subsets in the oligomycin injected setup. (**H**) Minimal OCR values at the measurement point 5 (47 min) after respective oligomycin or thioA injection were normalized to the non-mitochondrial respiration (last time point after rotenone/antimycin injection). Statistical analysis was performed using one-way ANOVA followed by Tukey´s post-hoc analysis; n=3 (quadruplicates).

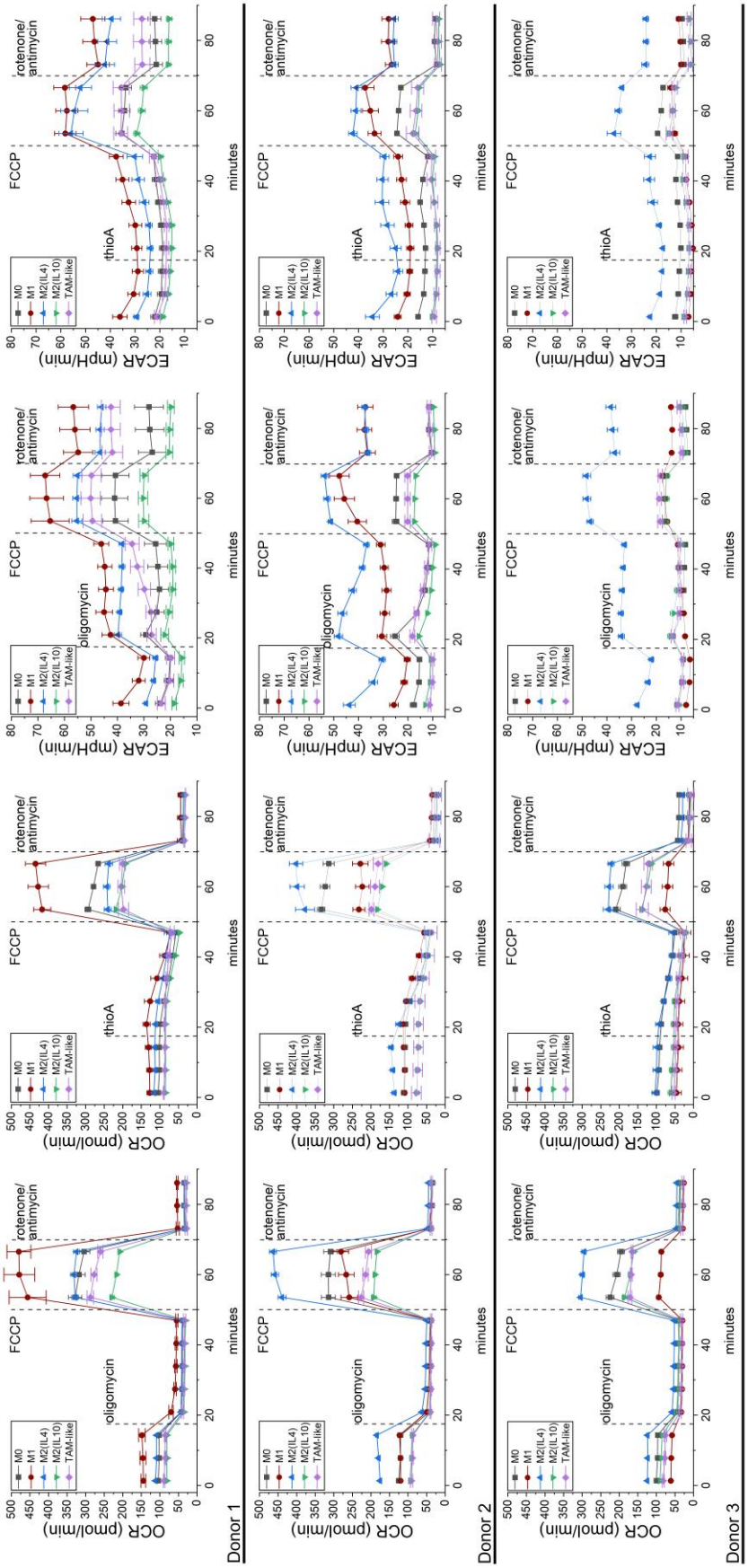

Figure 20. Donor-specific differences in metabolism of *in vitro* differentiated and polarized HMDMs. Continued.

Figure 20 continued. HMDMs were polarized into M0, M1, M2(IL4), M2(IL10), and TAM-like macrophages for 24 h. OCR and ECAR were measured in a mito stress test using a Seahorse 96XF instrument. 1 µM oligomycin was injected to shut down OXPHOS-dependent ATP production or 1 µM thioA was injected instead. Values are shown for three individual donors. n=3 (quadruplicates).

3.1.2.7 Thioholgamide A alters the macrophage phenotype

Macrophage phenotypes are linked to their metabolic features. Due to the distinct impact of thioA on macrophage metabolism, we hypothesized an effect on macrophage polarization. In order to determine sub-toxic thioA concentrations for polarized HMDMs, we stained the cells for caspase 3/7 activity and membrane permeability and monitored their viability over 3 days (**Figure 21**).

We chose the concentration of 50 nM for further experiments as it showed no toxic effects in all polarization states during the first 16 h treatment. Potential alterations in the macrophage phenotype were assessed regarding morphology, expression of marker genes, surface markers, as well as phagocytosis.

Macrophage polarization is characterized by distinct morphological features, as seen by a high proportion of elongated cells in M2 macrophages, and predominantly round cells in M1 macrophages. After thioA treatment, M2(IL10) macrophages showed a more M1-like morphology as they comprised a higher proportion of round cells (**Figure 22 A, B**).

Since morphological changes suggested that thioA treatment in sub-toxic concentrations skewed anti-inflammatory macrophages towards a less pronounced M2 phenotype, we analyzed gene expression of polarization markers. We found that thioA caused a reduction in the expression of the anti-inflammatory gene *IL10* in M2-macrophages, while the pro-inflammatory gene *IP10* was induced in M2(IL4) macrophages. The expression of *TNF* and *MMP9* showed no significant alterations (**Figure 22 C**).

Flow cytometry analyses revealed that the M2-associated surface marker CD163 was significantly downregulated in M2(IL10) macrophages by thioA. The expression of the M1 markers CD80 and HLA-DR remained unchanged (**Figure 22 D**).

For the evaluation of macrophage functional activity, the efficiency of phagocytosis was analyzed after thioA treatment by flow cytometry. In this setup, M0 and M2(IL10) macrophages exhibited the highest phagocytic capacity. ThioA decreased phagocytosis in M0, M2(IL4), and TAM-like macrophages (**Figure 22 E**).

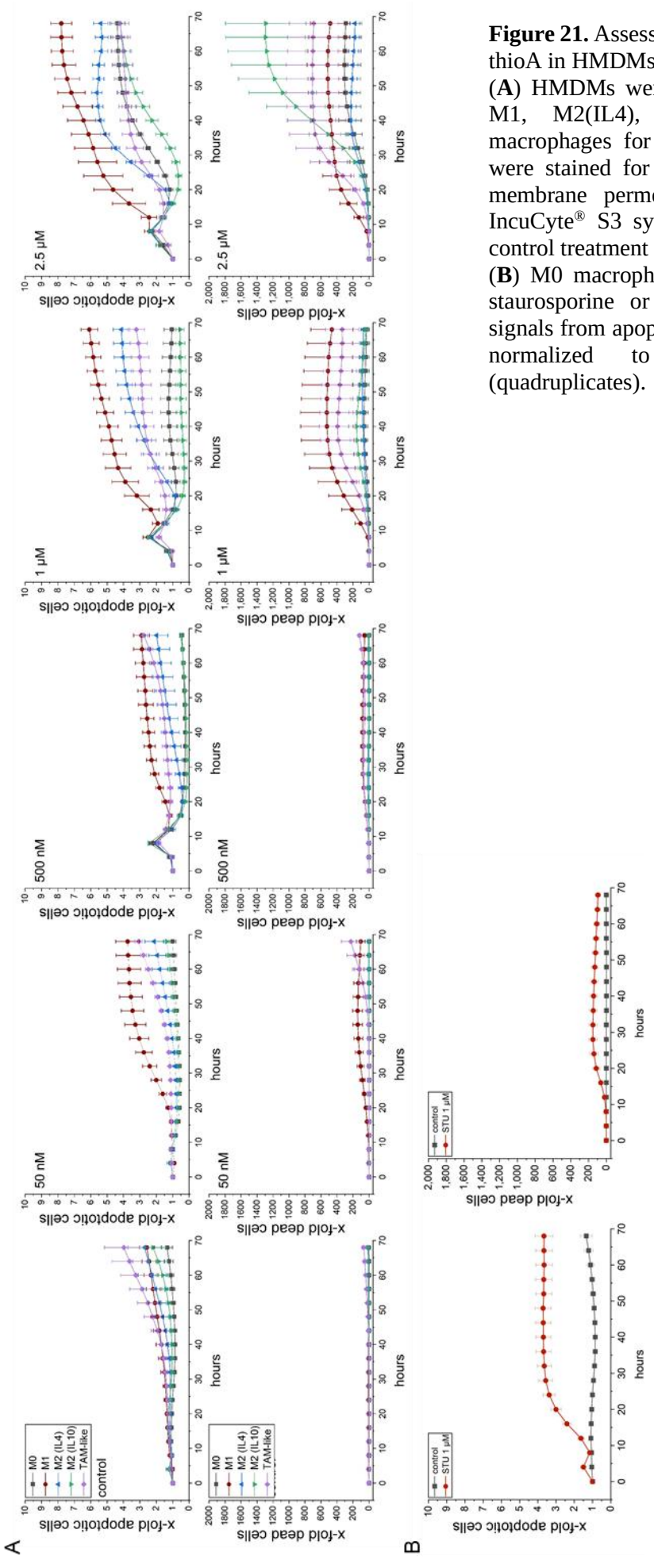

Figure 21. Assessment of toxic concentrations of thioA in HMDMs.
(**A**) HMDMs were polarized *in vitro* into M0, M1, M2(IL4), M2(IL10), and TAM-like macrophages for 24 h. Polarized macrophages were stained for caspase 3/7 activity and cell membrane permeability and analyzed in an IncuCyte® S3 system during thioA or vehicle control treatment for 68 h.
(**B**) M0 macrophages were treated with 1 µM staurosporine or vehicle control. Fluorescent signals from apoptotic and permeable cells were normalized to cell confluency; n=3 (quadruplicates).

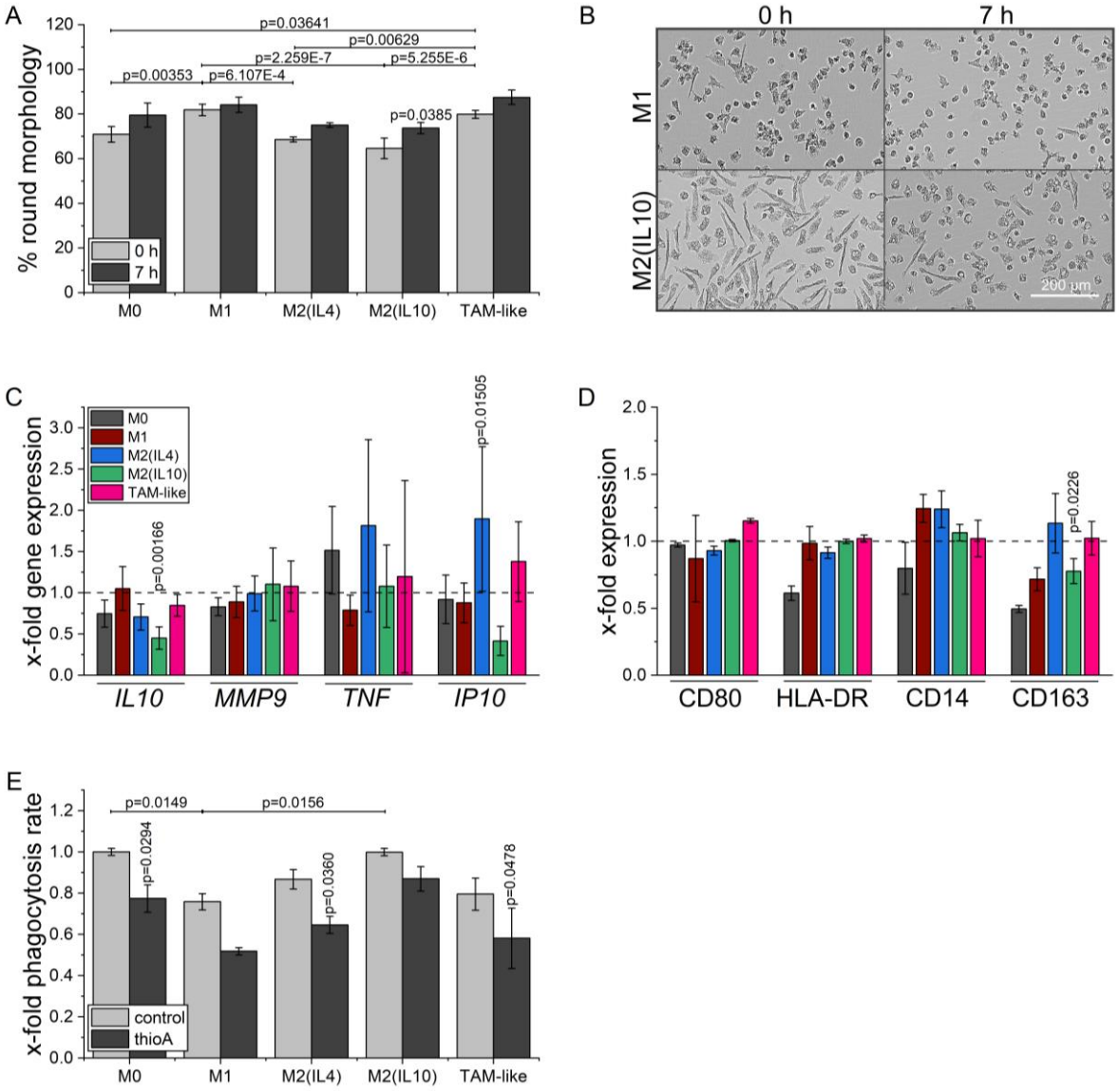

Figure 22. ThioA reduces M2 polarization markers.
(**A**) HMDMs were differentiated and polarized *in vitro* into M0, M1, M2(IL4), M2(IL10), and TAM-like macrophages for 24 h, followed by 50 nM thioA treatment. Cells were imaged at the beginning and at the end of 7 h treatment using automated microscopy. Cells were grouped based on their eccentricity in an elongated or round phenotype by the IncuCyte cell by cell analysis software; n=3 (quadruplicates).
(**B**) Representative pictures of M1 and M2(IL10) macrophages are shown.
(**C**) Macrophages polarized for 21 h were treated with 50 nM thioA for 7h. Gene expression of *IL10*, *MMP9*, *TNF*, and *IP10* were measured after treatment by qPCR. Expression values were normalized to *18S* as a housekeeping gene, followed by normalization to vehicle control-treated cells of the respective polarization state; n=3 (triplicates).
(**D**) Surface marker expression of M1-associated CD80 and HLA-DR, and M2-associated CD14 and CD163 was analyzed by flow cytometry after a 7 h treatment of macrophages polarized for 21 h. Expression values were normalized to vehicle control-treated cells of the respective polarization state; n=2 (duplicates).
(**E**) Macrophages polarized for 24 h were treated with thioA (1 µM) for 30 min, followed by incubation with fluorescent latex beads for 15 min. The proportion of macrophages that engulfed beads was quantified by flow cytometry. Bead-positive macrophages were normalized to M0 cells of the respective donor; n=3 (duplicates).
Statistical analysis was performed using one-way ANOVA followed by Tukey´s post-hoc analysis.

3.1.3 Discussion

The group of RiPPs has attracted increased attention in recent years due to the description of a range of biological activities against bacteria, fungi, and cancer cells. Following the initial observation of apoptosis induction by thioviramide in 3Y1 cancer cells (Hayakawa et al., 2006), further anti-cancer actions were described for the thioviridamide-like compounds prethioviridamide (Takase et al., 2019) and thioalbamide (Frattaruolo et al., 2019) *in vitro*. We are the first to provide a comprehensive biological profile of the thioviridamide-like RiPP thioA, using 2D- and 3D-cell culture models. To the best of our knowledge, this is the first study describing *in vivo* anti-tumor activities of a RiPP group member. Most importantly, this study addresses the critical role of thioA on the tumor microenvironment by investigating its effects on the polarization of macrophages as crucial players in the tumor microenvironment.

Using time-resolving automated microscopy approaches, we identified thioA as a potent anti-proliferative agent with IC_{50} values in the low nanomolar range. The anti-proliferative activity was confirmed in an *in vivo* zebrafish embryo model. The xenotransplantation of human cancer cells into zebrafish embryos extends the scope of early pre-clinical drug testing and offers new opportunities, such as real-time visualization of tumor growth and investigation of new compounds, from which only minor amounts are available (Veinotte et al., 2014; Yan et al., 2019). In this *in vivo* model, thioA effectively inhibited tumor growth without showing toxic effects on the embryo. The low toxic activity of thioA was further confirmed in human non-tumorigenic cells.

Treatment with concentrations even lower than those inhibiting proliferation resulted in reduced cell migration as another important hallmark of cancer. Another well-known hallmark of cancer is a metabolic reprogramming associated with increased glycolysis to sustain proliferation even in the presence of enough oxygen supply (Vander Heiden and DeBerardinis, 2017; Vander Heiden et al., 2009). Even though many cancers preferentially use glycolysis for energy production, the inhibition of OXPHOS, the suggested mechanism of action for thioA, could serve as an attractive anti-cancer target. In fact, different cancer subsets (Tan et al., 2019) and chemoresistant tumor cells (Matassa et al., 2016) showed an increased OXPHOS dependency. To investigate the anti-cancer potential of other OXPHOS inhibitors, they are currently under study *in vitro* and *in vivo* (Ashton et al., 2018).

While thioA acts in nanomolar concentrations on different hallmarks of cancer, distinctly higher concentrations are required to actually induce cell death in cancer cells. Takase et al. identified

the ATP synthase as a target of the derivative prethioviramide, causing the initiation of the ISR (Takase et al., 2019). The ISR functions primarily as a pro-survival response setting cells in a resting state to handle stress situations, such as amino acid deprivation or ER stress. If homeostasis cannot be restored, apoptotic pathways are finally entered (Pakos-zebrucka et al., 2016).

Our data show that thioA affected mitochondrial morphology and reduced the OCR of treated cells in a dose-dependent fashion to a similar extent as the ATP synthase inhibitor oligomycin. Moreover, a toxic thioA concentration caused an induction on mRNA level of the ISR-associated transcription factor *ATF4* and its downstream target *CHOP*, which is an important pro-apoptotic mediator (Quirós et al., 2017). This finding suggests the ATP synthase as a shared target for the derivatives prethioviramide (Takase et al., 2019) and thioA. The subsequent ISR initiation would explain the mainly anti-proliferative action of thioA, as cells first enter a resting state before they undergo apoptosis. Interestingly, Takase et al. (2019) did not investigate whether prethioviramide in fact induced cell death but reported effects on cell viability in a metabolic assay similar to the MTT assay we employed.

In addition to the challenges in the development of potent anti-cancer therapies driven by the complexity of malignant cells themselves, the TME actively contributes to their efficiency. The TME is composed of tissue-resident and a large proportion of recruited immune cells, with macrophages playing a central regulatory role (DeNardo and Ruffell, 2019). The beneficial effect of anti-cancer agents targeting both tumor cells and macrophages has been shown for the natural compound trabectedin. The compound originally isolated from *Ecteinascidia turbinata* was initially approved as an anti-proliferative drug for the treatment of advanced soft tissue sarcoma (Carter and Keam, 2007). The drug later demonstrated to reduce the number of tumor-infiltrating macrophages (Germano et al., 2013). This supplementary property substantially contributes to the activity of this clinically useful anti-cancer agent. Besides TAM depletion and inhibition of recruitment, a reprogramming of TAMs represents a promising approach [6]. Shifting TAM polarization from a tumor-supporting (M2) towards an actively tumor-rejecting (M1) phenotype would rebalance the TME and effectively support anti-tumor strategies. In this context, we focused the biological profiling of thioA not only on tumor cells but also investigated its effect on the polarization, viability, and activity of different macrophage subsets. The paradigm of a rather clear cut between M2 macrophages supporting cancer and M1 macrophages antagonizing cancer has been challenged by recent sequencing studies of immune cells from the TME, and TAMs exhibited some characteristics of both M1 and M2

polarization depending on localization and tumor stage (Azizi et al., 2018; Müller et al., 2017). In fact, TAM-like macrophages displayed an intermediate phenotype regarding, e.g., morphology and phagocytosis in our study.

As demonstrated in tumor cells, thioA inhibited OXPHOS-dependent ATP production also in macrophages. The link between macrophage metabolism and their phenotypes has become a highly studied focus of research in recent years. It has been shown that inflammatory M1 macrophages have an enhanced glycolytic metabolism to fulfill their energy demands, while anti-inflammatory macrophages mainly rely on OXPHOS (Van den Bossche et al., 2017; Vitale et al., 2019). Our bioenergetic data of *in vitro* polarized HMDMs revealed an overall quiescent profile for M0, M2(IL10), and TAM-like macrophages, as indicated by low basal OCR and ECAR values. M1, as well as M2(IL4) macrophages, showed higher metabolic activities, even though macrophages from different donors responded to varying degrees to the respective polarization stimuli. The slower OCR reduction caused by thioA compared to oligomycin might be caused by a lower cell penetration or target binding affinity.

Macrophage subtypes also differed in their SRC, which is defined as the difference between the basal and the maximal respiration. As many cells operate at a basal level that only requires a part of their total metabolic capacity, the SRC provides information on how the cell can deal with changing energy demands and withstand periods of stress (Divakaruni et al., 2014). The low SRC of M2(IL10) and TAM-like macrophages implies an increased sensitivity of these cells towards an OXPHOS inhibition. The fact that these cells also show just a small degree of subsequent glycolysis increase after thioA or oligomycin injection leads to the conclusion that M2(IL10) and TAM-like macrophages might have a specific reaction in response to the inhibition of OXPHOS.

To test the implications of thioA-mediated modulation of macrophage metabolism on polarization state, we used a thioA concentration that mainly inhibited tumor cell proliferation without showing distinct cytotoxic activities against either tumor cells or macrophages during the observed treatment periods. Overall, this low concentration of 50 nM, thioA weakened the extent of M2 polarization. ThioA reduced the anti-inflammatory polarization marker *IL10* (Zeni et al., 2007; Zhao et al., 2015) on gene expression level in M2 macrophages and increased the pro-inflammatory *IP10* (Cao et al., 2017) in M2(IL4) and TAM-like macrophages. The expression of the M2-associated surface marker CD163 (Yang et al., 2019; Ye et al., 2019) was also reduced after treatment in M2(IL10) macrophages. Moreover, morphology was skewed

towards an M1-like phenotype during treatment, which has also been described after oligomycin treatment of mouse macrophages (Chen et al., 2018).

Tumors are often referred to as “wounds that never heal”. In this context, apoptotic cells inside the tumor can polarize macrophages into an M2 status, which in turn try to maintain tissue homeostasis by engulfing cell debris, promoting tissue repair, and resolving inflammatory reactions (Dehne et al., 2017; Murray and Wynn, 2011; Weigert et al., 2016). Hence, this phenotype comprises a high efficiency in the phagocytosis of apoptotic cells (Rey-Giraud et al., 2012; Schaper et al., 2016; Xu et al., 2006), while inflammatory and microbicidal M1 macrophages excrete a preferential engulfment of bacteria (Krysko et al., 2011; Varin et al., 2010). In this study, M2 macrophages exhibited a higher phagocytic activity compared to M1 macrophages, which was reduced after thioA treatment in all phenotypes. The inhibition of phagocytosis after OXPHOS inhibition was described before for neutrophils (Li et al., 2019).

In conclusion, thioA exhibits an interesting biological profile for new tumor therapeutic strategies. As a metabolic regulator, it can play a pivotal role in orchestrating different hallmarks of cancer in cancer cells and macrophages. In combination with its low toxicity in non-tumorigenic cells and *in vivo*, thioA represents an interesting candidate for further preclinical testing.

Results presented in this chapter have been published in:

Charlotte Dahlem, Wei X. Siow, Maria Lopatniuk, William K.F. Tse, Sonja M Kessler, Susanne H. Kirsch, Jessica Hoppstädter, Angelika M. Vollmar, Rolf Müller, Andriy Luzhetskyy, and Alexandra K. Kiemer. 2020. “Thioholgamide A, a new anti-proliferative anti-tumor agent, modulates macrophage polarization and metabolism.” *Cancers* 12 (5): E1288. https://doi.org/https://doi.org/10.3390/cancers12051288.

3.2 **Chapter 2.** Anti-tumor activity of thioholgamide A derivatives

3.2.1 Introduction

Due to its peptide structure, the natural compound thioA offers many possibilities of structural modifications. The group of Andriy Luzhetskyy (Pharmaceutical Biotechnology, Saarland University) conducted thioA derivatization in *Streptomyces* hosts (unpublished data). Their approaches provided many thioA derivatives, of which two derivatives were tested in this study for their biological activity. **Figure 23** demonstrates the structural changes of the derivatives thioA2 and thioA3 in comparison to thioA.

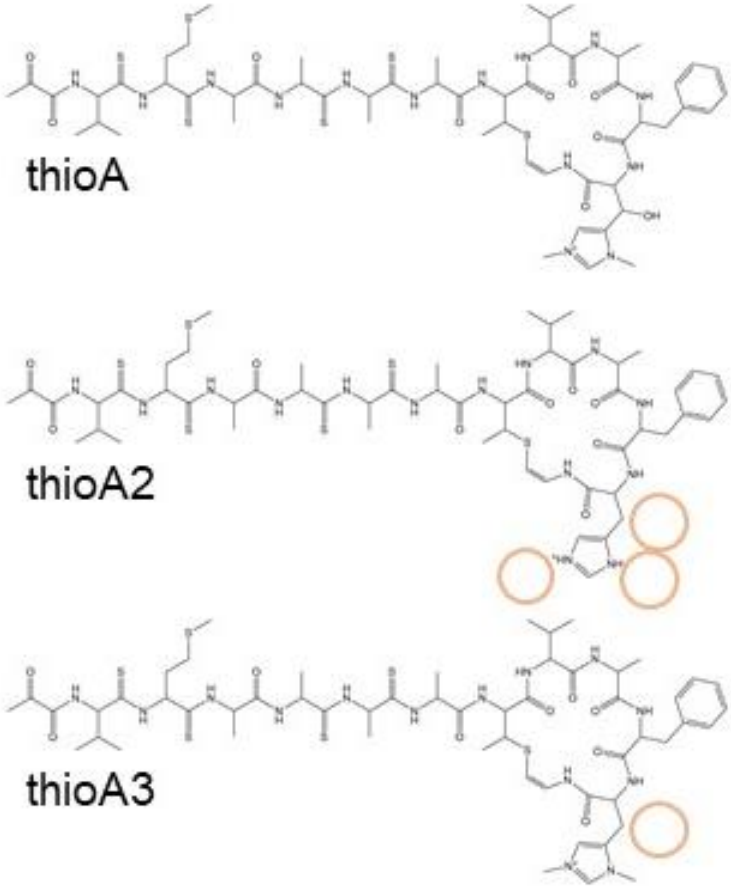

Figure 23. Structures of the thioA derivatives thioA2 and thioA3.

3.2.2 Results

The two thioA derivatives thioA2 and thioA3 were tested for their biological activity in human cancer cell lines. Measuring the metabolic activity of treated cells by an MTT assay, structural changes resulted in a decreased activity (**Figure 24**, IC_{50} values in **Table 4**) compared to thioA. The more substantial structural changes in thioA2 caused the lowest activity in HCT116 and Huh7.5 cells (**Figure 24 A, B**). Moreover, its activity was abolished entirely in A549 cells up to 20 µM (**Figure 24 C**). Structural modifications did not affect the activity in the 3D HCT116 spheroid model (**Figure 24 D**).

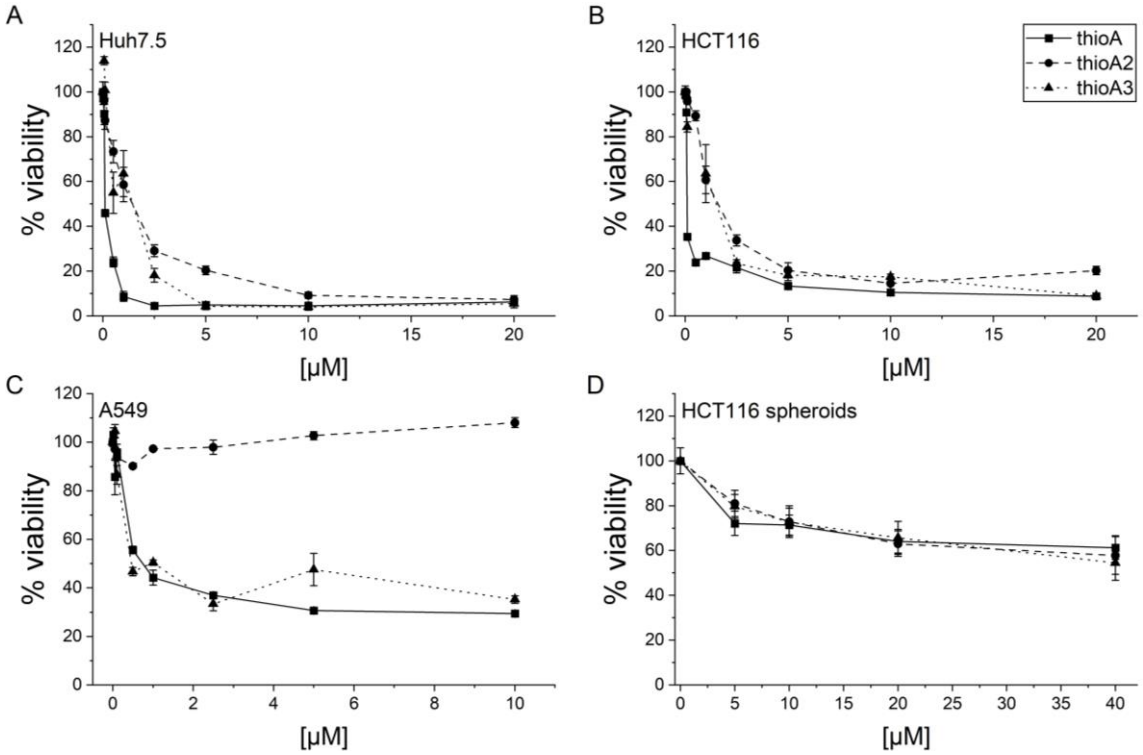

Figure 24. Effects of thioA and its derivatives on tumor cell viability.
(**A-C**) A set of tumor cell lines was treated with increasing concentrations of thioA and its derivatives thioA2, and thioA3. Cell viability was determined after 48 h treatment in an MTT assay.
(**D**) 3-day old HCT116 spheroids were treated with thioA, thioA2, or thioA3 for 48 h, followed by an APH assay to assess viability.
Vehicle control-treated cells were used for data normalization; n=3 (triplicates).

Table 4. MTT-based IC_{50} [µM] values of thioA and its derivatives.
Activity against a panel of tumor cell lines was measured in an MTT assay after 48 h treatment.

cell line	*thioA*	*thioA2*	*thioA3*
Huh7.5	0.141	1.243	0.961
HCT116	0.176	1.698	1.206
A549	1.158	> 20	1.514

The selectivity of anti-cancer agents towards degenerated cells is of utmost importance in preclinical drug development. Therefore, we employed a model of differentiated Huh7.5 cells to test the selectivity of thioA and its derivatives. Long-time culturing of hepatocellular carcinoma Huh7.5 cells in media supplemented with 2% human serum differentiates the hepatoma cells into a more normal hepatocyte-like phenotype (El-Shamy et al., 2015). Differentiated cells were described to display alterations in morphology from a spindle-shaped to a cobble-stone phenotype, which is associated with a switch from unrestrained growth to contact inhibition and induction of hepatocyte-specific genes. We monitored cell morphology microscopically during differentiation and observed the typical cobble-stone shape after 3 weeks cultivation (**Figure 25 A**). ThioA demonstrated a significant selectivity for undifferentiated tumor cells (**Figure 25 B**). This selectivity towards undifferentiated cells was even more pronounced in thioA2-treated cells (**Figure 25 C**). ThioA3 showed no preferential activity against undifferentiated cancer cells (**Figure 25 D**).

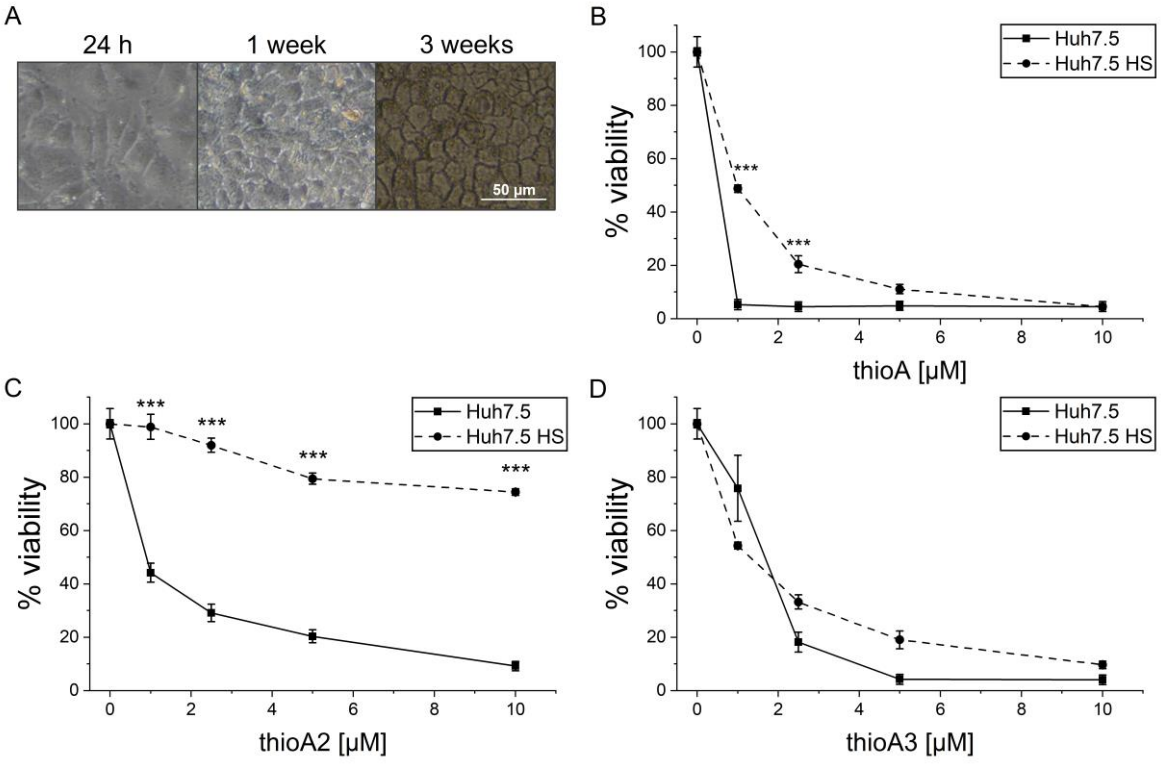

Figure 25. Selectivity of thioA and its derivatives towards proliferating non-differentiated tumor cells. Huh7.5 cells were differentiated in media supplemented with 2% human serum (HS) for 3 weeks.
(**A**) Cell morphology was monitored microscopically 24 h, 1 week, and 3 weeks after medium change. (**B-D**) Differentiated and non-differentiated cells were treated with increasing concentrations of (**B**) thioA and its derivatives (**C**) thioA2, and (**D**) thioA3. Cell viability was determined after 48 h treatment in an MTT assay.
Vehicle control-treated cells were used for data normalization; n=3 (triplicates).

Also in non-tumorigenic HUVEC, thioA and its derivatives demonstrated only a moderate activity, while thioA2 reduced cell viability to the lowest extent (**Figure 26**).

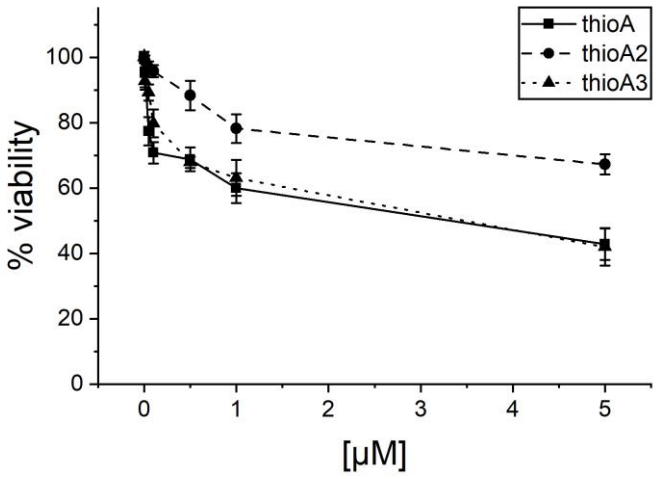

Figure 26. Effects of thioA and its derivatives on HUVEC viability.
HUVECs were treated with increasing concentrations of thioA, thioA2, or thioA3 respectively, and cell viability was determined after 48 h treatment in an MTT assay. Vehicle control-treated cells were used for data normalization; n=3 (quadruplicates).

3.2.3 Discussion

The natural compound thioholgamide A exhibits a striking biological profile against different hallmarks of cancer (see part I, chapter 1). We hypothesized that structural modifications could improve its pharmacokinetics and increase its efficiency, e.g., by a stronger target binding or better cell penetration. However, none of the two tested derivatives demonstrated a superior activity compared to thioA.

In her master thesis, Julia Wildfeuer produced further diverse thioA derivatives, introducing structural changes in two “tail” positions Val2, Met3, and the ring position Ala10. None of the derivatives exceeded the activity of the mother compound in MTT assays. The introduction of the polar amino acid asparagine at position 2 and 3 (Val2Asn, Met3Asn) demolished activity. The ring position 10 was even more sensitive for structural changes, as the introduction of glycine, tyrosine and histidine (Ala10Gly, Ala10Thr, Ala10His) reduced activity significantly. These findings are in line with the hypothesis that the tail of thioA is needed for cell membrane penetration, while the ring exerts the interaction with the target.

The derivatives tested in this study, possessed structural changes in the position 12 (histidine) in the thioA ring. They showed a comparable activity in Huh7 and HCT116 cells, while thioA2 lost its activity in A549 and non-tumorigenic cells. This interesting finding in combination with the activity studies of Julia Wildfeuer should be addressed in future studies.

Moreover, a high target specificity could reduce potential adverse off-target effects of the compound. Nonetheless, the evaluation of such parameters would require the final target identification of thioA. This result would be needed to confirm the direct inhibition of the ATP synthase by thioA and to answer the question if this inhibition is the direct link to all aspects of the subsequent biological profile of the compound or if thioA might have more than one target.

3.3 **Chapter 3.** Anti-tumor profiling of new natural compounds

Auratryptanon

3.3.1 Introduction

Myxobacteria belong to the group of Gram-negative eubacteria (Reichenbach, 1999), and are among the top producers of new and unique natural products. Due to their rich secondary metabolism, myxobacteria serve as an attractive source for lead structures in drug discovery. More than 100 core structures and even more derivatives, exhibiting unusual modes of action, have been described (Weissman and Müller, 2010).

Natural products from myxobacteria demonstrated to target cellular structures that are rarely targeted by secondary metabolites from other producers. For instance, several compounds showed to inhibit electron transport, interact with the cytoskeleton, or inhibit vacuolar ATPases (V-ATPases) in mammalian cells (Huss and Wieczorek, 2009; Kingston, 2009; Reichenbach, 2001; Sasse et al., 1999; Weissman and Müller, 2010).

The natural product auratryptanon was found in the extract of *Stigmatella aurantiaca Sga32* during a screening for novel anti-infectives. The tryptophan-based compound demonstrated to be highly active against several Gram-negative strains, e.g., *Staphylococcus aureus*, *Streptococcus pneumoniae, Staphylococcus* spp., and *Micrococcus luteus* (unpublished data). Its structure is demonstrated in **Figure 27**.

In this study, we aimed to characterize the biological activity of auratryptanon in cancer cells and macrophages as important players in the TME.

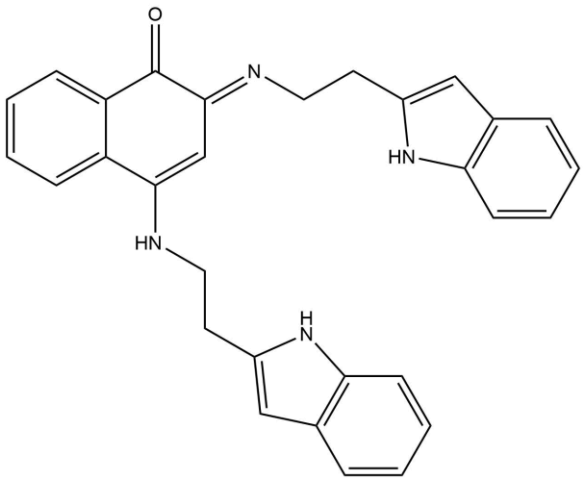

Figure 27. Structure of auratryptanon.

3.3.2 Results

Auratryptanon was first tested for its effects on the viability of human cancer cell lines (**Figure 28 A, B**) *via* MTT assays and showed IC_{50} values in the nano to low micromolar range (**Table 5**). Also in a 3D model, auratryptanon reduced the viability of HCT116 cells growing in spheroids (**Figure 28 C**).

In comparison to the widely used chemotherapeutic agent doxorubicin, auratryptanon demonstrated a more potent activity in Huh7 cells. Moreover, auratryptanon efficiently reduced the viability of doxorubicin-resistant Huh7 cells (**Figure 28 D**).

Interestingly, the activity of auratryptanon was abolished completely in Huh7.5 cells that were differentiated for 3 weeks in human serum. These cells feature a growth arrest and a more normal phenotype and metabolism (**Figure 28 E,** see also **3.3.2**).

Table 5. MTT-based IC_{50} [µM] values of auratryptanon.
Activity against a panel of tumor cell lines was measured in an MTT assay after 48 h treatment.

cell line	*IC_{50}*
Huh7.5	1.18
HCT116	3.35
A549	1.53
MCF7	1.51
SkMel5	0.58
SW620	1.08
HeLa	1.72
CCSW	1.85

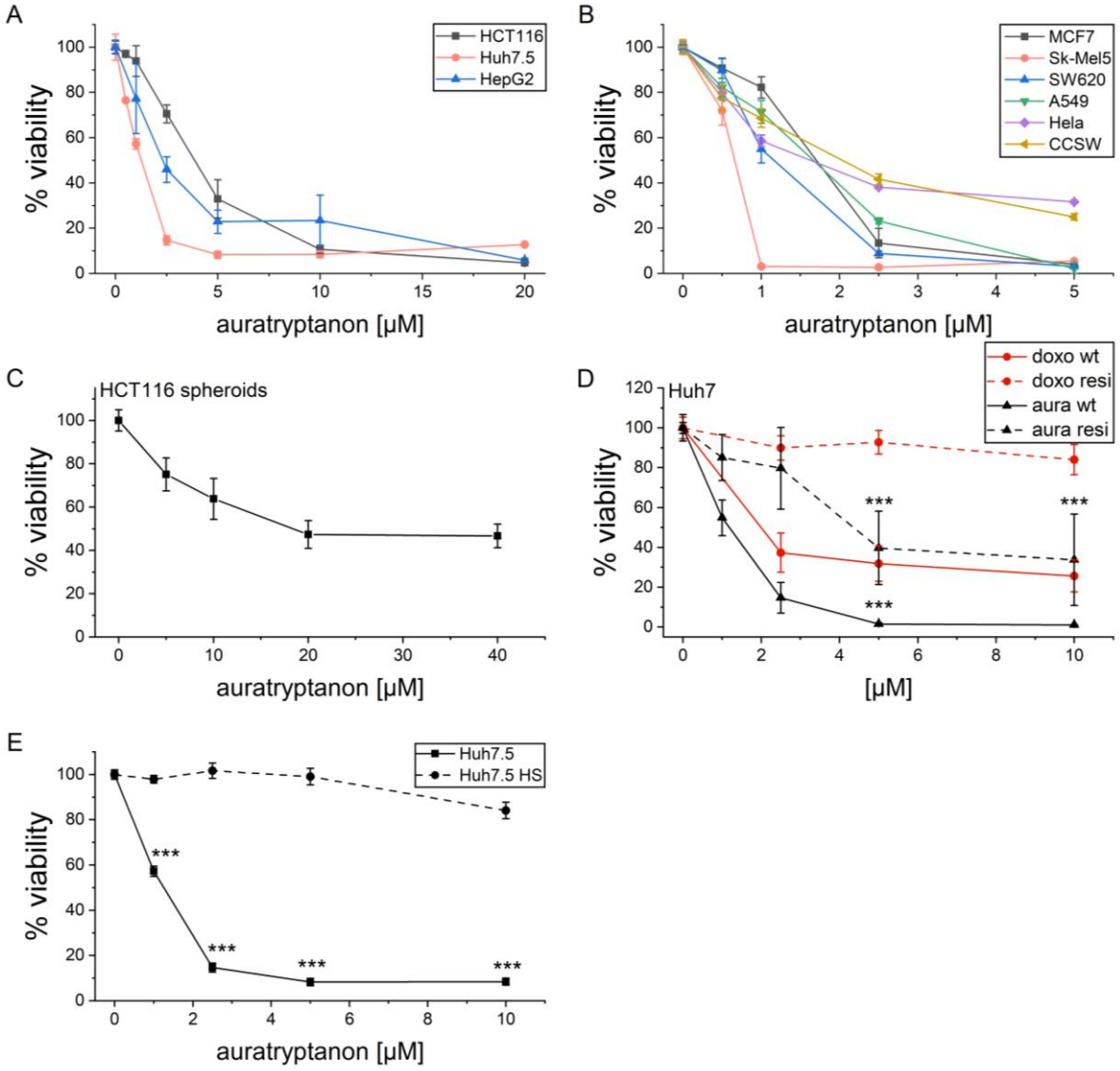

Figure 28. Effects of auratryptanon on tumor cell viability in different *in vitro* models.
A set of tumor cell lines was treated with increasing concentrations of auratryptanon or vehicle control. (**A, B**) Cell viability was determined after 48 h treatment in an MTT assay (**A**: n=3 (quadruplicates); **B**: n=2 (sextuplicates)).
(**C**) 3-day old HCT116 spheroids were treated with auratryptanon or vehicle control for 48 h, followed by an APH assay to assess viability; n=3 (quadruplicates).
(**D**) Huh7 wildtype (wt) and doxorubicin-resistant Huh7 (resi) cells were treated with increasing concentrations of auratryptanon or doxorubicin, and cell viability was determined after 48 h treatment in an MTT assay. Statistical analysis compared auratryptanon treatment *vs*. doxorubicin treatment in wildtype and resistant cells, respectively; n=3 (triplicates).
(**E**) Huh7.5 cells were differentiated in media supplemented with 2% human serum (HS) for 3 weeks. Differentiated and non-differentiated cells were treated with increasing concentrations of auratryptanon. Cell viability was determined after 48 h treatment in an MTT assay. Statistical analysis compared cell viability at the individual concentrations; n=3 (quadruplicates).
Statistical analysis was performed using one-way ANOVA followed by Bonferroni's post-hoc analysis, $p < 0.001$ (***).

As auratryptanon lost its activity in growth-arrested Huh7.5 cells, we hypothesized that it might have anti-proliferative actions. Hence, we tested the effects of auratryptanon on tumor cell proliferation using different 2D and 3D models (**Figure 29**). Concentrations similar to their MTT-based IC_{50}s inhibited the proliferation of A549 (**Figure 29 A**) and HCT116 cells (**Figure 29 B**) as assessed by automated microscopy and electric cell impedance sensing. Moreover, the concentration of 20 µM auratryptanon, which resulted in 50% reduced viability of tumor spheroids, caused a growth arrest of 3D HCT116 tumor spheroids (**Figure 29 C**).

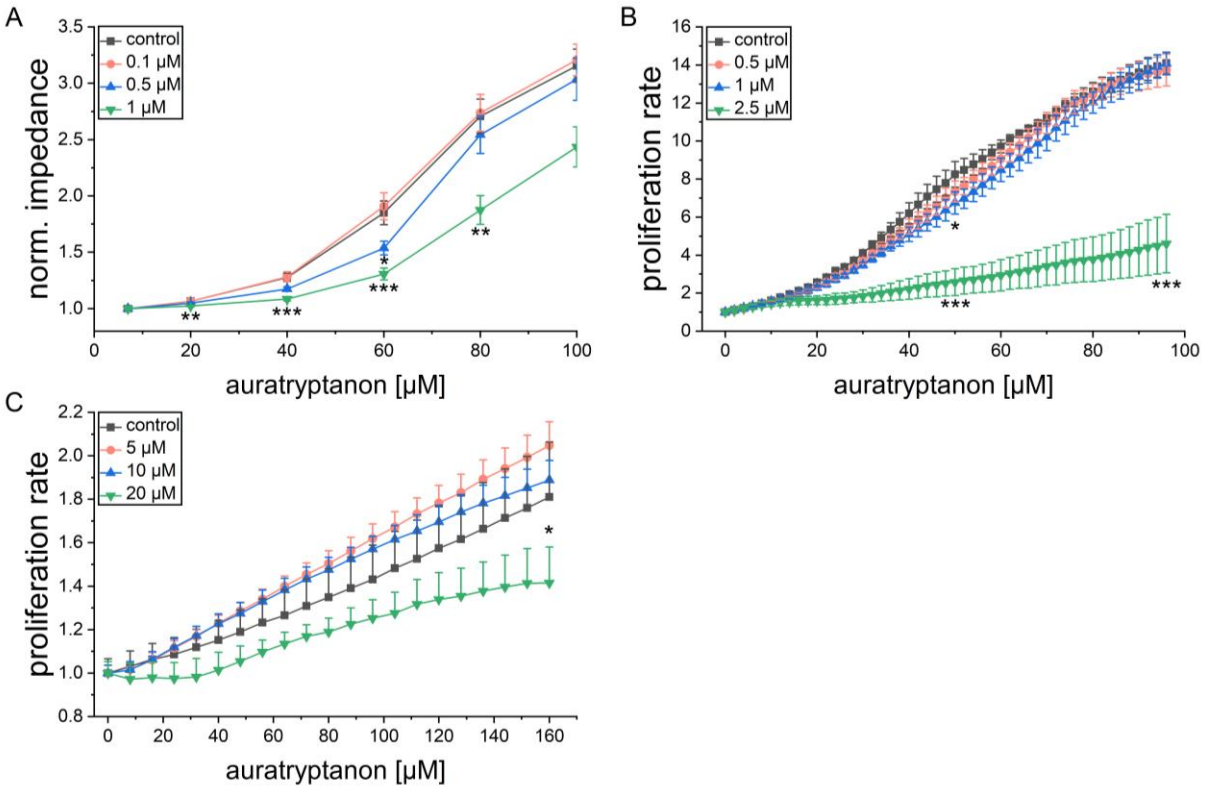

Figure 29. Effects of auratryptanon on tumor cell proliferation.
Cell proliferation was measured kinetically in different tumor cell lines treated with increasing concentrations of auratryptanon or vehicle control.
(**A**) Proliferation of treated A549 cells was measured using the electric cell-substrate impedance sensing (ECIS®) system. Cells were treated 5 h after seeding, and impedance was normalized to the value at 7 h after seeding; n=3 (quadruplicates).
(**B**) HCT116 cell proliferation was monitored in an IncuCyte® S3 system after auratryptanon or vehicle control treatment. Cell confluency was normalized to time point 0 h; n=2 (quadruplicates).
(**C**) 3-day old HCT116 tumor spheroids were treated with auratryptanon or vehicle control, and the spheroid area was analyzed by automated microscopy in an IncuCyte® S3 system; n=2 (quadruplicates).
Statistical analysis was performed for the indicated time points using one-way ANOVA followed by Bonferroni's post-hoc analysis, * $p < 0.05$, ** $p < 0.01$ ***, $p < 0.001$.

In order to test whether auratryptanon affects other hallmarks of cancer, we evaluated the metastatic capacity of tumor cells as modeled by cell migration in a scratch wound assay. Auratryptanon showed no effects on the migration of HCT116 cells up to 2.5 µM treatment (**Figure 30**).

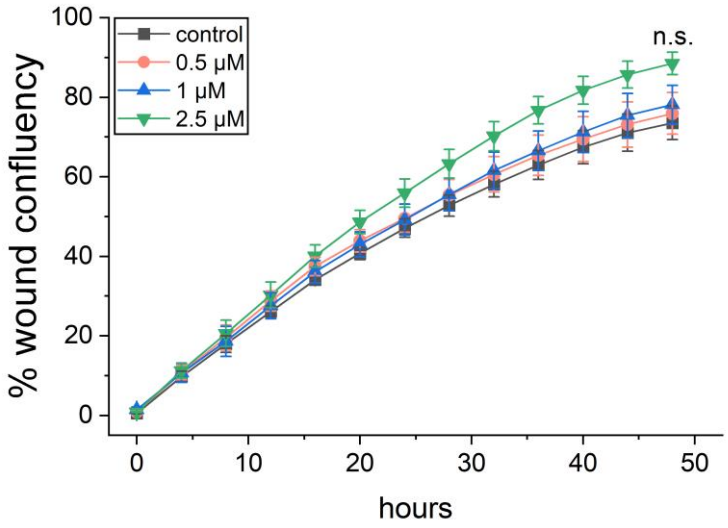

Figure 30. Effects of auratryptanon on tumor cell migration.
HCT116 cells were treated with thioA, and wound closure was analyzed in an IncuCyte® S3 system over 48 h. Statistical analysis was performed for the last acquired time point using one-way ANOVA followed by Bonferroni's post-hoc analysis; n=3 (quadruplicates).

Moreover, we measured the production of reactive oxygen species (ROS) in auratryptanon treated tumor cells. As assessed by HVA assay, treatment of 2.5 µM auratryptanon provoked an increased ROS production in A549 and Huh7.5 cells (**Figure 31**).

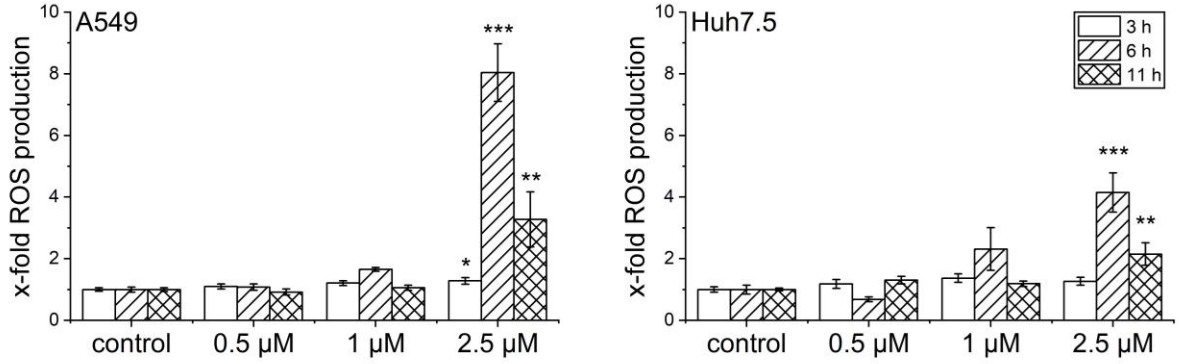

Figure 31. Effects of auratryptanon on ROS production of tumor cells.
A549 (left panel) and Huh7.5 (right panel) cells were treated with different concentrations of auratryptanon or vehicle control for the indicated time points. ROS production was assessed by HVA assays. Statistical analysis was performed for the indicated time points using one-way ANOVA followed by Bonferroni's post-hoc analysis, comparing auratryptanon-treated to control-treated cells, * $p < 0.05$, ** $p < 0.01$ ***, $p < 0.001$; n=3 (triplicates).

To test if auratryptanon exhibits selective effects on different macrophage subtypes, we differentiated and polarized HMDMs *in vitro* into M0, M1, M2(IL4), M2(IL10), and TAM-like macrophages and treated them for 48 h with the compound. Cell viability was assessed by MTT assays and demonstrated M1 macrophages to be the significantly most sensitive subtype towards the compound (p-values: **0.1 µM**: n.s., **0.5 µM** n.s.; **1 µM**: n.s.; **2.5 µM**: M1 to M2(IL4) p=0.0312, to M2(IL10) p=0.0015, to TAM-like p=2.255 x 10^{-6}; TAM-like to M0 p=0.0019; **5 µM**: M1 to M2(IL4) p=0.0241, to M2(IL10) p=9.052 x 10^{-7}, to TAM-like p<10^{-10}; TAM-like to M0 p=5.812 x 10^{-7}, to M2(IL4) p=8.451 x 10^{-4}; M0 to M2(IL10) p=0.0029). TAM-like macrophages were the least sensitive cells and showed 85% viability after 5 µM treatment for 48 h (**Figure 32**).

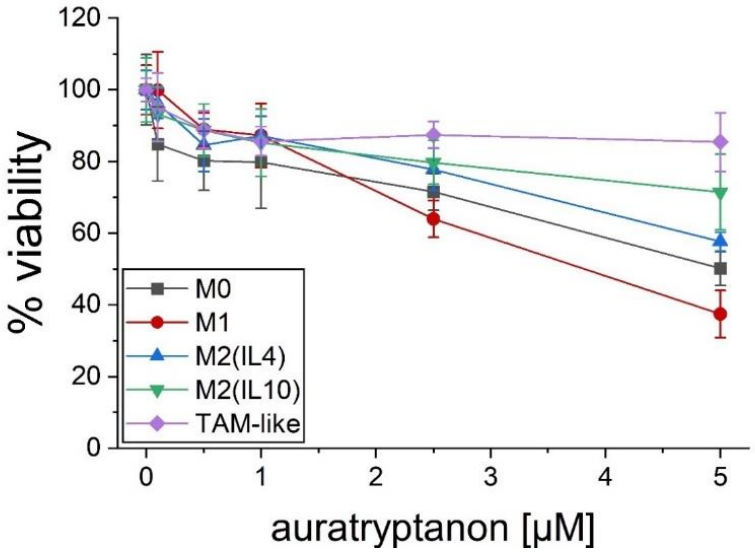

Figure 32. Effects of auratryptanon on the viability of different macrophage subsets.
HMDMs were differentiated and polarized *in vitro* into M0, M1, M2(IL4), M2(IL10), and TAM-like macrophages for 24 h. Polarized macrophages were treated with increasing concentrations of auratryptanon or vehicle control. Cell viability was determined after 48 h treatment in an MTT assay. Vehicle control-treated cells of the respective polarization status were used for data normalization. Statistical analysis was performed using one-way ANOVA followed by Tukey's post-hoc analysis; n=4 (triplicates).

3.3.3 Discussion

The newly identified bacterial natural product auratryptanon demonstrated a potent biological activity against human tumor cells from different tumor entities, which was superior to doxorubicin in Huh7 cells. The viability-reducing effect was not associated with a strong anti-proliferative activity, as only concentrations similar to the MTT-based IC_{50} values inhibited cell growth in 2D and 3D models.

The balance of intracellular ROS and antioxidants plays a pivotal role in the homeostasis of healthy cells, and elevated levels of ROS have been linked to cancer initiation and resistance to cancer therapy. During cancer development increased ROS production leads to DNA damage, genomic instability, and modified gene expression. However, pushing the ROS production beyond a breaking point leads to the activation of different cell death pathways and thereby offers a therapeutic strategy against tumor cells (Dharmaraja, 2017; Doering et al., 2012; Galadari et al., 2017).

Considering mitochondria as major ROS producers, the disruption of mitochondrial homeostasis can lead to increased ROS levels (Yang et al., 2016). In our study, auratryptanon showed an induction of hydrogen peroxide levels. As most ROS are converted to cell-permeable hydrogen peroxide (Weinberg et al., 2019), measuring hydrogen peroxide in an HVA assay provides an indirect measurement of the overall ROS status (Tarpey et al., 2004).

Deciphering the origin of auratryptanon-induced ROS levels was not part of this study. Other myxobacteria-derived compounds inhibited different parts of the mitochondrial respiratory chain complex (Weissman and Müller, 2010). Since the blockage of electron transport allows the electrons to react with oxygen to produce the ROS superoxide (Sabharwal and Schumacker, 2014), one could suggest a similar action for auratryptanon.

One prominent target of other natural products produced by myxobacteria is the eukaryotic cytoskeleton. Several compounds stabilize or destabilize actin, even though the compounds belong to distinctly different classes of metabolites (Weissman and Müller, 2010), as shown for e.g. chivosazoles (Diestel et al., 2009) and chondramide A (Schmauder et al., 2010). Since tumor cell migration, as an important hallmark of cancer, relies on the dynamic assembly and disassembly of actin filaments, we also tested the effects of auratryptanon on cell migration. However, even concentrations clearly above the MTT-based IC_{50} showed no effect on tumor cell migration.

Summarizing the effects of auratryptanon on tumor cells, auratryptanon exhibited an interesting profile mainly affecting tumor cell viability associated with increased ROS levels. Furthermore, the weak activity in differentiated Huh7.5 could be an indicator for a low toxicity against healthy cells.

We further aimed to investigate the effects of auratryptanon on macrophages as an essential component of the TME. Hence, we assessed the viability of different *in vitro* differentiated and polarized macrophage subsets after auratryptanon treatment. Auratryptanon exhibited the most potent effects against M1 macrophages, while TAM-like macrophages were barely affected.

In the context of the TME in a solid tumor, anti-inflammatory M2 macrophages exhibit tumor-promoting functions, while inflammatory M1 macrophages possess the ability to fight malignant cells. Therefore, the depletion of M1 macrophage by a tumor-toxic compound could lead to the accumulation of M2-like TAMs in the TME. Since apoptotic cells promote tumor-supporting functions of M2 macrophages (Weigert et al., 2016), this phenotype might be further enhanced in the remaining macrophages, causing an overall poor prognosis for the patients.

Therefore, considering auratryptanon for further preclinical studies, an in-depth analysis of its effects on tumor-associated macrophages needs to be performed to prevent an overestimation of its anti-cancer effects by solely focusing on tumor cells.

Perquinolines

3.3.4 Introduction

Perquinolines (**Figure 33**) belong to the group of bacterial tetrahydroisoquinolines and were identified in *Streptomyces* sp. IB2014/016-6 (Rebets et al., 2019). Isoquinoline structures are widely found in natural products, and plant-derived compounds of the benzisoquinoline alkaloid family, such as morphine or noscapine, exhibit a broad range of biological activities of high therapeutically importance (Kittakoop et al., 2014; Qiu et al., 2014; Weber and Opatz, 2019).

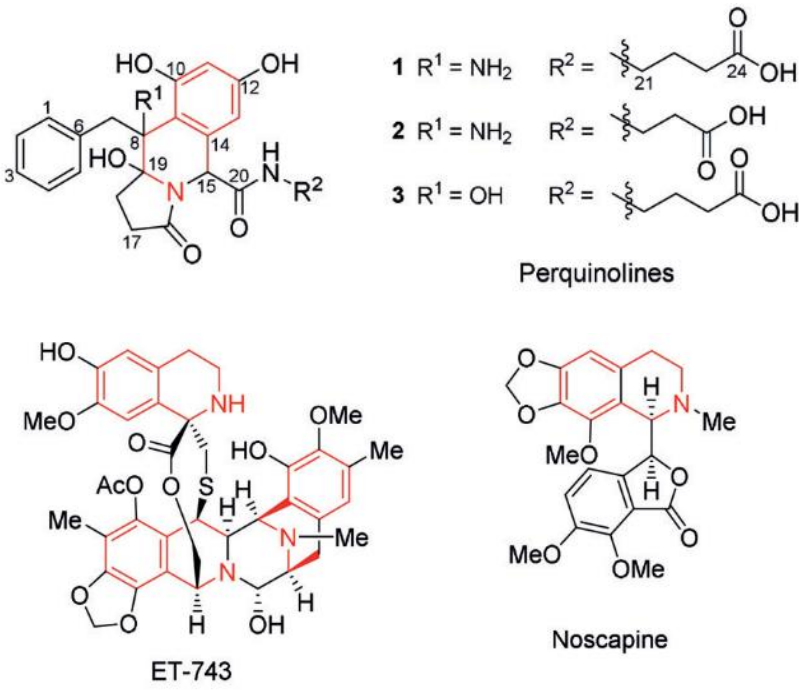

Figure 33. Structure of perquinolines A–C (1–3), ecteinascidin ET-743, and noscapine. Tetrahydroisoquinoline rings are highlighted in red (Rebets et al., 2019).

Non-plant-derived tetrahydroisoquinolines are less common. However, group members, such as saframycins A, produced by *Streptomyces lavendulae* and ecteinsacidins, isolated from the sea squirt species *Ecteinascidia turbinata*, attracted attention due to potent anti-tumor activities (Aune et al., 2002; Xing et al., 2004).

Ecteinascidin ET-743, also named trabectedin (Yondelis®), has been approved by the Food and Drug Administration (FDA) and the European Medicines Agency (EMA) as an anti-proliferative agent in cancer therapy (Carter and Keam, 2007). The drug further demonstrated

selective cytotoxicity towards monocytes and macrophages and, as a consequence, reduced numbers of tumor-infiltrating macrophages. This additional action on immune cells of the tumor microenvironment demonstrated to contribute substantially to its anti-cancer activity (Germano et al., 2013).

In this study, we characterized four different perquinolines in their effects on the viability of human cancer cells, macrophages, and monocytes.

3.3.5 Results

The three derivatives of the perquinoline group were first tested for their effects on the viability of human cancer cell lines *via* MTT assay (**Figure 34**). The derivatives perquinoline A and B demonstrated a moderate activity, especially against Huh7 cells (**Figure 34 A, B,** for IC_{50} values see **Table 6**). Perquinoline C demonstrated a very low activity in all three tested cell lines and reduced the viability to 50-60% after treatment with 200 µM (**Figure 34 C**).

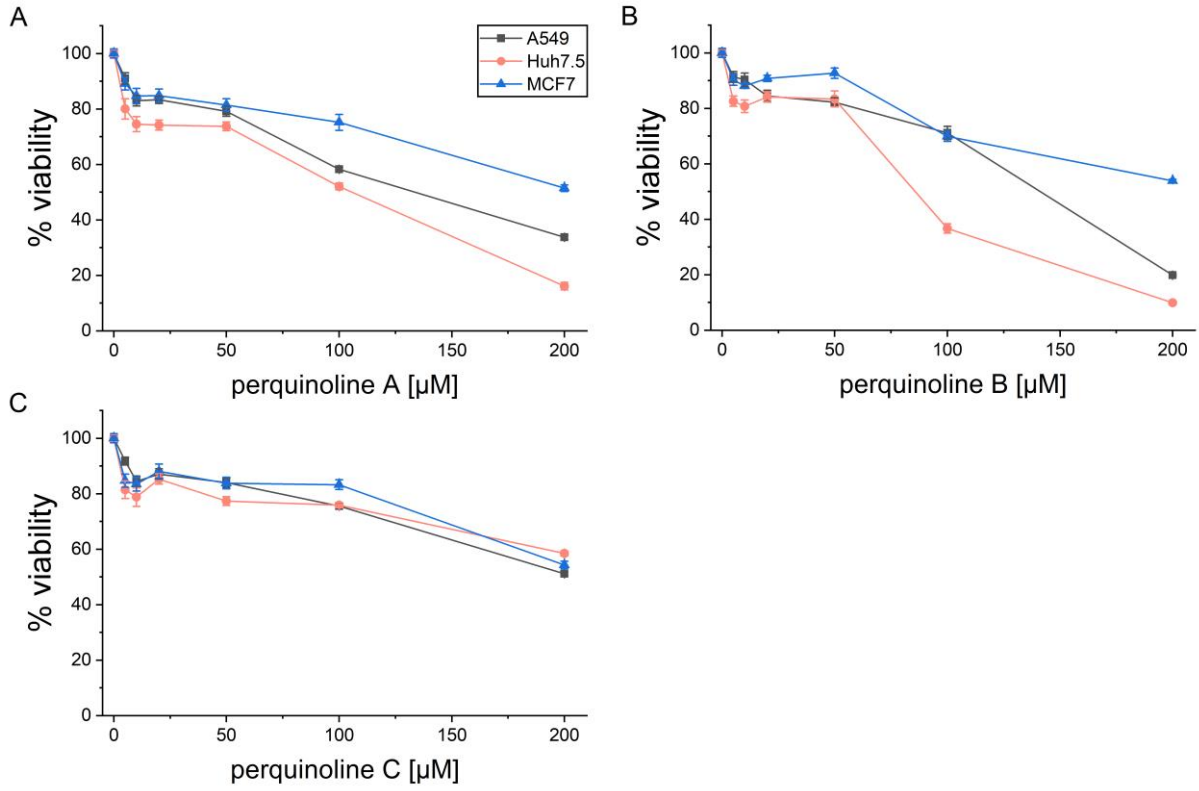

Figure 34. Effects of perquinolines on tumor cell viability.
A set of tumor cell lines was treated with increasing concentrations of perquinolines or vehicle control. Cell viability was determined after 48 h treatment in an MTT assay. Vehicle control-treated cells were used for data normalization; n=3 (quadruplicates).

Table 6. MTT-based IC_{50} [µM] values of perquinolines.
Activity against a panel of tumor cell lines was measured in an MTT assay after 48 h treatment.

cell line	*A*	*B*	*C*
A549	130.37	125.91	n.d.
Huh7.5	78.41	82.68	n.d.
MCF7	n.d.	n.d.	n.d.

n.d. (not detectable in concentrations up to 200 µM perquinolines)

Since the structurally related compound trabectedin selectively kills cells from the myeloid lineage, we hypothesized a similar activity for the perquinolines. However, all perquinoline derivatives showed no effects on the viability of differentiated and polarized macrophages derived from the monocyte cell line THP-1 (**Figure 35**), after 48 h treatment in concentrations up to 20 µM.

MTT assay and cell counting of undifferentiated THP-1 cells suggested no effect on monocyte viability and proliferation (data not shown, n=1).

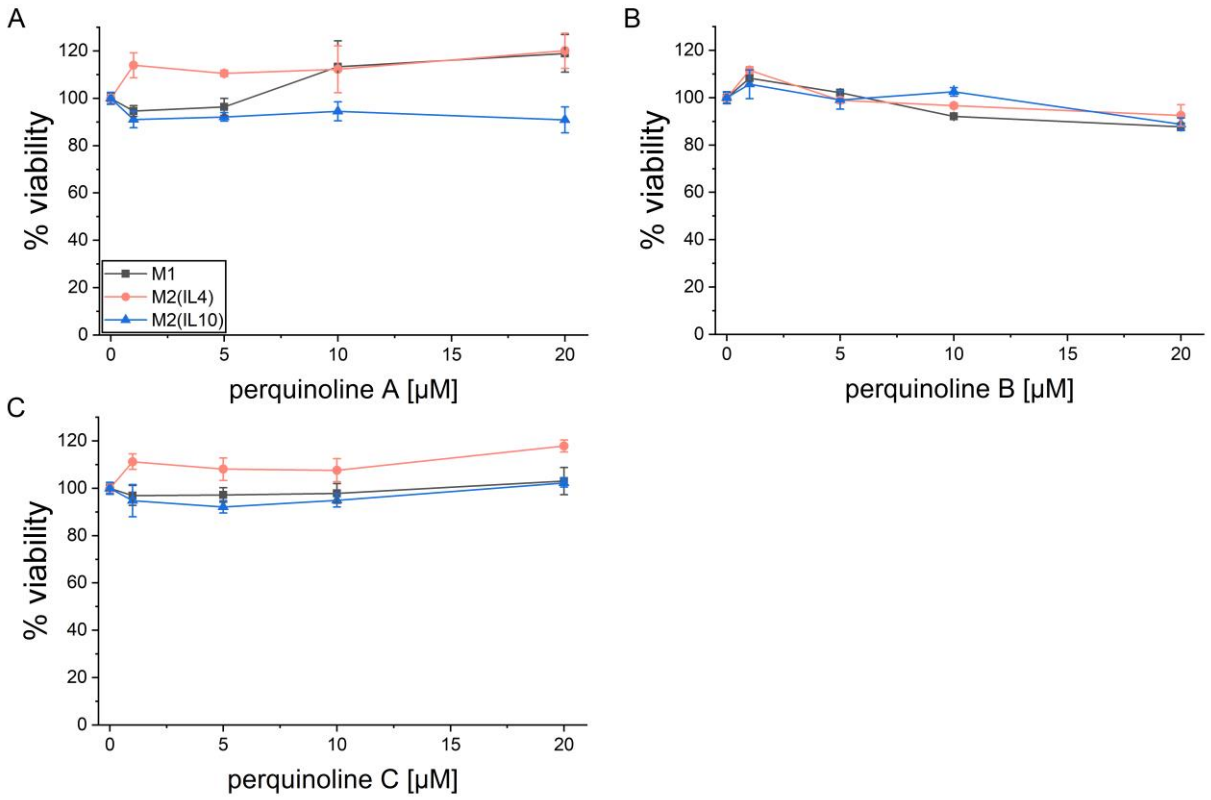

Figure 35. Effects of perquinolines on the viability of different macrophage subsets.
THP-1 cells were PMA-differentiated and polarized into M1, M2(IL4), and M2(IL10) macrophages for 24 h. Polarized macrophages were treated with increasing concentrations of perquinolines. Cell viability was determined after 48 h treatment in an MTT assay. Vehicle control-treated cells of the respective polarization status were used for data normalization; n=1 (quadruplicates).

3.3.6 Discussion

Perquinolines showed no prominent biological activity in human cancer cell lines, macrophages, and monocytes in the employed assays. However, due to their prominent core structure, the compounds could serve as interesting hits looking for other targets *via* library screenings.

Parts of the results presented in this chapter have been published in:

Yuriy Rebets, Suvd Nadmid, Constanze Paulus, **Charlotte Dahlem**, Jennifer Herrmann, Harald Hübner, Christian Rückert, Akexandra K. Kiemer, Peter Gmeiner, Jörn Kalinowski, Rolf Müller, and Andriy Luzhetskyy. 2019. "Perquinolines A-C: unprecedented bacterial tetrahydroisoquinolines involving an intriguing biosynthesis." *Angewandte Chemie International Edition* 58 (37): 12930–12934. https://doi.org/10.1002/anie.201905538.

Bakailomycins

3.3.7 Introduction

Organisms found in poorly studied ecosystems represent a promising source of new natural products serving as advantageous drugs or drug lead structures. The group of baikalomycins is produced by *Streptomyces sp*. IB201691-2A strain, which was found in the Lake Baikal endemic gastropod *Benedictia baicalensis* (Voitsekhovskaia et al., 2020).

Baikalomycins A-C were found by an activity-guided screening and belong to the family of aquayamycin-type angucyclines. The strain also contains large quantities of rabelomycin (Liu et al., 1970) and 5-hydroxy-rabelomycin, known shunt products in angucyclines biosynthesis. Structures are shown in **Figure 36** (Voitsekhovskaia et al., 2020).

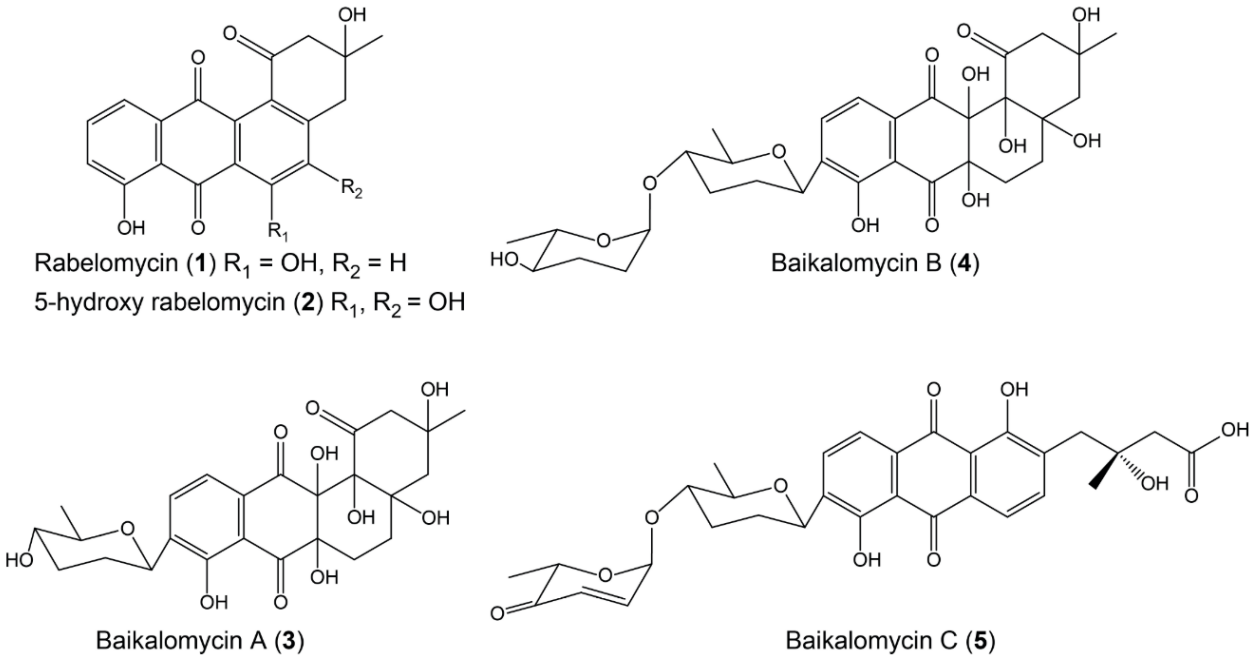

Figure 36. Structures of angucycline aglycons rabelomycin, 5-hydroxy-rabelomycin, and aquayamycin-type baikalomycins A-C (Voitsekhovskaia et al., 2020).

Angucyclines, characterized by a tetracyclic benz[a]anthracene core, are a class of compounds produced by *Streptomyces sp*., exhibiting a broad spectrum of biological activities such as anti-cancer and anti-bacterial activities *in vitro* (Kharel et al., 2012). In addition to the cytotoxic activities, other family members of the angucycline group have been reported to, e.g., inhibit the inducible nitric oxide synthase (iNOS) activity (Alvi et al., 2000), xanthin oxidase

(Kirschning et al., 2000), and to induce the peroxisome proliferator-activated receptor PPAR-γ (Potterat et al., 2007).

In this study, we aimed to characterize the baikalomycins A-C as well as rabelomycin and 5-hydroxy-rabelomycin in their biological activity against cancer cells.

3.3.8 Results

The baikalomycins A-C, rabelomycin, and 5-hydroxy-rabelomycin were tested for their effects on the viability of a set of human cancer cell lines *via* MTT assay. Baikalomycin A and B showed a moderate to no activity depending on the cell line. In comparison, baikalomycin C, rabelomycin, and 5-hydroxy-rabelomycin exerted a more potent activity with IC_{50} values in the low micromolar range in all four tested cell lines (**Figure 37 A**; for IC_{50} values, see **Table 7**).

As the overall lowest IC_{50} values were obtained in A549 cells, this cell line was chosen to analyze potential anti-proliferative actions in an electric cell impedance-based assay. Anti-proliferative effects correlated with cytotoxic activities observed in A549 cells: Baikalomycins A-C showed no effects on proliferation, while rabelomycin and, to a greater extent, 5-hydroxy-rabelomycin reduced cell proliferation in sub-toxic concentrations (cell viability > 80% after 48 h treatment) (**Figure 37 B**).

Table 7. MTT-based IC_{50} [µM] values of baikalomycins.
Activity against a panel of tumor cell lines was measured in an MTT assay after 48 h treatment.

cell line	*baikalo. A*	*baikalo. B*	*baikalo. C*	*rabelomycin*	*5-hydroxy-rabelomycin*
A549	58.51 ± 5.15	46.26 ± 0.52	42.43 ± 3.71	9.78 ± 0.49	9.11 ± 0.59
Huh7.5	n.d.	n.d.	7.62 ± 0.47	7.21 ± 0.70	11.91 ± 2.94
MCF7	53.19 ± 3.36	n.d.	13.35 ± 1.33	21.94 ± 1.59	27.39 ± 2.17
SW620	n.d.	n.d.	3.87 ± 0.69	7.82 ± 0.40	13.43 ± 0.72

n.d. (not detectable in concentrations up to 20 µM baikalomycins)

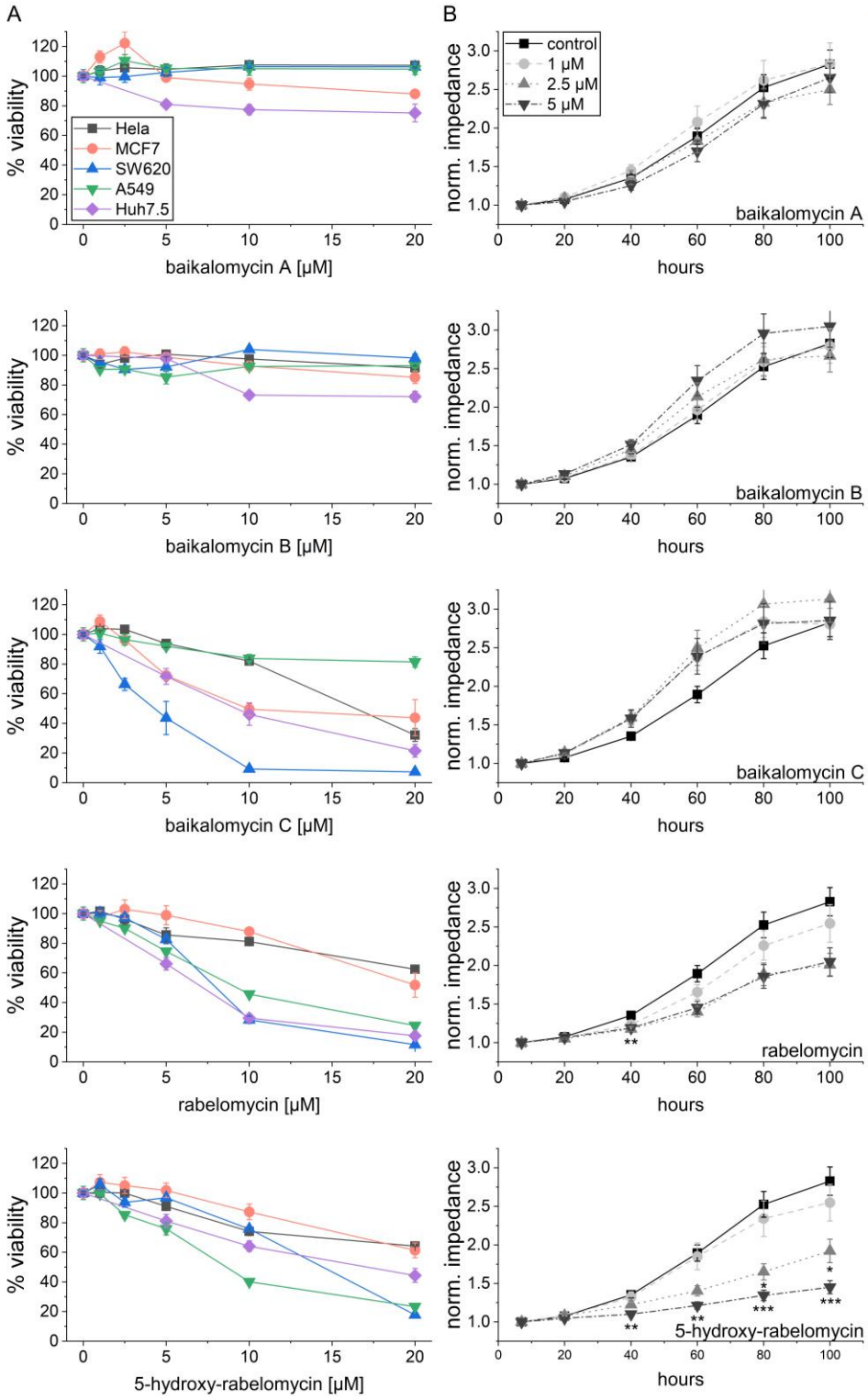

Figure 37. Effects of baikalomycins on tumor cell viability and proliferation.
(**Column A**) A set of tumor cell lines was treated with increasing concentrations of compounds or vehicle control. Cell viability was determined after 48 h treatment in an MTT assay.
(**Column B**) Proliferation of treated A549 cells was measured using the electric cell-substrate impedance sensing (ECIS®) system. Cells were treated 5 h after seeding and impedance was normalized to the value at 7 h after seeding. Statistical analysis was performed for the indicated time points using one-way ANOVA followed by Bonferroni's post-hoc analysis, comparing compound-treated to vehicle control-treated cells, ** $p < 0.01$ ***, $p < 0.001$; n=3 (quadruplicates).

3.3.9 Discussion

Baikalomycins A-C demonstrated a varying degree of moderate anti-cancer activities, with baikalomycin C being the most active derivative. None of the new compounds exceeded the viability-reducing and anti-proliferative effects of the commonly-found simple family member rabelomycin (Kharel et al., 2010).

To the best of our knowledge, we are the first to describe anti-proliferative effects for rabelomycin, in concentrations distinctly below IC_{50} values, which we found after 48 h treatment in an MTT assay. The fact that cell line-dependent IC_{50} values for rabelomycin vary in the literature between 1.52 µM and 9.91 µM (Bao et al., 2018; Zhang et al., 2012) demonstrates the need for a detailed description of methods and treatment times during the assessment of biological activities of newly described compounds.

Despite their structural and biological diversity, none of the angucycline family members have been developed into clinically applicable drugs so far, due to toxicity or solubility problems (Kharel et al., 2012). We did not observe any solubility issues in concentrations up to 20 µM.

Even though the baikalomycins are not characterized by strong anti-tumor properties, they are interesting candidates for further direct target identifications and target binding studies in other contexts since some angucyclines characterized by poor anti-tumoral and anti-bacterial activities exhibit potent enzyme inhibition (Kharel et al., 2012).

Parts of the results presented in this chapter have been published in:

Irina Voitsekhovskaia, Paulus Constanze, **Charlotte Dahlem**, Yuriy Rebets, Suvd Nadmid, Josef Zapp, Denis Axenov-Gribanov, Christan Rückert, Maxim Timofeyev, Jörn Kalinowski, Alexandra K. Kiemer, and Andriy Luzhetskyy. 2020. “Baikalomycins A-C, new aquayamycin-type angucyclines isolated from Lake Baikal derived *Streptomyces* sp. IB201691-2A.” *Microorganisms* 8 (5): E680. https://doi.org/10.3390/microorganisms8050680.

3.4 **Chapter 4.** Macrophage targeting by nanoparticles loaded into yeast

3.4.1 Introduction

In cancer drug development, the delivery of biologically active compounds to specific cells and tissues remains one major challenge. The systematic administration provides access to most of the tissues, reaching not only the tumor itself but also metastatic sites. This strategy provides an effective drug route that is nevertheless restricted for chemotherapeutic agents targeting pathways specifically found in malignant cells. To overcome off-target cytotoxicity, but also issues such as low drug bioavailability and uptake efficiency of chemotherapeutic agents, nanomedicines were developed. Nanomedicines are characterized as therapeutics composed of or formulated in carrier materials smaller than 100 nm. Nanoparticles proved to alter pharmacokinetics of drugs but also showed to accumulate in tumors through the enhanced permeation and retention (EPR) effect (Murthy, 2007; Wong et al., 2015).

The targeting of myeloid cells using nanomedicine reveals an attractive approach since, e.g., macrophages and dendritic cells represent logical targets due to their phagocytic capacity (Amoozgar and Goldberg, 2015; Torres Andón and Alonso, 2015). In this context, yeast cells have demonstrated to be an effective delivery vehicle for different contents such as DNA, mRNA, proteins, and vaccines to phagocytic cells (Seif et al., 2016, 2017; Stubbs et al., 2001; Walch-Rückheim et al., 2016; Walch et al., 2011).

In this study, we aimed to demonstrate a macrophage-specific targeting, employing the baker's yeast *Saccharomyces cervisiae* as a nano-in-micro delivery system for poly(lactic-co-glycolic acid) (PLGA) nanoparticles (NPs).

Ruth Kiefer (Molecular and cell biology, Saarland University) successfully loaded chitosan-coated rhodamine-labeled PLGA NPs to *Saccharomyces cerevisiae* BY4742 yeast cells. This loading included the binding of NPs to the cell wall as well as their internalization. The complexation under hypotonic (5 mM NaCl) conditions resulted in a higher loading efficiency compared to isotonic (154 mM NaCl) conditions. Interestingly, the complexation of NPs with yeast under hypotonic conditions revealed the highest percentage of NP-positive cells, when M1 and M2 polarized THP-derived macrophages were incubated with either free or complexed (isotonic/hypotonic) NPs (Kiefer et al., 2019).

3.4.2 Results

In order to assess the specific targeting of phagocytic cells by NPs complexed with yeast cells, we used a co-culture model consisting of fluorescently labeled HeLa tumor cells and HMDMs. The co-culture was incubated for 0.5 h or 4 h with NPs either as free NP or as NP/yeast complexes, followed by flow cytometric analysis.

A small fraction of analyzed cells (4.2% ± 2.1 SD) was double-positive for both the macrophage and tumor cell staining. These cells were excluded from further analysis, as we suggested that this occurred from the uptake of tumor cell debris by macrophages during co-culture.

After 4 h incubation, macrophages and tumor cells showed both a shift in the rhodamine channel when incubated with free NPs. Incubation with the yeast-complexed NPs revealed a clear bias of NP uptake towards macrophages already after 30 min incubation (**Figure 38**).

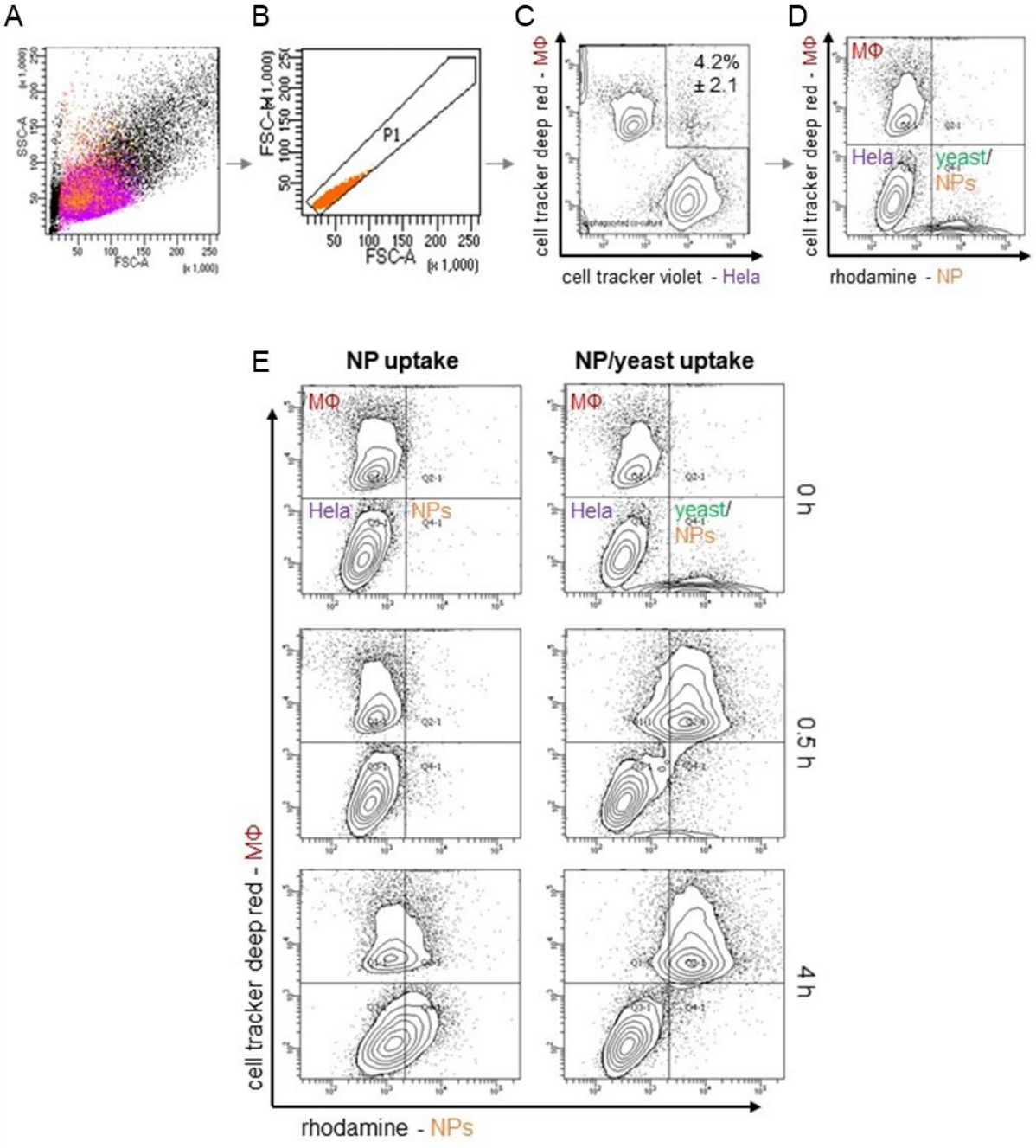

Figure 38. NP uptake in HeLa /HMDM co-culture.
Uptake of rhodamine-labeled nanoparticles (NPs) by co-cultured HeLa cells (cell tracker violet-stained) and human monocyte-derived macrophages (MΦ, cell tracker deep red-stained) was analyzed by flow cytometry.
(**A**) All events were plotted in an FSC-A *vs*. SSC-A scatter plot.
(**B**) Singlet cells were selected in an FSC-A *vs*. FSC-H scatter plot.
(**C**) Cells double positive for cell tracker deep red and violet were excluded from further analysis.
(**D**) The cell tracker deep red-positive (MΦ) and deep red-negative (HeLa) cell populations were analyzed for their uptake of rhodamine-labeled NPs, as indicated by increased signals in the rhodamine channel.
(**E**) Representative contour plots for the timepoints 0, 0.5, and 4 h are shown. Co-cultures were incubated with either plain hypotonic NPs or opsonized NP-loaded yeast (CFSE-stained).

The signal quantification manifested that free NPs were taken up to equal extents in HeLa cells and macrophages after 4 h (**Figure 39 A**), while the complexation of NPs to yeast specifically targeted macrophages already after 0.5 h incubation (**Figure 39 B**). Moreover, complexation increased rhodamine-positive macrophages from 34% to 91% after 4 h, indicating a more efficient NP delivery.

The uptake of free NPs in isotonic *vs*. hypotonic solution into macrophages showed no differences (**Figure 39 C**). Comparing NPs complexed under isotonic *vs.* hypotonic conditions, macrophages incubated with hypotonic NP/yeast complexes revealed a significantly higher fraction of rhodamine-positive cells after 0.5 h (40% *vs*. 76%). This effect was abolished after 4 h incubation (**Figure 39 D**). This observation could not be explained by a reduced yeast uptake, as 95-99% of macrophages were CFSE-positive already after 0.5 h, indicating a fast and efficient yeast uptake by macrophages (**Figure 39 E**).

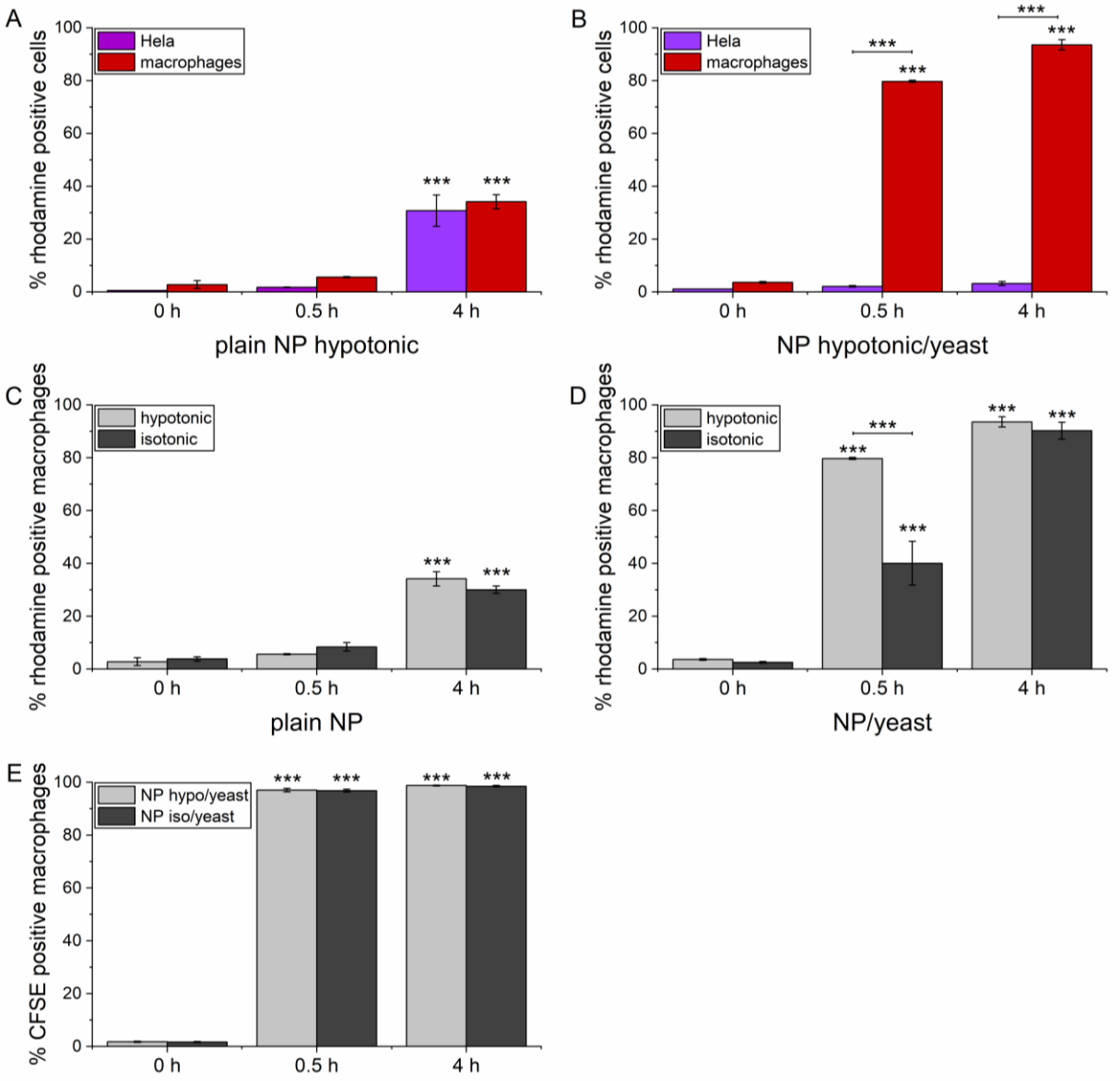

Figure 39. Quantification of NP uptake in HeLa/HMDM co-culture.
Uptake of rhodamine-labeled nanoparticles (NPs) by co-cultured HeLa cells (cell tracker violet-stained) and human monocyte-derived macrophages (MΦ, cell tracker deep red-stained) was analyzed by flow cytometry.
(**A, B**) Quantitative analysis comparing the uptake of (**A**) plain hypotonic NPs and (**B**) hypotonic NP/ yeast complexes in HeLa cells and macrophages.
(**C, D**) Quantitative analysis comparing uptake of isotonic and hypotonic NPs in macrophages, either (**C**) as plain NPs or (**D**) as NP/yeast complexes.
(**E**) Quantitative analysis of yeast (CFSE-stained) uptake in macrophages comparing yeast complexed under isotonic and hypotonic conditions.
Data are presented as mean values ± SEM of two independent experiments performed in cells from two different donors, measured in duplicates. Statistical analysis was performed by one-way ANOVA followed by Tukey´s post-hoc analysis $p < 0.001$ (***).

3.4.3 Discussion

In our study, the baker´s yeast *Saccharomyces cerevisiae* demonstrated to be an attractive vehicle to deliver NPs effectively and selectively to macrophages. The administration of NPs inside the nano-in-micro particle not only specifically targeted the NPs to phagocytic cells, but also delivered higher amounts of NPs compared to NPs alone. As the complexation of yeast with NPs under isotonic conditions resulted in a lower binding capacity (Kiefer et al., 2019), it is not surprising that those complexes led to a lower NP delivery to macrophages.

Our study underlines the advantages of yeast cells as a delivery vehicle for NPs. Beyond the cell-specific targeting, the complexation of NPs to *Saccharomyces cerevisiae* offers the possibility of cargo protection and further modifications of the cell surface. Besides local injection, NP-complexed yeast could be administered *via* the oral route, since yeast cells showed to protect its cargo from degradation by proteases and acid pH during stomach passage and demonstrated to be viable in the intestine for up to one week (Kenngott et al., 2016). Moreover, surface-modified yeast was taken up by M cells of the Peyer's patches in the gastrointestinal mucosa (Kenngott et al., 2016), where they could be engulfed by macrophages, which can be found beneath the surface of the Peyer's patches.

Considering the achievements already earned by using NPs for immunotherapy (Irvine and Dane, 2020; Kumar et al., 2020), the combination with yeast cells for cell-specific targeting to phagocytic cells might lead to substantial progress in different therapeutic approaches.

The results presented in this chapter have been published in:

Ruth Kiefer, Marijas Jurisic, **Charlotte Dahlem**, Marcus Koch, Manfred J. Schmitt, Alexandra K. Kiemer, Marc Schneider, and Frank Breinig. 2019. “Targeted delivery of functionalized PLGA nanoparticles to macrophages by complexation with the yeast *Saccharomyces cerevisiae*.” *Biotechnology and Bioengineering* 117 (3): 776-788. https://doi.org/10.1002/bit.27226.

4 **Part II:** The RNA binding protein IGF2BP2/ IMP2 as potential target in cancer therapy

4.1 **Chapter 1.** The insulin-like growth factor 2 mRNA binding protein IMP2/IGF2BP2 is overexpressed and correlates with poor survival in pancreatic cancer

4.1.1 Introduction

Pancreatic adenocarcinoma is the seventh leading cause of cancer-related deaths worldwide (Rawla et al., 2019). Prognosis is poor and 5-year survival is only 9%. Most of the patients have advanced stage tumors at the time of diagnosis making tumor resection impossible. Insulin-like growth factor 2 (*IGF2*) mRNA binding proteins (IGF2BPs/IMPs) have been described to be oncogenic in several types of cancer including pancreatic cancer (Barghash et al., 2015, 2016; Bell et al., 2013; Dai et al., 2017; Janiszewska et al., 2012; Kessler et al., 2015a). The IMP family member IMP3 has originally been identified in pancreatic cancer tissues (Müeller-Pillasch et al., 1997) and studied in this cancer type in more detail compared to the other two IMPs (Morimatsu et al., 2013; Schaeffer et al., 2010; Wachter et al., 2011; Zhao et al., 2007). In lung cancer IMP1 has been reported to increase Kras signaling (Rosenfeld et al., 2019), which is frequently altered in pancreatic cancer tissue. Recently, *IMP2* has been reported to be the most abundant of the three members of the IMP family in most cancer types including pancreatic ductal adenocarcinoma (PDAC) (Dai et al., 2017). However, beside gene expression in pancreatic cancer samples of the TCGA data set little is known about its role in pancreatic cancer progression and its prognostic relevance. A well-known precursor of PDAC is Pancreatic Intraepithelial Neoplasia (PanIN). PanIN lesions progress from intraepithelial to invasive PDAC. Early detection of PanINs would help to interfere with PanIN progression to PDAC. IMP2 has been shown to promote carcinogenesis in the liver and to worsen chronic liver disease as a risk factor for liver cancer development (Kessler et al., 2015a; Simon et al., 2014). This study shows for the first time that IMP2 expression is linked to progression and poor survival in pancreatic cancer.

4.1.2 Results and discussion

4.1.2.1 IMP2 is overexpressed in precursor lesions, PDAC and linked to lower rate of survival

In order to study the expression of *IMP2* in pancreatic cancer, publicly available datasets were investigated. Dai et al. recently showed that *IMP2* is overexpressed in PDAC tissues of the publicly available TCGA cohort compared to normal tissues (Dai et al., 2017). In concordance, we observed *IMP2* overexpression in tumor tissues compared to normal tissues from a dataset containing matched normal and tumor samples (**Figure 40 A**). Survival analysis revealed that high *IMP2* expression is linked to lower survival rate (**Figure 40 B**). Interestingly, *IMP2* was overexpressed in PanIN lesions, which bear a high risk to develop into pancreatic cancer (**Figure 40 C**). In contrast to IMP2, IMP3 was shown to be highly specific for pancreatic tumor tissue and negative in premalignant tissues (Yantiss et al., 2005). However, since biomarkers for early detection are needed to detect progression from PanIN towards PDAC, IMP2 might fulfill this need.

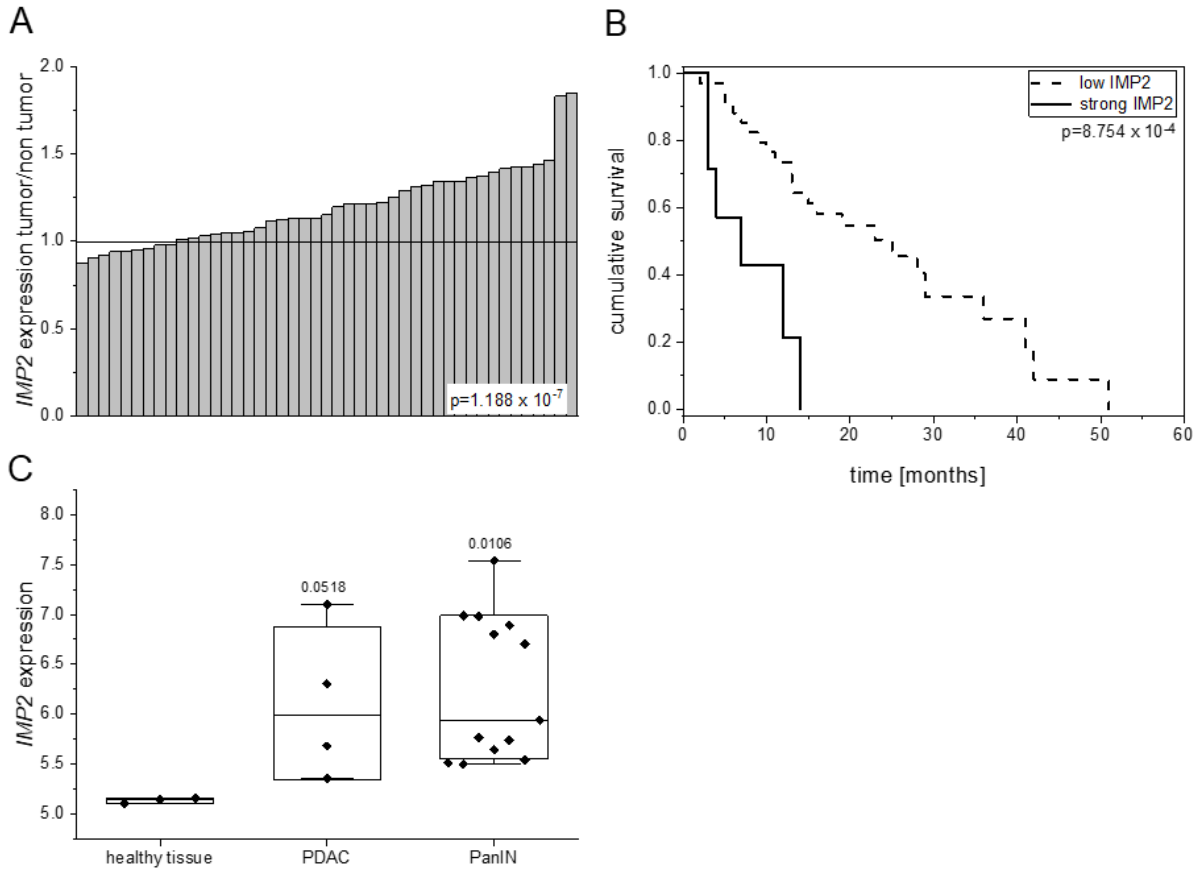

Figure 40. *IMP2* is overexpressed in PanINs and PDAC and leads to lower rate of survival.
(**A**) Expression levels of *IMP2* in human PDAC cohort as compared with matched normal pancreatic tissue (GEO ID: GSE28735; $p = 1.188 \times 10^{-7}$; n = 45).
Continued.

Figure 40 continued.
(**B**) Kaplan-Meier estimated cumulative survival of PDAC patients with strong or low IMP2 expression (GEO ID: GSE28735; p = 8.754 × 10−4; low IMP2 expression in tumor tissue < 6, n = 35; strong IMP2 expression > 6, n = 7). Continued.
(**C**) IMP2 expression levels ± SEM in human PDAC and PanIN lesions (GEO ID: GSE43288).

Strict correlation analysis (threshold $R^2 > 0.75$) revealed 22 genes highly positively and 9 genes highly negatively correlating with *IMP2* (**Table 8**). Besides genes involved in the inhibition of apoptosis (*Bcl-XL*), especially factors involved in ubiquitination were strongly correlated with IMP2 expression: *SMURF1* and *FBXO45*. Moreover, protein kinase C (*PKC*) signaling pathway was distinctly affected: *DXS1179E* encoding PKC iota, PKC substrate *PLEK2*, and inositol triphosphate receptor *IP3R3*. Negatively correlated genes are involved in apoptosis regulation and DNA repair (*APO-J* and *CAF*) as well as epigenetic regulation (*AAM-B*). Interestingly, *IMP2* negatively correlated with *KIAA0922*, which antagonizes Wnt signaling, a pathway which has been described to be essential for pancreatic carcinogenesis (Sano et al., 2016; Zhang et al., 2013b).

Table 8. Genes correlating with *IMP2* expression.
Table shows correlation coefficients for highly positively and negatively correlating genes (threshold $R^2 > 0.75$ or $R^2 < -0.75$, respectively). Correlation analysis was performed by Ahmad Barghash (Department of Computer Science, German Jordanian University).

Positive correlation		*Negative correlation*	
Gene	**Correlation coefficient R^2**	**Gene**	**Correlation coefficient R^2**
ERO1-alpha	0.867	*DMDL*	-0.833
CD318	0.830	*CAF*	-0.814
ARVD12	0.825	*SEPP1*	-0.801
BEN	0.818	*AAM-B*	-0.796
BCL-XL/S	0.793	*ADAMTSL3*	-0.779
IP3R3	0.787	*8B*	-0.774
BM600-125KD	0.783	*KIAA0922*	-0.765
PLEK2	0.781	*SEB*	-0.761
TM9SF4	0.776	*GGTA1*	-0.760
DYT17	0.774	*APO-J*	-0.753
TMCC1	0.772	*DCL2*	-0.752
DXS1179E	0.770		
HSNOV1	0.764		
SDC4	0.762		
TFGA	0.761		
SMURF1	0.761		
FAD104	0.760		
CT31	0.759		
FGD6	0.758		
FBXO45	0.750		

4.1.2.2 IMP2 is involved in metastasis

Epithelial-mesenchymal transition (EMT) is important for tumor cells to gain migratory and invasive potential. In glioblastoma, IMP2 promotes EMT and migration *via* the IGF2/PI3K/Akt pathway (Mu et al., 2015). EMT can be induced in cell culture by treatment of cancer cells with TGF-β. In fact, TGF-β induced EMT was associated with increased *IMP2* expression (**Figure 41 A**).

Metastases are a result of circulating tumor cells (CTC) that detach from the primary cancer and settle down in distant organs. In the publicly available dataset GDS4329 CTC, haematological cells, original tumour, and non-tumoural pancreatic control tissue were isolated from PDAC patients. CTC showed high *IMP2* expression, significantly increased compared to

healthy pancreatic tissue as well as to haematological cells (**Figure 41 B**), suggesting a role for IMP2 in metastasis of pancreatic tumors.

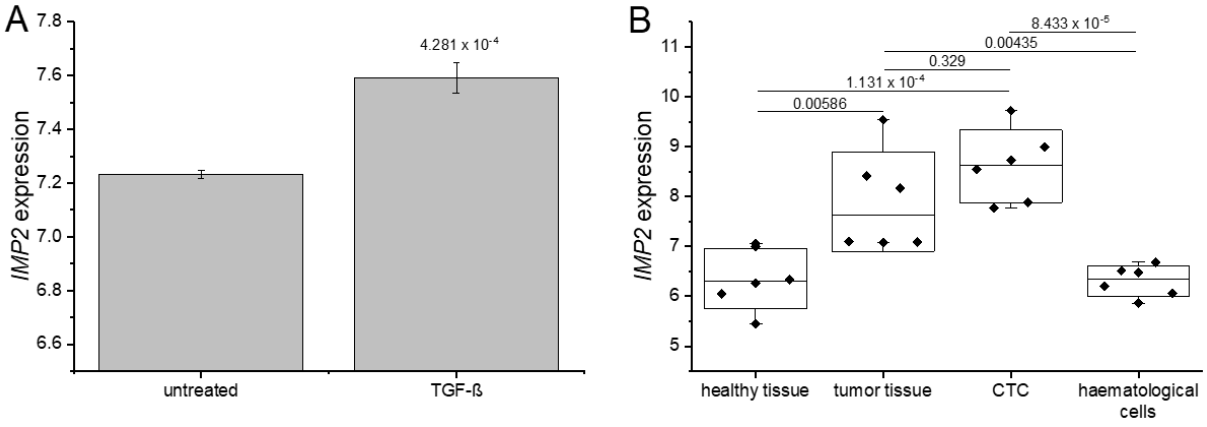

Figure 41. *IMP2* is associated with metastasis.
(**A**) *IMP2* expression in Panc-1 cells after EMT induction by treatment with 5 ng/mL TGF beta for 48 h (GEO ID: GSE23952, data ± SD; n = 3).
(**B**) *IMP2* expression in tumor tissue and CTC compared to healthy tissue and heamatological cells of the same donor as controls (GEO ID: GDS4329, data ± SD).

IMP2 protein expression is linked to the occurrence of metastasis in esophageal cancer (Barghash et al., 2016). IMP2 was further described to be involved in tumor growth and metastasis in non-small cell lung cancer (NSCLC) and to be targeted by the tumor suppressive microRNA miR-485-5p (Huang et al., 2018). Png and colleagues reported that IMP2 is secreted from metastatic cells and recruits endothelial cells during metastasis (Png et al., 2012) underlining the role of IMP2 in tumor progression.

4.1.2.3 IMP2 protein is overexpressed in PDAC tissue compared to healthy tissue and associated with lower rate of one-year survival

Since increased protein levels are crucial for the usage of IMP2 as a biomarker, tissue microarrays of a PDAC sample collection from 210 PDAC patients in total were analyzed by immunohistochemistry. IMP2 was significantly overexpressed in tumor tissue ($p = 0.26 \times 10^{-4}$; **Figure 42 A**). In healthy tissues IMP2 immunoreactivity was found in 91% of samples. (score 0: 9%; score 1: 55%; score 2: 27%; score 3: 9%). All tumor tissues (n = 204) were positive for IMP2: score 1: 7.4%; score 2: 40%; score 2/3: 2.9%; score 3: 49.5%). Kaplan-Meier analysis showed no effect of IMP2 staining intensity on overall survival, but strong IMP2 expression (score3) was linked to lower rate of one-year survival (**Figure 42 B**). This is in accordance to

findings in several other malignancies, in which a subgroup of tumors with highest IMP2 expression is linked to short survival (Barghash et al., 2015, 2016; He et al., 2018; Janiszewska et al., 2012; Kessler et al., 2013, 2017). In conclusion, IMP2 is frequently overexpressed in PDAC and significantly associated with poor prognosis. IMP2 seems to promote tumor progression of PDAC. Thus, it might be an interesting prognostic marker as well as a novel target for the treatment of PDAC.

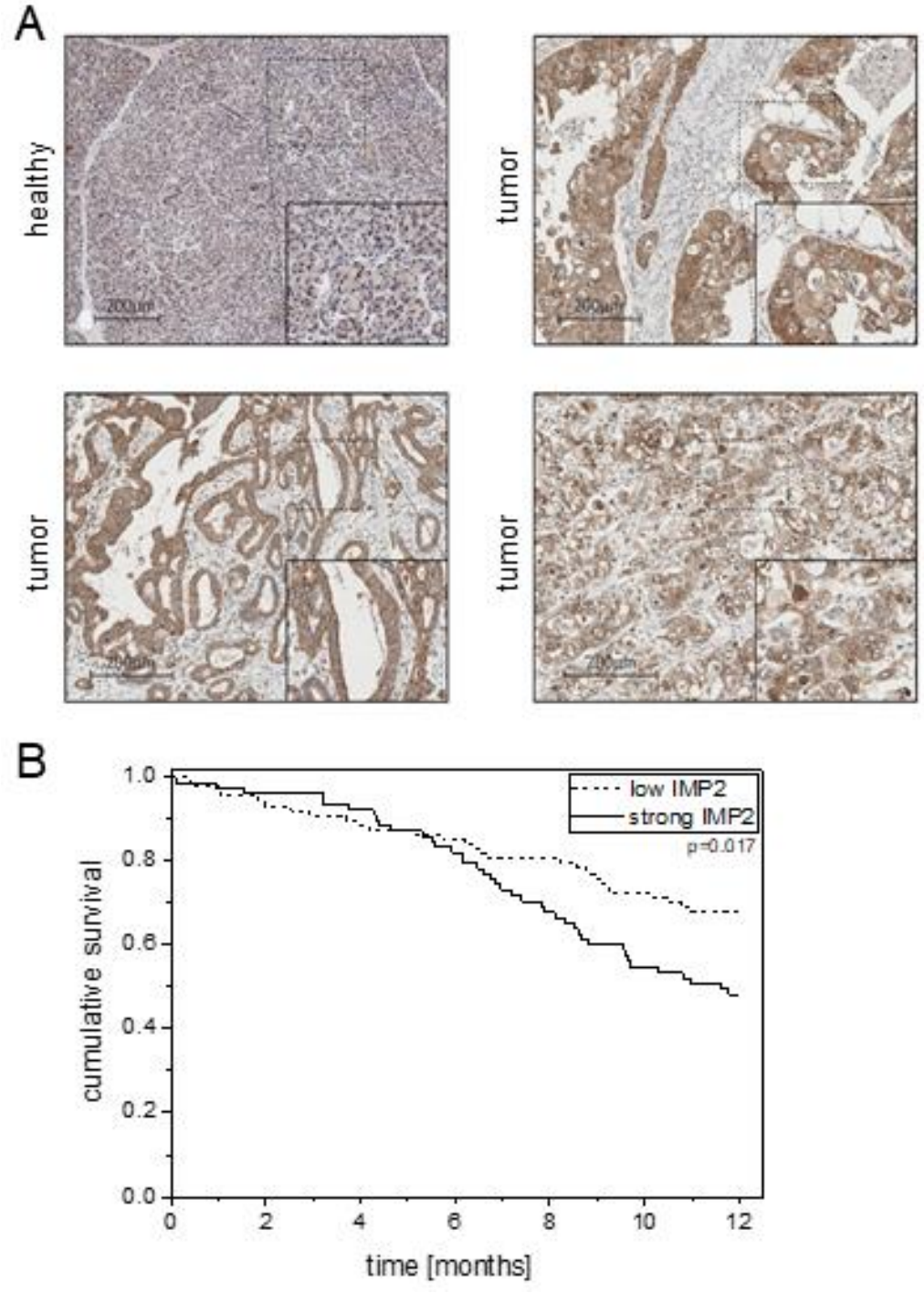

Figure 42. IMP2 protein is linked to poor one-year survival.

Figure 42 continued.
(**A**) Tissue microarrays of PDAC sample collection from n = 210 PDAC patients (tumor tissue: n = 210 healthy tissue: n = 11) were analyzed by immunohistochemistry. IMP2 was significantly overexpressed in tumor tissue ($p = 0.26 \times 10^{-4}$). In healthy tissues IMP2 immunoreactivity was found in 91% of samples (score 0: 9%; score 1: 55%; score 2: 27%; score 3: 9%). All tumor tissues (n = 204) were positive for IMP2 expression: score 1: 7.4%; score 2: 40%; score 2/3: 2.9%; score 3: 49.5%).
(**B**) Kaplan-Meier analysis of one-year survival of patients with strong IMP2 staining (score 3) *vs.* low IMP2 staining in pancreatic tumor tissues.
Data were generated by Sonja M Kessler (Pharmaceutical Biology, Saarland University), Philip Puchas and Johannes Haybaeck (Institute of Pathology, Medical University of Graz).

The results presented in this chapter have been published in:

Charlotte Dahlem, Ahmad Barghash, Philip Puchas, Johannes Haybaeck, and Sonja M. Kessler. 2019. "The insulin-like growth factor 2 mRNA binding protein IMP2/IGF2BP2 is overexpressed and correlates with poor survival in pancreatic cancer." *International Journal of Molecular Sciences* 20 (13): 3204. https://doi.org/10.3390/ijms20133204.

Sonja M. Kessler participated in writing this chapter.

4.2 **Chapter 2.** IMP2 target validation and *in vivo* testing of IMP2 inhibitors

4.2.1 Introduction

Insulin-like growth factor 2 (*IGF2*) mRNA binding proteins (IGF2BPs/IMPs/VICKZs) are oncofetal RBPs that are suggested to play a crucial role in carcinogenesis and tumor progression (see chapters 1.6 and 4.1).

RBPs are emerging targets in cancer therapy due to their role in various physiological functions, but also in cancer initiation and progression. Different studies focus on the application of small molecules inhibiting RBP function by, e.g., the inhibition of RBP-RNA interactions, prevention of functional modifications of RBPs, or the inhibition of the enzymatic activity of RBPs towards the target mRNA (Mohibi et al., 2019).

In this study, we validated IMP2 as a novel and attractive anti-cancer target due to its suggested role in carcinogenesis and tumor progression, using *in vitro* and *in vivo* approaches.

Ali Abuhaliema (Pharmaceutical Biology, Saarland University) screened different (natural) compound libraries for IMP2 inhibitors *via* fluorescence polarization assays (Abuhaliema et al. 2020, *submitted*). In this study, a selection of the hit compounds was further characterized in their anti-proliferative actions in a zebrafish xenograft *in vivo* model.

4.2.2 Results

4.2.2.1 IMP2 knockout reduces tumor proliferation and migration in vitro

To validate IMP2 as a potential anti-cancer target, its role in different hallmarks of cancer was evaluated by comparison of IMP2 knockout *vs*. parental colon cancer cells. Tarek Kröhler (Pharmaceutical Biology, Saarland University) performed a CRISPR/Cas9-mediated knockout of IMP2 and its splice variant p62 in HCT116 cells (Abuhaliema et al. 2020, *submitted*).

The impact of IMP2 on tumor cell proliferation was tested in a comprehensive time-dependent live-cell microscopic analysis. By monitoring cell confluency of parental and knockout cells in conventional 2D cultures over 4.5 days, we observed a minor inhibition of proliferation by IMP2 knockout (**Figure 43 A**).

Since previous studies demonstrated that IMP2 knockout affects proliferation of 2D cell cultures only to a minor extent (Kessler et al., 2013; Xing et al., 2019), and *in vivo* tumor phenotypes can be simulated more accurately by CRISPR phenotypes in 3D cell cultures (Han et al., 2020), we assessed the proliferation of parental and IMP2 knockout HCT116 cells also in a 3D spheroid model. Live-cell analysis revealed a strongly reduced proliferation in the absence of IMP2 (**Figure 43 B, C**).

In order to assess the influence of IMP2 on another hallmark of cancer, we modeled the metastatic capacity of parental *vs*. knockout cells in a scratch wound assay. In this model, IMP2 knockout significantly reduced cell migration (**Figure 43 D, E**).

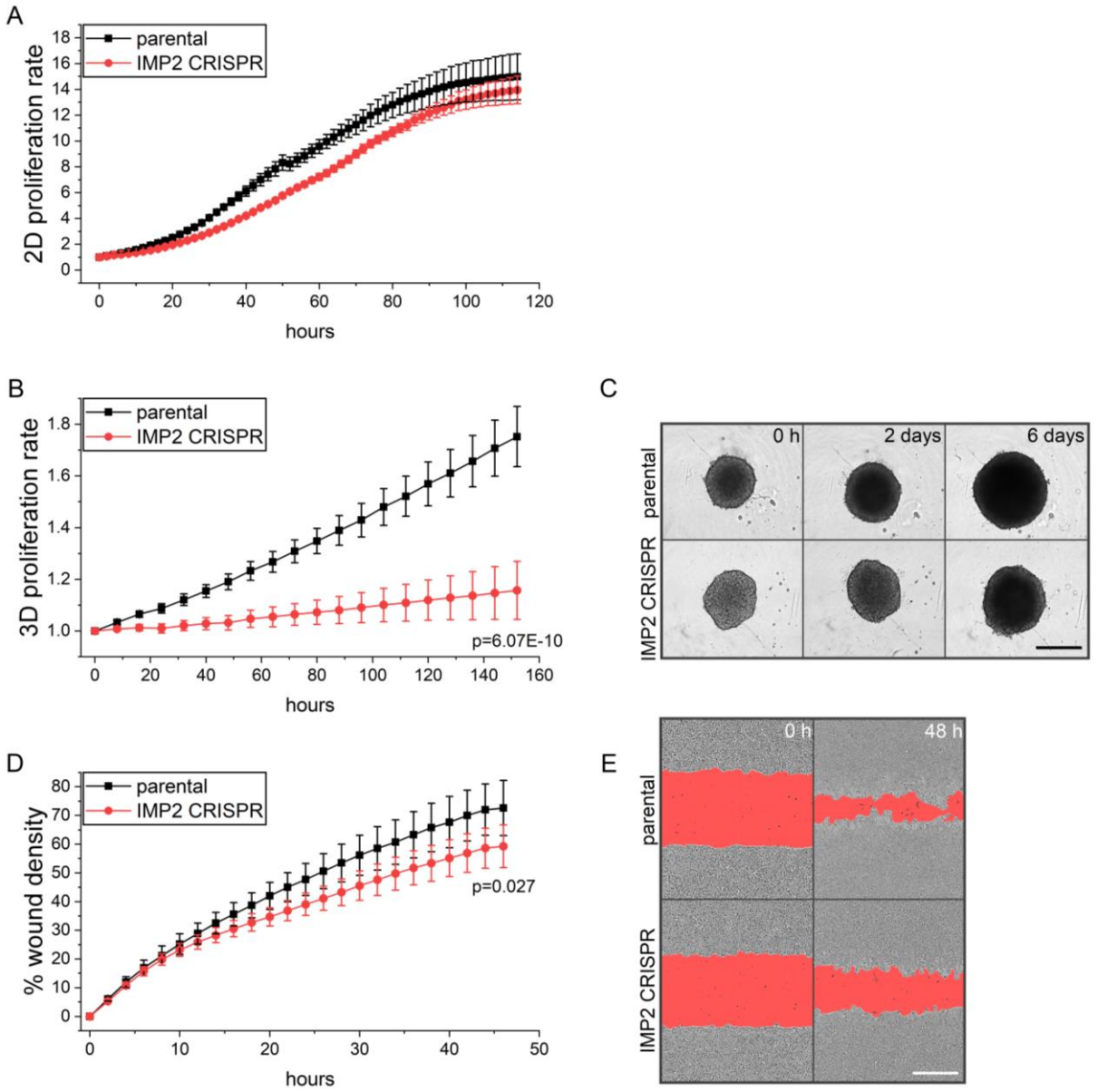

Figure 43. *In vitro* IMP2 target validation on tumor cell proliferation and migration.
IMP2 CRISPR knockout and parental HCT116 cells were monitored in an IncuCyte® S3 system.
(**A**) Cell confluency of 2D cell cultures was analyzed by the IncuCyte basic analyzer and normalized to the time point 0 h (10% confluency); n=3 (quadruplicates).
(**B**) After spheroid formation for 3 days, spheroid area growth was analyzed using the IncuCyte spheroid analyzer. Spheroid area was normalized to 3 day old spheroids (0 h); n=2 (quadruplicates).
(**C**) Representative pictures are shown for the starting point (0 h), 2 days, and 6 days after measurement initiation.
(**D**) Migratory activity was analyzed in a scratch wound assay. % wound density was analyzed by the IncuCyte migration analyzer and normalized to the time point of scratch performance (0 h); n=3 (quadruplicates).
(**E**) Representative pictures demonstrate the wound area in red at the starting point (0 h) and 48 h after wounding.
Data are presented as mean values ± SEM. Statistical analysis was performed by a two-tailed student's t-test.

4.2.2.2 IMP2 knockout reduces tumor growth in vivo

Since IMP2 knockout strongly decreased 3D proliferation of HCT116 cells, we further evaluated its effects in a zebrafish embryo *in vivo* xenograft model. Indeed, the absence of IMP2 resulted in a significantly diminished tumor growth after 3 days (**Figure 44**).

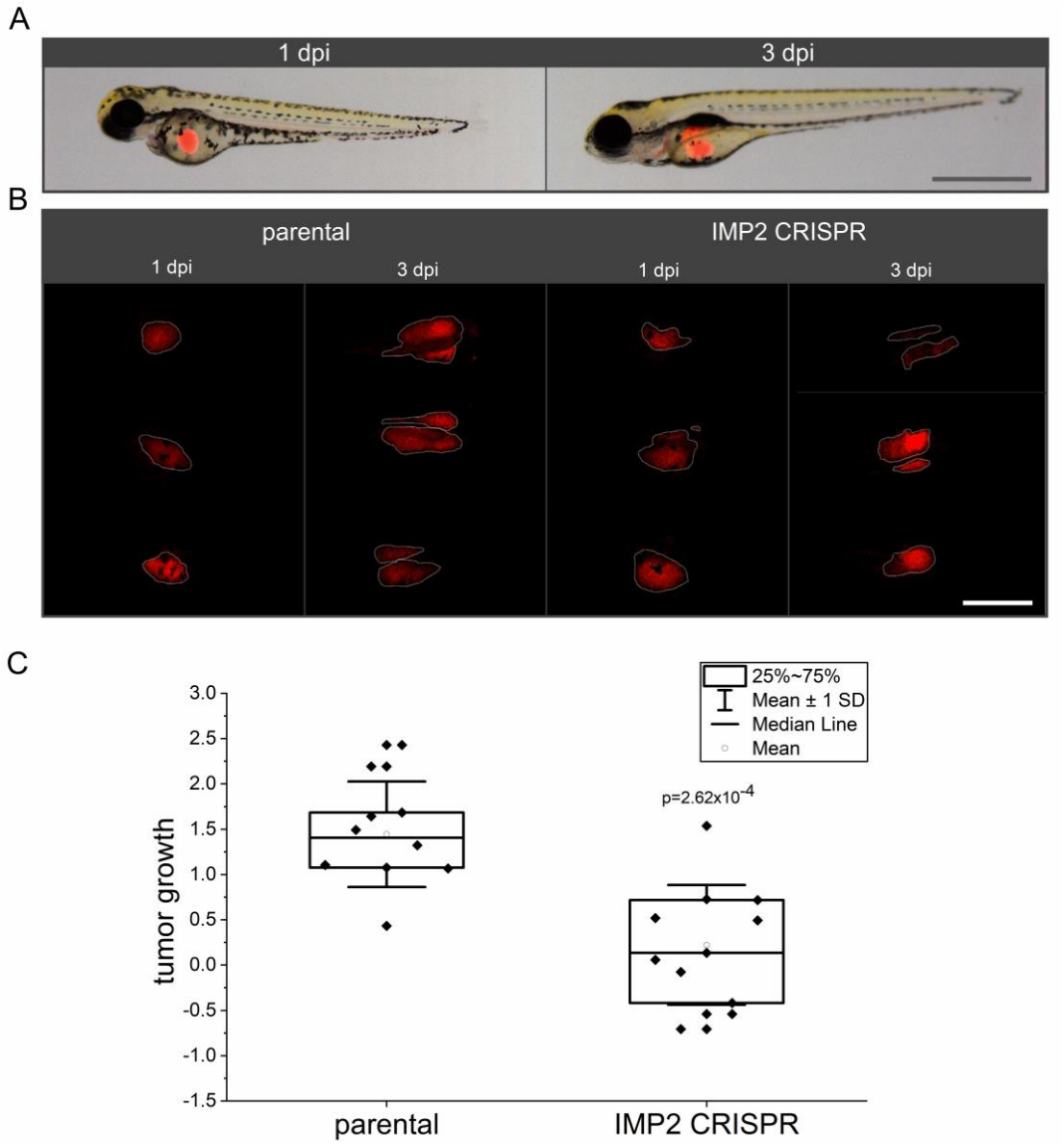

Figure 44. *In vivo* IMP2 target validation on tumor cell proliferation.
Fluorescence-labeled parental or IMP2 CRISPR knockout HCT116 cells were injected into the yolk sac of 2 dpf zebrafish embryos.
(**A**) Embryos (brightfield) and tumor mass (fluorescent channel) were imaged at 1 dpi and 3 dpi. Representative, merged images are shown; scale bar = 1 mm.
(**B**) Tumor areas were analyzed using ImageJ based on red fluorescent signals; scale bar = 0.5 mm.
(**C**) Quantification of tumor growth is represented as individual values in a box blot.
Statistical analysis was performed by a two-tailed student's t-test.

4.2.2.3 Biological activity of IMP2 inhibitors in vivo

Ali Abuhaliema (Pharmaceutical Biology, Saarland University) screened different compound libraries for IMP2 inhibitors using a fluorescence polarization assay. Hit compounds were tested for their biological activity and demonstrated a specificity for cells expressing high levels of IMP2 in a metabolic viability assay and an impedance-based proliferation assay (Abuhaliema et al. 2020, *submitted*).

In order to assess the biological activity of the hit compounds *in vivo,* we selected 3 promising compounds based on their activity in HCT116 cells *in vitro* (low IC_{50} values, target specificity, low toxicity in differentiated Huh7 cells) for *in vivo* studies in zebrafish embryos. The compounds were synthesized by Ben Zoller (Department of Microbial Natural Products, Helmholtz Institute for Pharmaceutical Research Saarland (HIPS)).

To test their toxicity in zebrafish embryos, compounds 4, 6, and 9 (**Figure 45**) were first administered in the fish water of 2 dpf embryos. Embryos were observed microscopically for normal development, heartbeat, and pigmentation. The concentration of 30 µM resulted in a 100% toxicity after 1 day treatment for all compounds (**Table 9**). Lower concentrations of compounds 4 and 9 showed no effects after 1 day treatment but affected embryo viability and development from day two on.

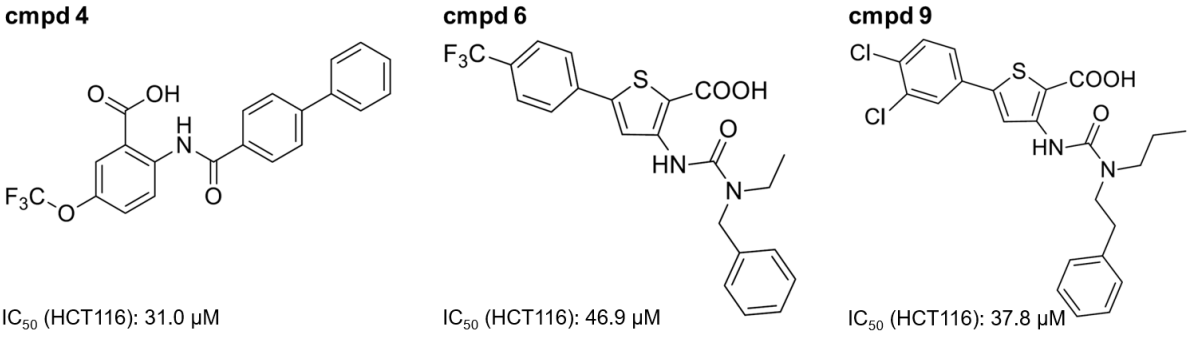

Figure 45. Structures IC_{50} values of IMP2 inhibitors.
Compounds (cmpd) inhibiting IMP2 were identified, and MTT-based IC_{50} values for HCT116 cells were calculated by Ali Abuhaliema (Pharmaceutical Biology, Saarland University).

Table 9. Toxicity of IMP2 inhibitors in zebrafish embryos.
8-10 2 dpf embryos were treated with the respective treatment and observed microscopically 1, 2, and 3 days after treatment. Table includes the percentage of dead embryos.

		1 day treatment	2 days treatment	3 days treatment
cmpd 4	5 µM	0%	50%	75%
	10 µM	0%	100%	
	30 µM	100%		
	100 µM	100%		
	300 µM	100%		
cmpd 6	30 µM	100%		
	100 µM	100%		
	300 µM	100%		
cmpd 9	5 µM	0%	12.5% hunched axis	12.5% hunched axis
	10 µM	0%	25% hunched axis	25% hunched axis
	30 µM	100%		
	100 µM	100%		
	300 µM	100%		

Since concentrations below the IC_{50} for HCT116 cells administered in the fish water led to a disturbed embryonal development, compounds were injected together with HCT116 tumor cells for the zebrafish embryo xenograft model.

In this model, compounds 4 and 6 significantly inhibited tumor growth (**Figure 46 A**). Embryos showed no compound-induced toxicity after 3 days of treatment. Tumor-bearing and compound-injected embryos showed normal development, but compound 4 (50 µM) caused a somewhat hunched body axis in 22.7% of the embryos at 3 dpi (**Figure 46 B**).

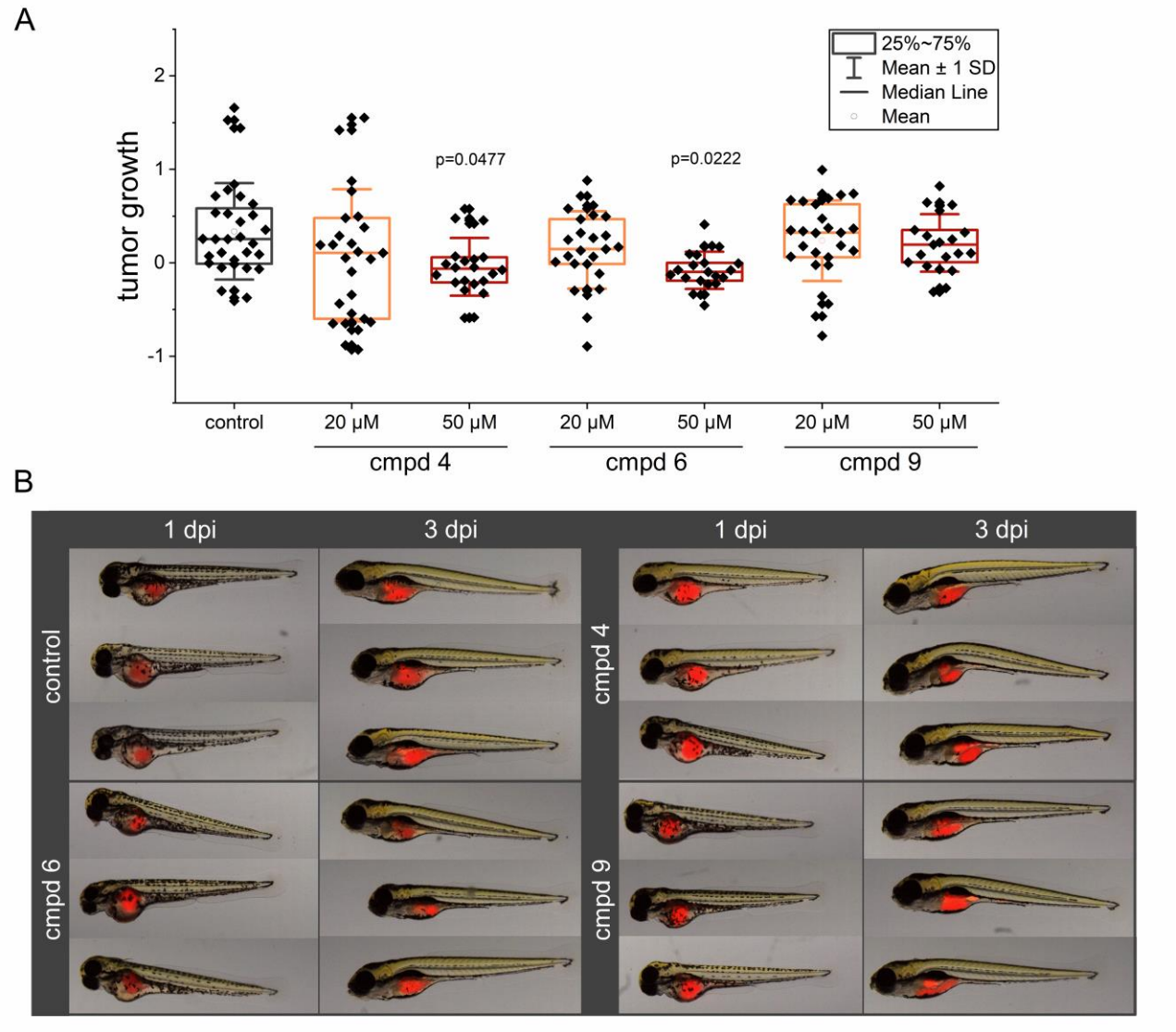

Figure 46. *In vivo* actions of IMP2 inhibitors in a xenograft zebrafish embryo model.
Fluorescence-labeled HCT116 cells suspended in compounds (cmpd) 4, 6, 9 (20 µM and 50 µM) or solvent control containing PBS/BSA were injected into the yolk sac of 2 dpf zebrafish embryos. Embryos were imaged at 1 and 3 dpi, and tumor area was quantified based on red fluorescent signals using ImageJ.
(**A**) Quantification is represented as individual growth values in a box plot.
(**B**) Representative pictures of 50 µM or control-treated embryos are shown.
Statistical analysis was performed using one-way ANOVA followed by Tukey´s post-hoc analysis.

4.2.3 Discussion

RBPs have raised attention as potential drug targets in cancer treatment due to their important role in various physiological functions (Mohibi et al., 2019). In this context, the RBP HuR has been studied rather extensively, and small molecule inhibitors have been identified (Meisner et al., 2007; Nasti et al., 2017; Della Volpe et al., 2019).

The RBP IMP2 has been suggested to promote tumorigenesis and tumor progression in several cancers. *IMP2* amplification is a frequent event in many cancer entities, and its abundance exceeds that of the paralogues *IMP1* and *IMP3* (Dai et al., 2017).

In our study, we validated IMP2 as a promising anti-cancer drug target *in vitro* and *in vivo* in colorectal cancer cells. CRISPR-mediated IMP2 knockout HCT116 cells revealed reduced proliferative and migratory capacities compared to their parental counterparts. These data are in line with findings, which describe a reduced colony proliferation of shRNA knockdown colon cancer cells (Ye et al., 2016). IMP2 overexpression resulted in increased tumor growth of pancreatic cancer cells in a mouse xenograft model (Xu et al., 2019). To the best of our knowledge, this study provides the first *in vivo* data underscoring the importance of IMP2 in a colon cancer xenograft model.

These promising results were the basis for a compound screening for small molecules inhibiting IMP2 - target interactions, performed by Ali Abuhaliema (Pharmaceutical Biology, Saarland University).

In vitro experiments of these hit compounds, performed by Ali Abuhaliema, revealed biological activity by inhibition of cell proliferation and target specificity by a reduced effect on IMP2 knockout cells. In addition to target specificity, two out of three tested compounds, tested in this study, also reduced tumor growth *in vivo* in a zebrafish xenograft model.

The exposure of zebrafish embryos to inhibitor-containing fish water caused severe toxicity, while administration *via* injection into the yolk sac was well tolerated. Zebrafish possess 69% human orthologues displaying 70% identity. However, functional domains, which often serve as drug binding targets, are more conserved (Langheinrich, 2003; Maurer and Quimby, 2015). In the case of human IGF2BP2, homologs have been identified in *Danio rerio* (Gaynes et al., 2015). Three viable *Igf2bp2* mutants, carrying a transgenic insertion at 3 different positions in the introns, have been obtained in large-scale mutagenesis of the zebrafish genome (Varshney et al., 2013). In wild-type embryos *Igf2bp2* was expressed equally in 1, 3, and 5 dpf embryos,

and morpholino antisense oligonucleotide-mediated knockdown resulted in viable embryos, which showed a somewhat hunched body axis (O'Hare et al., 2016). An explanation of the discrepancy between compound-induced toxicity seen after external exposure and injection remains elusive. It is conceivable that IGF2BP2 also plays a role in zebrafish development, and the comparably higher total compound amount in the fish water results in embryonic toxicity. Another possible explanation might be that yolk sac-injected compounds act mainly locally in the yolk sac without large tissue distribution or are metabolized differently, leading to lower toxicity.

In mouse models, IGF2BP2 total knockdown results in viable pups having a reduced body length and body weight, and a longer life than their littermates (Dai et al., 2015). On the other hand, *Igf2bp2* null females show reduced fertility, and maternal deletion of *Igf2bp2* in mouse embryos caused early embryonic developmental arrest *in vitro* at the 2-cell-stage and only 6% of embryos developed into the blastocyst-stage (Liu et al., 2019).

BTYNB, a small molecule inhibitor, was identified to inhibit the interaction between IMP1 and its target *c-Myc* and thereby inhibiting tumor cell proliferation in ovarian cancer and melanoma cells (Mahapatra et al., 2017). To the best of our knowledge, ours is the first study to show active inhibitors of an IMP family member *in vivo*.

Taken together, our data describe the RBP IMP2 as a novel druggable target for the treatment of gastrointestinal tumors.

5 Summary and conclusion

This study pursued different strategies to identify novel therapeutic approaches for solid tumors. A phenotypic approach was conducted in the first part, integrating different hallmarks of cancer. Besides the tumor-centric evaluation of effects exerted by natural compounds, macrophage phenotypes were included since they represent critical players in the tumor microenvironment. In this approach, 12 newly identified natural compounds from 4 distinct classes of bacterial secondary metabolites were characterized.

In conclusion, the metabolic modulator thioholgamide A exhibits an interesting biological profile orchestrating different hallmarks of cancer in cancer cells and macrophages. In combination with its low toxicity in non-tumorigenic cells and *in vivo*, thioholgamide A represents an interesting candidate for further preclinical testing. The first structural modifications of thioholgamide A in two derivatives did not lead to improved biological activity. The observed anti-tumor effects, in combination with macrophage repolarization initiated by the inhibition of oxidative phosphorylation, could serve as an attractive tumor therapeutic strategy.

The characterization of natural products from other classes revealed moderate activities against tumor growth. In this evaluation, auratryptanon stood out because of its induction of reactive oxygen species production. In macrophages, auratryptanon showed the most substantial effects on M1 macrophage viability. In the context of the tumor microenvironment, their depletion could lead to further undesirable immunocompromising effects in the tumor tissue.

In general, different strategies can be used to specifically target macrophages of the tumor microenvironment. In addition to the identification of macrophage-selective targets, the delivery of compounds into macrophages by taking advantage of their phagocytic activity represents a promising approach. In this study, we identified *Saccharomyces cerevisiae* as a macrophage-specific delivery vehicle for nanoparticles.

In the second part of this study, the role of IMP2 in pancreatic ductal adenocarcinoma was investigated. High IMP2 expression demonstrated to correlate with cancer progression and poor survival, making it an interesting diagnostic and prognostic marker as well as a novel target for the treatment of pancreatic ductal adenocarcinoma.

In a target-centric approach, IMP2 was validated *in vitro* and *in vivo* as an anti-cancer target in another malignancy in the gastrointestinal system, i.e., colon cancer.

Anti-proliferative activities of potential IMP2 inhibitors were moreover demonstrated in an *in vivo* xenograft zebrafish embryo model, revealing IMP2 as an interesting novel target for cancer therapy.

6 References

Ahmed, Y., Rebets, Y., Estévez, M.R., Zapp, J., Myronovskyi, M., and Luzhetskyy, A. (2020). Engineering of *Streptomyces lividans* for heterologous expression of secondary metabolite gene clusters. Microb. Cell Fact. *19*, 5.

Alvi, K.A., Baker, D.D., Stienecker, V., Hosken, M., and Nair, B.G. (2000). Identification of inhibitors of inducible nitric oxide synthase from microbial extracts. J. Antibiot. *53*, 496–501.

Amoozgar, Z., and Goldberg, M.S. (2015). Targeting myeloid cells using nanoparticles to improve cancer immunotherapy. Adv. Drug Deliv. Rev. *91*, 38–51.

Ashton, T.M., Gillies McKenna, W., Kunz-Schughart, L.A., and Higgins, G.S. (2018). Oxidative phosphorylation as an emerging target in cancer therapy. Clin. Cancer Res. *24*, 2482–2490.

Astanina, K., Koch, M., Jüngst, C., Zumbusch, A., and Kiemer, A.K. (2015). Lipid droplets as a novel cargo of tunnelling nanotubes in endothelial cells. Sci. Rep. *5*, 1–13.

Aune, G.J., Furuta, T., and Pommier, Y. (2002). Ecteinascidin 743: a novel anticancer drug with a unique mechanism of action. Anticancer. Drugs *13*, 545–555.

Azizi, E., Carr, A.J., Plitas, G., Cornish, A.E., Konopacki, C., Prabhakaran, S., Nainys, J., Wu, K., Kiseliovas, V., Setty, M., et al. (2018). Single-cell map of diverse immune phenotypes in the breast tumor microenvironment. Cell *174*, 1293-1308.e36.

Baker, D.D., Chu, M., Oza, U., and Rajgarhia, V. (2007). The value of natural products to future pharmaceutical discovery. Nat. Prod. Rep. *24*, 1225–1244.

Bao, J., He, F., Li, Y., Fang, L., Wang, K., Song, J., Zhou, J., Li, Q., and Zhang, H. (2018). Cytotoxic antibiotic angucyclines and actinomycins from the *Streptomyces* sp. XZHG99T. J. Antibiot. *71*, 1018–1024.

Barghash, A., Helms, V., and Kessler, S.M. (2015). Overexpression of *IGF2* mRNA-binding protein 2 (IMP2/p62) as a feature of basal-like breast cancer correlates with short survival. Scand. J. Immunol. *82*, 142–143.

Barghash, A., Golob-Schwarzl, N., Helms, V., Haybaeck, J., and Kessler, S.M. (2016). Elevated expression of the *IGF2* mRNA binding protein 2 (IGF2BP2/IMP2) is linked to short survival and metastasis in esophageal adenocarcinoma. Oncotarget *7*, 49743–49750.

Bell, J.L., Wächter, K., Mühleck, B., Pazaitis, N., Köhn, M., Lederer, M., and Hüttelmaier, S. (2013). Insulin-like growth factor 2 mRNA-binding proteins (IGF2BPs): post-transcriptional drivers of cancer progression? Cell. Mol. Life Sci. *70*, 2657–2675.

Biswas, S.K., Chittezhath, M., Shalova, I.N., and Lim, J.Y. (2012). Macrophage polarization and plasticity in health and disease. Immunol. Res. *53*, 11–24.

Bonapace, L., Coissieux, M.M., Wyckoff, J., Mertz, K.D., Varga, Z., Junt, T., and Bentires-Alj, M. (2014). Cessation of CCL2 inhibition accelerates breast cancer metastasis by promoting angiogenesis. Nature *515*, 130–133.

Van den Bossche, J., Baardman, J., Otto, N.A., van der Velden, S., Neele, A.E., van den Berg, S.M., Luque-Martin, R., Chen, H.J., Boshuizen, M.C.S., Ahmed, M., et al. (2016). Mitochondrial dysfunction prevents repolarization of inflammatory macrophages. Cell Rep. *17*, 684–696.

Van den Bossche, J., O'Neill, L.A., and Menon, D. (2017). Macrophage immunometabolism: where are we (going)? Trends Immunol. *38*, 395–406.

Boudoukha, S., Cuvellier, S., and Polesskaya, A. (2010). Role of the RNA-binding protein IMP-2 in muscle cell motility. Mol. Cell. Biol. *30*, 5710–5725.

Bray, F., Ferlay, J., Soerjomataram, I., Siegel, R.L., Torre, L.A., and Jemal, A. (2018). Global cancer statistics 2018: GLOBOCAN estimates of incidence and mortality worldwide for 36 cancers in 185 countries. CA. Cancer J. Clin. *68*, 394–424.

Cao, J., Mu, Q., and Huang, H. (2018). The roles of insulin-like growth factor 2 mRNA-binding protein 2 in cancer and cancer stem cells. Stem Cells Int. 4217259.

Cao, Y., Huang, H., Wang, Z., and Zhang, G. (2017). The inflammatory CXC chemokines, GROα^{high}, IP-10^{low}, and MIG^{low}, in tumor microenvironment can be used as new indicators for non-small cell lung cancer progression. Immunol. Invest. *46*, 361–374.

Carmona-Fontaine, C., Deforet, M., Akkari, L., Thompson, C.B., Joyce, J.A., and Xavier, J.B. (2017). Metabolic origins of spatial organization in the tumor microenvironment. Proc. Natl. Acad. Sci. U. S. A. *114*, 2934–2939.

Carter, N.J., and Keam, S.J. (2007). Trabectedin: a review of its use in the management of soft tissue sarcoma and ovarian cancer. Drugs *67*, 2257–2276.

Cassetta, L., and Pollard, J.W. (2018). Targeting macrophages: therapeutic approaches in cancer. Nat. Rev. Drug Discov. *17*, 887–904.

Chang, C.H., Qiu, J., O'Sullivan, D., Buck, M.D., Noguchi, T., Curtis, J.D., Chen, Q., Gindin, M., Gubin, M.M., Van Der Windt, G.J.W., et al. (2015). Metabolic competition in the tumor microenvironment is a driver of cancer progression. Cell *162*, 1229–1241.

Chen, X., and Song, E. (2019). Turning foes to friends: targeting cancer-associated fibroblasts. Nat. Rev. Drug Discov. *18*, 99–115.

Chen, W., Sandoval, H., Kubiak, J.Z., Li, X.C., Ghobrial, R.M., and Kloc, M. (2018). The phenotype of peritoneal mouse macrophages depends on the mitochondria and ATP/ADP homeostasis. Cell. Immunol. *324*, 1–7.

Chevrier, S., Levine, J.H., Zanotelli, V.R.T., Silina, K., Schulz, D., Bacac, M., Ries, C.H., Ailles, L., Jewett, M.A.S., Moch, H., et al. (2017). An immune atlas of clear cell renal cell carcinoma. Cell *169*, 736-749.e18.

Chopra, A., Willmore, W.G., and Biggar, K.K. (2019). Protein quantification and visualization *via* ultraviolet-dependent labeling with 2,2,2-trichloroethanol. Sci. Rep. *9*, 1–8.

Christiansen, J., Kolte, A.M., Hansen, T.V.O., and Nielsen, F.C. (2009). *IGF2* mRNA-binding protein 2: biological function and putative role in type 2 diabetes. J. Mol. Endocrinol. *43*, 187–195.

Chung, W., Eum, H.H., Lee, H.O., Lee, K.M., Lee, H.B., Kim, K.T., Ryu, H.S., Kim, S., Lee, J.E., Park, Y.H., et al. (2017). Single-cell RNA-seq enables comprehensive tumour and immune cell profiling in primary breast cancerng. Nat. Commun. *8*, 1–12.

Courtnay, R., Ngo, D.C., Malik, N., Ververis, K., Tortorella, S.M., and Karagiannis, T.C. (2015). Cancer metabolism and the Warburg effect: the role of HIF-1 and PI3K. Mol. Biol. Rep. *42*, 841–851.

Crnogorac-Jurcevic, T., Chelala, C., Barry, S., Harada, T., Bhakta, V., Lattimore, S., Jurcevic, S., Bronner, M., Lemoine, N.R., and Brentnall, T.A. (2013). Molecular analysis of precursor lesions in familial pancreatic cancer. PLoS One *8*, 1–14.

Cuccarese, M.F., Dubach, J.M., Pfirschke, C., Engblom, C., Garris, C., Miller, M.A., Pittet, M.J., and Weissleder, R. (2017). Heterogeneity of macrophage infiltration and therapeutic response in lung carcinoma revealed by 3D organ imaging. Nat. Commun. *8*.

Czepukojc, B., Abuhaliema, A., Barghash, A., Tierling, S., Naß, N., Simon, Y., Körbel, C., Cadenas, C., van Hul, N., Sachinidis, A., et al. (2019). *IGF2* mRNA binding protein 2 transgenic mice are more prone to develop a ductular reaction and to progress toward cirrhosis. Front. Med. *6*, 1–16.

Dai, N., Rapley, J., Ange, M., Yanik, F.M., Blower, M.D., and Avruch, J. (2011). mTOR phosphorylates IMP2 to promote *IGF2* mRNA translation by internal ribosomal entry. Genes Dev. *25*, 1159–1172.

Dai, N., Zhao, L., Wrighting, D., Krämer, D., Majithia, A., Wang, Y., Cracan, V., Borges-Rivera, D., Mootha, V.K., Nahrendorf, M., et al. (2015). IGF2BP2/IMP2-deficient mice resist obesity through enhanced translation of *Ucp1* mRNA and other mRNAs encoding mitochondrial proteins. Cell Metab. *21*, 609–621.

Dai, N., Ji, F., Wright, J., Minichiello, L., Sadreyev, R., and Avruch, J. (2017). *IGF2* mRNA binding protein-2 is a tumor promoter that drives cancer proliferation through its client mRNAs *IGF2* and *HMGA1*. elife *6*, 1–21.

Degrauwe, N., Suvà, M.L., Janiszewska, M., Riggi, N., and Stamenkovic, I. (2016). IMPs: an RNA-binding protein family that provides a link between stem cell maintenance in normal development and cancer. Genes Dev. *30*, 2459–2474.

Dehne, N., Mora, J., Namgaladze, D., Weigert, A., and Brüne, B. (2017). Cancer cell and macrophage cross-talk in the tumor microenvironment. Curr. Opin. Pharmacol. *35*, 12–19.

DeNardo, D.G., and Ruffell, B. (2019). Macrophages as regulators of tumour immunity and immunotherapy. Nat. Rev. Immunol. *19*, 369–382.

Desbats, M.A., Giacomini, I., Prayer-Galetti, T., and Montopoli, M. (2020). Metabolic plasticity in chemotherapy resistance. Front. Oncol. *10*.

Dharmaraja, A.T. (2017). Role of reactive oxygen species (ROS) in therapeutics and drug resistance in cancer and bacteria. J. Med. Chem. *60*, 3221–3240.

Diestel, R., Irschik, H., Jansen, R., Khalil, M.W., Reichenbach, H., and Sasse, F. (2009). Chivosazoles A and F, cytostatic macrolides from myxobacteria, interfere with actin. ChemBioChem *10*, 2900–2903.

Divakaruni, A.S., Paradyse, A., Ferrick, D.A., Murphy, A.N., and Jastroch, M. (2014). Analysis and interpretation of microplate-based oxygen consumption and pH data (Elsevier Inc.).

Doering, M., Diesel, B., Gruhlke, M.C.H., Viswanathan, U.M., Mániková, D., Chovanec, M., Burkholz, T., Slusarenko, A.J., Kiemer, A.K., and Jacob, C. (2012). Selenium- and tellurium-containing redox modulators with distinct activity against macrophages: possible implications for the treatment of inflammatory diseases. Tetrahedron *68*, 10577–10585.

Eder, J., Sedrani, R., and Wiesmann, C. (2014). The discovery of first-in-class drugs: origins and evolution. Nat. Rev. Drug Discov. *13*, 577–587.

El-Shamy, A., Eng, F.J., Doyle, E.H., Klepper, A.L., Sun, X., Sangiovanni, A., Iavarone, M., Colombo, M., Schwartz, R.E., Hoshida, Y., et al. (2015). A cell culture system for distinguishing hepatitis C viruses with and without liver cancer-related mutations in the viral core gene. J. Hepatol. *63*, 1323–1333.

Elia, I., Doglioni, G., and Fendt, S.M. (2018). Metabolic hallmarks of metastasis formation. Trends Cell Biol. *28*, 673–684.

Elliott, M.R., Koster, K.M., and Murphy, P.S. (2017). Efferocytosis signaling in the regulation of macrophage inflammatory responses. J. Immunol. *198*, 1387–1394.

Epelman, S., Lavine, K.J., and Randolph, G.J. (2014). Origin and Functions of Tissue Macrophages. Immunity *41*, 21–35.

Filho, V.C. (2018). Natural products as source of molecules with therapeutic potential.

Fouad, Y.A., and Aanei, C. (2017). Revisiting the hallmarks of cancer. Am. J. Cancer Res. *7*, 1016–1036.

Frattaruolo, L., Fiorillo, M., Brindisi, M., Curcio, R., Dolce, V., Lacret, R., Truman, A., Sotgia, F., Lisanti, M.P., and Cappello, A.R. (2019). Thioalbamide, a thioamidated peptide from amycolatopsis alba, affects tumor growth and stemness by inducing metabolic dysfunction and oxidative stress. Cells *8*, 1408.

Galadari, S., Rahman, A., Pallichankandy, S., and Thayyullathil, F. (2017). Reactive oxygen species and cancer paradox: to promote or to suppress? Free Radic. Biol. Med. *104*, 144–164.

Gaynes, J.A., Otsuna, H., Campbell, D.S., Manfredi, J.P., Levine, E.M., and Chien, C. Bin (2015). The RNA binding protein Igf2bp1 is required for zebrafish RGC axon outgrowth *in vivo*. PLoS One *10*, 1–20.

Geeraerts, X., Bolli, E., Fendt, S.M., and Van Ginderachter, J.A. (2017). Macrophage metabolism as therapeutic target for cancer, atherosclerosis, and obesity. Front. Immunol. *8*.

Germano, G., Frapolli, R., Belgiovine, C., Anselmo, A., Pesce, S., Liguori, M., Erba, E., Uboldi, S., Zucchetti, M., Pasqualini, F., et al. (2013). Role of macrophage targeting in the antitumor activity of trabectedin. Cancer Cell *23*, 249–262.

Gilkes, D.M., Semenza, G.L., and Wirtz, D. (2014). Hypoxia and the extracellular matrix: drivers of tumour metastasis. Nat. Rev. Cancer *16*, 430–439.

Ginhoux, F., Schultze, J.L., Murray, P.J., Ochando, J., and Biswas, S.K. (2016). New insights into the multidimensional concept of macrophage ontogeny, activation and function. Nat. Immunol. *17*, 34–40.

Gordon, S., Plüddemann, A., and Martinez Estrada, F. (2014). Macrophage heterogeneity in tissues: phenotypic diversity and functions. Immunol. Rev. *262*, 36–55.

Gürtler, A., Kunz, N., Gomolka, M., Hornhardt, S., Friedl, A.A., McDonald, K., Kohn, J.E., and Posch, A. (2013). Stain-Free technology as a normalization tool in Western blot analysis. Anal. Biochem. *433*, 105–111.

Hafner, M., Landthaler, M., Burger, L., Khorshid, M., Hausser, J., Berninger, P., Rothballer, A., Ascano, M., Jungkamp, A.C., Munschauer, M., et al. (2010). Transcriptome-wide identification of RNA-binding protein and microRNA target sites by PAR-CLIP. Cell *141*, 129–141.

Han, K., Pierce, S.E., Li, A., Spees, K., Anderson, G.R., Seoane, J.A., Lo, Y.H., Dubreuil, M., Olivas, M., Kamber, R.A., et al. (2020). CRISPR screens in cancer spheroids identify 3D growth-specific vulnerabilities. Nature *580*, 136–141.

Hanahan, D., and Weinberg, R.A. (2000). The hallmarks of cancer. Cell *100*, 57–70.

Hanahan, D., and Weinberg, R.A. (2011). Hallmarks of cancer: the next generation. Cell *144*, 646–674.

Hayakawa, Y., Sasaki, K., Adachi, H., Furihata, K., Nagai, K., and Shin-ya, K. (2006). Thioviridamide, a novel apoptosis inducer in transformed cells from streptomyces olivoviridis. J. Antibiot. *59*, 1–5.

He, X., Li, W., Liang, X., Zhu, X., Zhang, L., Huang, Y., Yu, T., Li, S., and Chen, Z. (2018). IGF2BP2 overexpression indicates poor survival in patients with acute myelocytic leukemia. Cell. Physiol. Biochem. *51*, 1945–1956.

Vander Heiden, M.G., and DeBerardinis, R.J. (2017). Understanding the intersections between metabolism and cancer biology. Cell *168*, 657–669.

Vander Heiden, M.G., Cantley, L.C., and Thompson, C.B. (2009). Understanding the Warburg effect: the metabolic requirements of cell proliferation. Science (80-.). *324*, 1029–1033.

Helm, O., Held-Feindt, J., Grage-Griebenow, E., Reiling, N., Ungefroren, H., Vogel, I., Krüger, U., Becker, T., Ebsen, M., Röcken, C., et al. (2014). Tumor-associated macrophages exhibit pro- and anti-inflammatory properties by which they impact on pancreatic tumorigenesis. Int. J. Cancer *135*, 843–861.

Hinshaw, D.C., and Shevde, L.A. (2019). The tumor microenvironment innately modulates cancer progression. Cancer Res. *79*, 4557–4567.

Huang, R. sheng, Zheng, Y. liang, Li, C., Ding, C., Xu, C., and Zhao, J. (2018). MicroRNA-485-5p suppresses growth and metastasis in non-small cell lung cancer cells by targeting IGF2BP2. Life Sci. *199*, 104–111.

Huang, S., Wu, Z., Cheng, Y., Wei, W., and Hao, L. (2019). Insulin-like growth factor 2 mRNA binding protein 2 promotes aerobic glycolysis and cell proliferation in pancreatic ductal adenocarcinoma *via* stabilizing *GLUT1* mRNA. Acta Biochim. Biophys. Sin. *51*, 743–752.

Hume, D.A., Irvine, K.M., and Pridans, C. (2019). The mononuclear phagocyte system: the relationship between monocytes and macrophages. Trends Immunol. *40*, 98–112.

Huss, M., and Wieczorek, H. (2009). Inhibitors of V-ATPases: old and new players. J. Exp. Biol. *212*, 341–346.

Irvine, D.J., and Dane, E.L. (2020). Enhancing cancer immunotherapy with nanomedicine. Nat. Rev. Immunol.

Jänicke, R.U., Sprengart, M.L., Wati, M.R., and Porter, A.G. (1998). Caspase-3 is required for DNA fragmentation and morphological changes associated with apoptosis. J. Biol. Chem. *273*, 9357–9360.

Janiszewska, M., Suvà, M.L., Riggi, N., Houtkooper, R.H., Auwerx, J., Clément-Schatlo, V., Radovanovic, I., Rheinbay, E., Provero, P., and Stamenkovic, I. (2012). Imp2 controls oxidative

phosphorylation and is crucial for preservin glioblastoma cancer stem cells. Genes Dev. *26*, 1926–1944.

Jemal, A., Ward, E.M., Johnson, C.J., Cronin, K.A., Ma, J., Ryerson, A.B., Mariotto, A., Lake, A.J., Wilson, R., Sherman, R.L., et al. (2017). Annual report to the nation on the status of cancer, 1975-2014, featuring survival. J. Natl. Cancer Inst. *109*, 1–22.

Kenngott, E.E., Kiefer, R., Schneider-Daum, N., Hamann, A., Schneider, M., Schmitt, M.J., and Breinig, F. (2016). Surface-modified yeast cells: a novel eukaryotic carrier for oral application. J. Control. Release *224*, 1–7.

Kessler, S., Haybaeck, J., and Kiemer, A. (2016). Insulin-like growth factor 2 - The oncogene and its accomplices. Curr. Pharm. Des. *22*, 5948–5961.

Kessler, S.M., Pokorny, J., Zimmer, V., Laggai, S., Lammert, F., Bohle, R.M., and Kiemer, A.K. (2013). *IGF2* mRNA binding protein p62/IMP2-2 in hepatocellular carcinoma: antiapoptotic action is independent of IGF2/PI3K signaling. Am. J. Physiol. - Gastrointest. Liver Physiol. *304*, 328–336.

Kessler, S.M., Laggai, S., Barghash, A., Schultheiss, C.S., Lederer, E., Artl, M., Helms, V., Haybaeck, J., and Kiemer, A.K. (2015a). IMP2/p62 induces genomic instability and an aggressive hepatocellular carcinoma phenotype. Cell Death Dis. *6*, 1–12.

Kessler, S.M., Laggai, S., Kiemer, A.K., Barghash, A., and Helms, V. (2015b). Hepatic hepcidin expression is decreased in cirrhosis and HCC. J. Hepatol. *62*, 977–979.

Kessler, S.M., Lederer, E., Laggai, S., Golob-Schwarzl, N., Hosseini, K., Petzold, J., Schweiger, C., Reihs, R., Keil, M., Hoffmann, J., et al. (2017). IMP2/IGF2BP2 expression, but not IMP1 and IMP3, predicts poor outcome in patients and high tumor growth rate in xenograft models of gallbladder cancer. Oncotarget *8*, 89736–89745.

Kharel, M.K., Pahari, P., Lian, H., and Rohr, J. (2010). Enzymatic total synthesis of rabelomycin, an angucycline group antibiotic. Org. Lett. *12*, 2814–2817.

Kharel, M.K., Pahari, P., Shepherd, M.D., Tibrewal, N., Nybo, S.E., Shaaban, K.A., and Rohr, J. (2012). Angucyclines: biosynthesis, mode-of-action, new natural products, and synthesis. Nat. Prod. Rep. *29*, 264–325.

Kiefer, R., Jurisic, M., Dahlem, C., Koch, M., Schmitt, M.J., Kiemer, A.K., Schneider, M., and Breinig, F. (2019). Targeted delivery of functionalized PLGA nanoparticles to macrophages by complexation with the yeast *Saccharomyces cerevisiae*. Biotechnol. Bioeng. *117*, 776-788.

Kingston, D.G.I. (2009). Tubulin-interactive natural products as anticancer agents. J. Nat. Prod. *72*, 507–515.

Kirchberger, S., Sturtzel, C., Pascoal, S., and Distel, M. (2017). Quo natas, Danio?—Recent progress in

modeling cancer in zebrafish. Front. Oncol. *7*.

Kirschning, A., Chen, G.W., Dräger, G., Schuberth, I., and Tietze, L.F. (2000). Syntheses and biological evaluation of new glyco-modified angucyclin-antibiotics. Bioorganic Med. Chem. *8*, 2347–2354.

Kittakoop, P., Mahidol, C., and Ruchirawat, S. (2014). Alkaloids as Important Scaffolds in Therapeutic Drugs for the Treatments of Cancer, Tuberculosis, and Smoking Cessation. Curr. Top. Med. Chem. *14*, 239–252.

Kjaerulff, L., Sikandar, A., Zaburannyi, N., Adam, S., Herrmann, J., Koehnke, J., and Müller, R. (2017). Thioholgamides: thioamide-containing cytotoxic RiPP natural products. ACS Chem. Biol. *12*, 2837–2841.

Krysko, O., Holtappels, G., Zhang, N., Kubica, M., Deswarte, K., Derycke, L., Claeys, S., Hammad, H., Brusselle, G.G., Vandenabeele, P., et al. (2011). Alternatively activated macrophages and impaired phagocytosis of *S. aureus* in chronic rhinosinusitis. Allergy. *66*, 396–403.

Kumar, S., Ramesh, A., Kulkarni, A., and Kumar, S. (2020). Targeting macrophages: a novel avenue for cancer drug discovery. Expert Opin. Drug Discov. *00*, 1–14.

Laggai, S., Kessler, S.M., Boettcher, S., Lebrun, V., Gemperlein, K., Lederer, E., Leclercq, I.A., Mueller, R., Hartmann, R.W., Haybaeck, J., et al. (2014). The *IGF2* mRNA binding protein p62/IGF2BP2-2 induces fatty acid elongation as a critical feature of steatosis. J. Lipid Res. *55*, 1087–1097.

Landwehr, W., Wolf, C., and Wink, J. (2016). Actinobacteria and myxobacteria—Two of the most important bacterial resources for novel antibiotics. Curr. Top. Microbiol. Immunol. *398*, 273–302.

Langheinrich, U. (2003). Zebrafish: a new model on the pharmaceutical catwalk. BioEssays *25*, 904–912.

Lavin, Y., Kobayashi, S., Leader, A., Amir, E. ad D., Elefant, N., Bigenwald, C., Remark, R., Sweeney, R., Becker, C.D., Levine, J.H., et al. (2017). Innate immune landscape in early lung adenocarcinoma by paired single-cell analyses. Cell *169*, 750–765.

Lebleu, V.S., O'Connell, J.T., Gonzalez Herrera, K.N., Wikman, H., Pantel, K., Haigis, M.C., De Carvalho, F.M., Damascena, A., Domingos Chinen, L.T., Rocha, R.M., et al. (2014). PGC-1α mediates mitochondrial biogenesis and oxidative phosphorylation in cancer cells to promote metastasis. Nat. Cell Biol. *16*, 992–1003.

Li, Y., Jia, A., Wang, Y., Dong, L., Wang, Y., He, Y., Wang, S., Cao, Y., Yang, H., Bi, Y., et al. (2019). Immune effects of glycolysis or oxidative phosphorylation metabolic pathway in protecting against bacterial infection. J. Cell. Physiol. *234*, 20298–20309.

Li, Y.C., Fung, K.P., Kwok, T.T., Lee, C.Y., Suen, Y.K., and Kong, S.K. (2004). Mitochondria-targeting drug oligomycin blocked P-glycoprotein activity and triggered apoptosis in doxorubicin-resistant HepG2 cells. Chemotherapy *50*, 55–62.

Liguori, M., Buracchi, C., Pasqualini, F., Bergomas, F., Pesce, S., Sironi, M., Grizzi, F., Mantovani, A., Belgiovine, C., and Allavena, P. (2016). Functional TRAIL receptors in monocytes and tumor-associated macrophages: a possible targeting pathway in the tumor microenvironment. Oncotarget *7*, 41662–41676.

Lim, S.Y., Yuzhalin, A.E., Gordon-Weeks, A.N., and Muschel, R.J. (2016). Targeting the CCL2-CCR2 signaling axis in cancer metastasis. Oncotarget *7*, 28697–28710.

Liu, D., Chang, C., Lu, N., Wang, X., Lu, Q., Ren, X., Ren, P., Zhao, D., Wang, L., Zhu, Y., et al. (2017). Comprehensive proteomics analysis reveals metabolic reprogramming of tumor-associated macrophages stimulated by the tumor microenvironment. J. Proteome Res. *16*, 288–297.

Liu, H. Bin, Muhammad, T., Guo, Y., Li, M.J., Sha, Q.Q., Zhang, C.X., Liu, H., Zhao, S.G., Zhao, H., Zhang, H., et al. (2019). RNA-binding protein IGF2BP2/IMP2 is a critical maternal activator in early zygotic genome activation. Adv. Sci. *6*, 1900295.

Liu, W., Parker, W.L., Slusarchyk, D.S., Greenwood, G.L., Graham, S.F., and Meyers, E. (1970). Isolation, characterization, and structure of rabelomycin, a new antibiotic. J. Antibiot. *XXIII*.

Liu, W., Li, Z., Xu, W., Wang, Q., and Yang, S. (2013). Humoral autoimmune response to IGF2 mRNA-Binding protein (IMP2/p62) and its tissue-specific expression in colon cancer. Scand. J. Immunol. *77*, 255–260.

Lu, M., Nakamura, R.M., Dent, E.D.B., Zhang, J.Y., Nielsen, F.C., Christiansen, J., Chan, E.K.L., and Tan, E.M. (2001). Aberrant expression of fetal RNA-binding protein p62 in liver cancer and liver cirrhosis. Am. J. Pathol. *159*, 945–953.

Mahapatra, L., Andruska, N., Mao, C., Le, J., and Shapiro, D.J. (2017). A novel IMP1 inhibitor, BTYNB, targets c-Myc and inhibits melanoma and ovarian cancer cell proliferation. Transl. Oncol. *10*, 818–827.

Maishi, N., and Hida, K. (2017). Tumor endothelial cells accelerate tumor metastasis. Cancer Sci. *108*, 1921–1926.

Mantovani, A., Biswas, S.K., Galdiero, M.R., Sica, A., and Locati, M. (2013). Macrophage plasticity and polarization in tissue repair and remodelling. J. Pathol. *229*, 176–185.

Mantovani, A., Marchesi, F., Malesci, A., Laghi, L., and Allavena, P. (2017). Tumour-associated macrophages as treatment targets in oncology. Nat. Rev. Clin. Oncol. *14*, 399–416.

Matassa, D.S., Amoroso, M.R., Lu, H., Avolio, R., Arzeni, D., Procaccini, C., Faicchia, D., Maddalena, F., Simeon, V., Agliarulo, I., et al. (2016). Oxidative metabolism drives inflammation-induced platinum resistance in human ovarian cancer. Cell Death Differ. *23*, 1542–1554.

Maurer, K.J., and Quimby, F.W. (2015). Animal Models in Biomedical Research (Elsevier Inc.).

McGuirk, S., Audet-Delage, Y., and St-Pierre, J. (2020). Metabolic Fitness and Plasticity in Cancer Progression. Trends in Cancer *6*, 49–61.

Meisner, N.C., Hintersteiner, M., Mueller, K., Bauer, R., Seifert, J.M., Naegeli, H.U., Ottl, J., Oberer, L., Guenat, C., Moss, S., et al. (2007). Identification and mechanistic characterization of low-molecular-weight inhibitors for HuR. Nat. Chem. Biol. *3*, 508–515.

Mohibi, S., Chen, X., and Zhang, J. (2019). Cancer the'RBP'eutics–RNA-binding proteins as therapeutic targets for cancer. Pharmacol. Ther. *203*.

Morimatsu, K., Aishima, S., Yamamoto, H., Hayashi, A., Nakata, K., Oda, Y., Shindo, K., Fujino, M., Tanaka, M., and Oda, Y. (2013). Insulin-like growth factor II messenger RNA-binding protein-3 is a valuable diagnostic and prognostic marker of intraductal papillary mucinous neoplasm. Hum. Pathol. *44*, 1714–1721.

Mu, Q., Wang, L., Yu, F., Gao, H., Lei, T., Li, P., Liu, P., Zheng, X., Hu, X., Chen, Y., et al. (2015). Imp2 regulates GBM progression by activating IGF2/PI3K/Akt pathway. Cancer Biol. Ther. *16*, 623–633.

Müeller-Pillasch, F., Lacher, U., Wallrapp, C., Micha, A., Zimmerhackl, F., Hameister, H., Varga, G., Friess, H., Büchler, M., Beger, H.G., et al. (1997). Cloning of a gene highly overexpressed in cancer coding for a novel KH-domain containing protein. Oncogene *14*, 2729–2733.

Müller, S., Kohanbash, G., Liu, S.J., Alvarado, B., Carrera, D., Bhaduri, A., Watchmaker, P.B., Yagnik, G., Di Lullo, E., Malatesta, M., et al. (2017). Single-cell profiling of human gliomas reveals macrophage ontogeny as a basis for regional differences in macrophage activation in the tumor microenvironment. Genome Biol. *18*, 1–14.

Murray, P.J., and Wynn, T.A. (2011). Protective and pathogenic functions of macrophage subsets. Nat. Rev. Immunol. *11*, 723–737.

Murray, P.J., Allen, J.E., Biswas, S.K., Fisher, E.A., Gilroy, D.W., Goerdt, S., Gordon, S., Hamilton, J.A., Ivashkiv, L.B., Lawrence, T., et al. (2014). Macrophage activation and polarization: nomenclature and experimental guidelines. Immunity *41*, 14–20.

Murthy, S.K. (2007). Nanoparticles in modern medicine: state of the art and future challenges. Int. J. Nanomedicine *2*, 129–141.

Nasti, R., Rossi, D., Amadio, M., Pascale, A., Unver, M.Y., Hirsch, A.K.H., and Collina, S. (2017). Compounds interfering with embryonic lethal abnormal vision (ELAV) protein-RNA complexes: an avenue for discovering new drugs. J. Med. Chem. *60*, 8257–8267.

Netea-Maier, R.T., Smit, J.W.A., and Netea, M.G. (2018). Metabolic changes in tumor cells and tumor-associated macrophages: a mutual relationship. Cancer Lett. *413*, 102–109.

Newman, D.J., and Cragg, G.M. (2020). Natural products as sources of new drugs over the nearly four decades from 01/1981 to 09/2019. J. Nat. Prod. *83*, 770–803.

Nielsen, J., Christiansen, J., Lykke-Andersen, J., Johnsen, A.H., Wewer, U.M., and Nielsen, F.C. (1999). A family of insulin-like growth factor II mRNA-binding proteins represses translation in late development. Mol. Cell. Biol. *19*, 1262–1270.

O'Hare, E.A., Yerges-Armstrong, L.M., Perry, J.A., Shuldiner, A.R., and Zaghloul, N.A. (2016). Assignment of functional relevance to genes at type 2 diabetes-associated loci through investigation of β-cell mass deficits. Mol. Endocrinol. *30*, 429–445.

Ostuni, R., Kratochvill, F., Murray, P.J., and Natoli, G. (2015). Macrophages and cancer: from mechanisms to therapeutic implications. Trends Immunol. *36*, 229–239.

Pakos-zebrucka, K., Koryga, I., Mnich, K., Ljujic, M., Samali, A., and Gorman, A.M. (2016). The integrated stress response. EMBO Rep. *17*, 1374–1395.

Pathria, P., Louis, T.L., and Varner, J.A. (2019). Targeting tumor-associated macrophages in cancer. Trends Immunol. *40*, 310–327.

Penny, H.L., Sieow, J.L., Adriani, G., Yeap, W.H., See Chi Ee, P., San Luis, B., Lee, B., Lee, T., Mak, S.Y., Ho, Y.S., et al. (2016). Warburg metabolism in tumor-conditioned macrophages promotes metastasis in human pancreatic ductal adenocarcinoma. Oncoimmunology *5*, 1–15.

Perdiguero, E.G., and Geissmann, F. (2016). The development and maintenance of resident macrophages. Nat. Immunol. *17*, 2–8.

Png, K.J., Halberg, N., Yoshida, M., and Tavazoie, S.F. (2012). A microRNA regulon that mediates endothelial recruitment and metastasis by cancer cells. Nature *481*, 190–196.

Potterat, O., Puder, C., Wagner, K., Bolek, W., Vettermann, R., and Kauschke, S.G. (2007). Chlorocyclinones A-D, chlorinated angucyclinones from *Streptomyces* sp. strongly antagonizing rosiglitazone-induced PPAR-γ activation. J. Nat. Prod. *70*, 1934–1938.

Qiu, S., Sun, H., Zhang, A.H., Xu, H.Y., Yan, G.L., Han, Y., and Wang, X.J. (2014). Natural alkaloids: basic aspects, biological roles, and future perspectives. Chin. J. Nat. Med. *12*, 401–406.

Quirós, P.M., Prado, M.A., Zamboni, N., D'Amico, D., Williams, R.W., Finley, D., Gygi, S.P., and

Auwerx, J. (2017). Multi-omics analysis identifies ATF4 as a key regulator of the mitochondrial stress response in mammals. J. Cell Biol. *216*, 2027–2045.

Rabinovitch, R.C., Samborska, B., Faubert, B., Ma, E.H., Gravel, S.P., Andrzejewski, S., Raissi, T.C., Pause, A., St.-Pierre, J., and Jones, R.G. (2017). AMPK maintains cellular metabolic homeostasis through regulation of mitochondrial reactive oxygen species. Cell Rep. *21*, 1–9.

Rawla, P., Sunkara, T., and Gaduputi, V. (2019). Epidemiology of pancreatic cancer: global trends, etiology and risk factors. World J. Oncol. *10*, 10–27.

Rebets, Y., Nadmid, S., Paulus, C., Dahlem, C., Herrmann, J., Hübner, H., Rückert, C., Kiemer, A.K., Gmeiner, P., Kalinowski, J., et al. (2019). Perquinolines A-C: unprecedented bacterial tetrahydroisoquinolines involving an intriguing biosynthesis. Angew. Chemie Int. Ed. *58*, 12930–12934.

Reichenbach, H. (1999). The ecology of the myxobacteria. Environ. Microbiol. *1*, 15–21.

Reichenbach, H. (2001). Myxobacteria, producers of novel bioactive substances. J. Ind. Microbiol. Biotechnol. *27*, 149–156.

Rey-Giraud, F., Hafner, M., and Ries, C.H. (2012). *In vitro* generation of monocyte-derived macrophages under serum-free conditions improves their tumor promoting functions. PLoS One *7*.

Rius, J., Guma, M., Schachtrup, C., Akassoglou, K., Zinkernagel, A.S., Nizet, V., Johnson, R.S., Haddad, G.G., and Karin, M. (2008). NF-κB links innate immunity to the hypoxic response through transcriptional regulation of HIF-1α. Nature *453*, 807–811.

Roma-Rodrigues, C., Mendes, R., Baptista, P. V., and Fernandes, A.R. (2019). Targeting tumor microenvironment for cancer therapy. Int. J. Mol. Sci. *20*.

Rosenfeld, Y.B.Z., Krumbein, M., Yeffet, A., Schiffmann, N., Mishalian, I., Pikarsky, E., Oberman, F., Fridlender, Z., and Yisraeli, J.K. (2019). VICKZ1 enhances tumor progression and metastasis in lung adenocarcinomas in mice. Oncogene *38*, 4169–4181.

Roth, G.A., Abate, D., Abate, K.H., Abay, S.M., Abbafati, C., Abbasi, N., Abbastabar, H., Abd-Allah, F., Abdela, J., Abdelalim, A., et al. (2018). Global, regional, and national age-sex-specific mortality for 282 causes of death in 195 countries and territories, 1980–2017: a systematic analysis for the Global Burden of Disease Study 2017. Lancet *392*, 1736–1788.

Sabharwal, S.S., and Schumacker, P.T. (2014). Mitochondrial ROS in cancer: initiators, amplifiers or an Achilles' heel? Nat. Rev. Cancer *14*, 709–721.

Saha, S., Shalova, I.N., and Biswas, S.K. (2017). Metabolic regulation of macrophage phenotype and function. Immunol. Rev. *280*, 102–111.

Sano, M., Driscoll, D.R., DeJesus-Monge, W.E., Quattrochi, B., Appleman, V.A., Ou, J., Zhu, L.J.,

Yoshida, N., Yamazaki, S., Takayama, T., et al. (2016). Activation of WNT/β-catenin signaling enhances pancreatic cancer development and the malignant potential *via* up-regulation of Cyr61. Neoplasia *18*, 785–794.

Sasse, F., Böhlendorf, B., Hermann, M., Kunze, B., Forche, E., Steinmetz, H., Höfle, G., and Reichenbach, H. (1999). Melithiazols, new β-methoxyacrylate inhibitors of the respiratory chain isolated from myxobacteria. Production, isolation, physico-chemical and biological properties. J. Antibiot. *52*, 721–729.

Schaeffer, D.F., Owen, D.R., Lim, H.J., Buczkowski, A.K., Chung, S.W., Scudamore, C.H., Huntsman, D.G., Ng, S.S.W., and Owen, D.A. (2010). Insulin-like growth factor 2 mRNA binding protein 3 (IGF2BP3) overexpression in pancreatic ductal adenocarcinoma correlates with poor survival. BMC Cancer *10*.

Schaper, F., de Leeuw, K., Horst, G., Bootsma, H., Limburg, P.C., Heeringa, P., Bijl, M., and Westra, J. (2016). High mobility group box 1 skews macrophage polarization and negatively influences phagocytosis of apoptotic cells. Rheumatol. *55*, 2260–2270.

Schetter, A., He, P., Hussain, S.P., Lee, D.H., Gaedcke, J., Funamizu, N., Maitra, A., Ghadimi, B.M., Alexander, H.R., Zhang, G., et al. (2012). DPEP1 inhibits tumor cell invasiveness, enhances chemosensitivity and predicts clinical outcome in pancreatic ductal adenocarcinoma. PLoS One *7*, e31507.

Schmauder, A., Sibley, D., David, S., and Maier, M.E. (2010). Total Synthesis and Configurational Assignment of Chondramide A. Chemistry (Easton). *16*, 4328–4336.

Schultheiss, C.S., Laggai, S., Czepukojc, B., Hussein, U.K., List, M., Barghash, A., Tierling, S., Hosseini, K., Golob-Schwarzl, N., Pokorny, J., et al. (2017). The long non-coding RNA H19 suppresses carcinogenesis and chemoresistance in hepatocellular carcinoma. Cell Stress *1*, 37–54.

Seif, M., Philippi, A., Breinig, F., Kiemer, A.K., and Hoppstädter, J. (2016). Yeast (Saccharomyces cerevisiae) polarizes both M-CSF- and GM-CSF-differentiated macrophages toward an M1-like phenotype. Inflammation *39*, 1690–1703.

Seif, M., Hoppstädter, J., Breinig, F., and Kiemer, A.K. (2017). Yeast-mediated mRNA delivery polarizes immuno-suppressive macrophages towards an immuno-stimulatory phenotype. Eur. J. Pharm. Biopharm. *117*, 1–13.

Sergeant, G., van Eijsden, R., Roskams, T., Van Duppen, V., and Topal, B. (2012). Pancreatic cancer circulating tumour cells express a cell motility gene signature that predicts survival after surgery. BMC Cancer *12*, 1–9.

Shapouri-Moghaddam, A., Mohammadian, S., Vazini, H., Taghadosi, M., Esmaeili, S.A., Mardani, F.,

Seifi, B., Mohammadi, A., Afshari, J.T., and Sahebkar, A. (2018). Macrophage plasticity, polarization, and function in health and disease. J. Cell. Physiol. *233*, 6425–6440.

Shen, C., Xuan, B., Yan, T., Ma, Y., Xu, P., Tian, X., Zhang, X., Cao, Y., Ma, D., Zhu, X., et al. (2020). M6A-dependent glycolysis enhances colorectal cancer progression. Mol. Cancer *19*, 1–19.

Sica, A., and Mantovani, A. (2012). Macrophage plasticity and polarization: *in vivo* veritas. J. Clin. Invest. *122*, 787–795.

Simões, R. V., Serganova, I.S., Kruchevsky, N., Leftin, A., Shestov, A.A., Thaler, H.T., Sukenick, G., Locasale, J.W., Blasberg, R.G., Koutcher, J.A., et al. (2015). Metabolic plasticity of metastatic breast cancer cells: adaptation to changes in the microenvironment. Neoplasia *17*, 671–684.

Simon, Y., Kessler, S.M., Bohle, R.M., Haybaeck, J., and Kiemer, A.K. (2014). The insulin-like growth factor 2 (*IGF2*) mRNA-binding protein p62/IGF2BP2-2 as a promoter of NAFLD and HCC? Gut *63*, 861–863.

Solinas, G., Germano, G., Mantovani, A., and Allavena, P. (2009). Tumor-associated macrophages (TAM) as major players of the cancer-related inflammation. J. Leuko *86*, 1065–1073.

Stubbs, A.C., Martin, K.S., Coeshott, C., Skaates, S. V., Kuritzkes, D.R., Bellgrau, D., Franzusoff, A., Duke, R.C., and Wilson, C.C. (2001). Whole recombinant yeast vaccine activates dendritic cells and elicits protective cell-mediated immunity. Nat. Med. *7*, 625–629.

Swinney, D.C. (2013). Phenotypic vs. target-based drug discovery for first-in-class medicines. Clin. Pharmacol. Ther. *93*, 299–301.

Swinney, D.C., and Anthony, J. (2011). How were new medicines discovered? Nat. Rev. Drug Discov. *10*, 507–519.

Takase, S., Kurokawa, R., Kondoh, Y., Honda, K., Suzuki, T., Kawahara, T., Ikeda, H., Dohmae, N., Osada, H., Shin-ya, K., et al. (2019). Mechanism of action of prethioviridamide, an anticancer ribosomally synthesized and post-translationally modified peptide with a polythioamide structure. ACS Chem. Biol. *14*, 1819–1828.

Takeya, M., and Komohara, Y. (2016). Role of tumor-associated macrophages in human malignancies: friend or foe? Pathol. Int. *66*, 491–505.

Tan, J.L., Li, F., Yeo, J.Z., Yong, K.J., Bassal, M.A., Ng, G.H., Lee, M.Y., Leong, C.Y., Tan, H.K., Wu, C. shuo, et al. (2019). New high-throughput screening identifies compounds that reduce viability specifically in liver cancer cells that express high levels of SALL4 by inhibiting oxidative phosphorylation. Gastroenterology *157*, 1615-1629.e17.

Tarpey, M.M., Wink, D.A., and Grisham, M.B. (2004). Methods for detection of reactive metabolites

of oxygen and nitrogen: *in vitro* and in vivo considerations. Am. J. Physiol. - Regul. Integr. Comp. Physiol. *286*.

Torres Andón, F., and Alonso, M.J. (2015). Nanomedicine and cancer immunotherapy - Targeting immunosuppressive cells. J. Drug Target. *23*, 656–671.

Tybl, E., Shi, F.D., Kessler, S.M., Tierling, S., Walter, J., Bohle, R.M., Wieland, S., Zhang, J., Tan, E.M., and Kiemer, A.K. (2011). Overexpression of the IGF2-mRNA binding protein p62 in transgenic mice induces a steatotic phenotype. J. Hepatol. *54*, 994–1001.

Varin, A., Mukhopadhyay, S., Herbein, G., and Gordon, S. (2010). Alternative activation of macrophages by IL-4 impairs phagocytosis of pathogens but potentiates microbial-induced signalling and cytokine secretion. Blood *115*, 353–362.

Varshney, G.K., Lu, J., Gildea, D.E., Huang, H., Pei, W., Yang, Z., Huang, S.C., Schoenfeld, D., Pho, N.H., Casero, D., et al. (2013). A large-scale zebrafish gene knockout resource for the genome-wide study of gene function. Genome Res. *23*, 727–735.

Veinotte, C.J., Dellaire, G., and Berman, J.N. (2014). Hooking the big one: the potential of zebrafish xenotransplantation to reform cancer drug screening in the genomic era. DMM Dis. Model. Mech. *7*, 745–754.

Vitale, I., Manic, G., Coussens, L.M., Kroemer, G., and Galluzzi, L. (2019). Macrophages and metabolism in the tumor microenvironment. Cell Metab. *30*, 36–50.

Voitsekhovskaia, I., Constanze, P., Dahlem, C., Rebets, Y., Nadmid, S., Zapp, J., Axenov-Gribanov, D., Rückert, C., Timofeyev, M., Kalinowski, J., et al. (2020). Baikalomycins A-C, new aquayamycin-type angucyclines isolated from lake baikal derived streptomyces sp. IB201691-2A. Microorganisms *8*, E680.

Della Volpe, S., Nasti, R., Queirolo, M., Unver, M.Y., Jumde, V.K., Dömling, A., Vasile, F., Potenza, D., Ambrosio, F.A., Costa, G., et al. (2019). Novel compounds targeting the RNA-binding protein HuR. Structure-based design, synthesis, and interaction studies. ACS Med. Chem. Lett. *10*, 615–620.

Wachter, D.L., Schlabrakowski, A., Hoegel, J., Kristiansen, G., Hartmann, A., and Riener, M.O. (2011). Diagnostic value of immunohistochemical IMP3 expression in core needle biopsies of pancreatic ductal adenocarcinoma. Am. J. Surg. Pathol. *35*, 873–877.

Walch-Rückheim, B., Kiefer, R., Geginat, G., Schmitt, M.J., and Breinig, F. (2016). Coexpression of human perforin improves yeast-mediated delivery of DNA and mRNA to mammalian antigen-presenting cells. Gene Ther. *23*, 103–107.

Walch, B., Breinig, T., Geginat, G., Schmitt, M.J., and Breinig, F. (2011). Yeast-based protein delivery to mammalian phagocytic cells is increased by coexpression of bacterial listeriolysin. Microbes Infect.

13, 908–913.

Weber, C., and Opatz, T. (2019). Bisbenzylisoquinoline Alkaloids (Elsevier Inc.).

Weigert, A., Mora, J., Sekar, D., Syed, S., and Brüne, B. (2016). Killing is not enough: How apoptosis hijacks tumor-associated macrophages to promote cancer progression. In Apoptosis in Cancer Pathogenesis and Anti-Cancer Therapy, C.D. Gregory, ed. (Springer International Publishing), pp. 205–239.

Weinberg, F., Ramnath, N., and Nagrath, D. (2019). Reactive oxygen species in the tumor microenvironment: an overview. Cancers (Basel). *11*, 1–20.

Weissman, K.J., and Müller, R. (2010). Myxobacterial secondary metabolites: bioactivities and modes-of-action. Nat. Prod. Rep. *27*, 1276–1295.

Wenes, M., Shang, M., Di Matteo, M., Goveia, J., Martín-Pérez, R., Serneels, J., Prenen, H., Ghesquière, B., Carmeliet, P., and Mazzone, M. (2016). Macrophage metabolism controls tumor blood vessel morphogenesis and metastasis. Cell Metab. *24*, 701–715.

Westerfield, M. (2000). The Zebrafish Book. A Guide for the Laboratory Use of Zebrafish (Danio rerio) (Eugene, OR, University of Oregon Press).

Wong, A.D., Ye, M., Ulmschneider, M.B., and Searson, P.C. (2015). Quantitative analysis of the Enhanced Permeation and Retention (EPR) effect. PLoS One *10*, 1–13.

Xing, C., LaPorte, J.R., Barbay, J.K., and Myers, A.G. (2004). Identification of GAPDH as a protein target of the saframycin antiproliferative agents. Proc. Natl. Acad. Sci. U. S. A. *101*, 5862–5866.

Xing, M., Li, P., Wang, X., Li, J., Shi, J., Qin, J., Zhang, X., Francia, G., and Zhang, J. (2019). Overexpression of p62/IMP2 can promote cell migration in hepatocellular carcinoma via activation of the Wnt / β -catenin pathway. Cancers *12*, 1–16.

Xu, W., Roos, A., Schlagwein, N., Woltman, A.M., Daha, M.R., and Kooten, C. Van (2006). IL-10–producing macrophages preferentially clear early apoptotic cells. Blood *107*, 4930–4937.

Xu, X., Yu, Y., Zong, K., Lv, P., and Gu, Y. (2019). Up-regulation of IGF2BP2 by multiple mechanisms in pancreatic cancer promotes cancer proliferation by activating the PI3K/Akt signaling pathway. J. Exp. Clin. Cancer Res. *38*, 1–14.

Xue, J., Schmidt, S. V, Sander, J., Draffehn, A., Krebs, W., Quester, I., Nardo, D. De, Gohel, T.D., Emde, M., Schmidleithner, L., et al. (2014). Resource transcriptome-based network analysis reveals a spectrum model of human macrophage activation. Immunity *40*, 274–288.

Yan, C., Brunson, D.C., Tang, Q., Do, D., Iftimia, N.A., Moore, J.C., Hayes, M.N., Welker, A.M., Garcia, E.G., Dubash, T.D., et al. (2019). Visualizing engrafted human cancer and therapy responses in

immunodeficient zebrafish. Cell *177*, 1903-1914.e14.

Yang, C., Wei, C., Wang, S., Shi, D., Zhang, C., Lin, X., Dou, R., and Xiong, B. (2019). Elevated CD163+/CD68+ ratio at tumor invasive front is closely associated with aggressive phenotype and poor prognosis in colorectal cancer. Int. J. Biol. Sci. *15*, 984–998.

Yang, Y., Karakhanova, S., Hartwig, W., D'Haese, J.G., Philippov, P.P., Werner, J., and Bazhin, A. V. (2016). Mitochondria and mitochondrial ROS in cancer: novel targets for anticancer therapy. J. Cell. Physiol. *231*, 2570–2581.

Yantiss, R.K., Woda, B.A., Fanger, G.R., Kalos, M., Whalen, G.F., Tada, H., Andersen, D.K., Rock, K.L., and Dresser, K. (2005). KOC (K homology domain containing protein overexpressed in cancer) A novel molecular marker that disthinguishes between benign and malignant lesions of the pancreas. Am. J. Surg. Pathol. *29*, 188–195.

Ye, L., Zhang, T., Kang, Z., Guo, G., Sun, Y., Lin, K., Huang, Q., Shi, X., Ni, Z., Ding, N., et al. (2019). Tumor-infiltrating immune cells act as a marker for prognosis in colorectal cancer. Front. Immunol. *10*, 1–12.

Ye, S., Song, W., Xu, X., Zhao, X., and Yang, L. (2016). IGF2BP2 promotes colorectal cancer cell proliferation and survival through interfering with RAF-1 degradation by miR-195. FEBS Lett. *590*, 1641–1650.

Zeni, E., Mazzetti, L., Miotto, D., Lo Cascio, N., Maestrelli, P., Querzoli, P., Pedriali, M., De Rosa, E., Fabbri, L.M., Mapp, C.E., et al. (2007). Macrophage expression of interleukin-10 is a prognostic factor in nonsmall cell lung cancer. Eur. Respir. J. *30*, 627–632.

Zhang, G., He, P., Tan, H., Budhu, A., Gaedcke, J., Michael Ghadimi, B., Ried, T., Yfantis, H.G., Lee, D.H., Maitra, A., et al. (2013a). Integration of metabolomics and transcriptomics revealed a fatty acid network exerting growth inhibitory effects in human pancreatic cancer. Clin. Cancer Res. *19*, 4983–4993.

Zhang, J.Y., Chan, E.K.L., Peng, X.X., and Tan, E.M. (1999). A novel cytoplasmic protein with RNA-binding motifs is an autoantigen in human hepatocellular carcinoma. J. Exp. Med. *189*, 1101–1110.

Zhang, W., Liu, Z., Li, S., Lu, Y., Chen, Y., Zhang, H., Zhang, G., Zhu, Y., Zhang, G., Zhang, W., et al. (2012). Fluostatins I-K from the South China sea-derived *Micromonospora rosaria* SCSIO N160. J. Nat. Prod. *75*, 1937–1943.

Zhang, Y., Morris IV, J.P., Yan, W., Schofield, H.K., Gurney, A., Simeone, D.M., Millar, S.E., Hoey, T., Hebrok, M., and Di Magliano, M.P. (2013b). Canonical Wnt signaling is required for pancreatic carcinogenesis. Cancer Res. *73*, 4909–4922.

Zhang, Y., Chen, M., Bruner, S.D., and Ding, Y. (2018). Heterologous production of microbial

ribosomally synthesized and post-translationally modified peptides. Front. Microbiol. *9*, 1–13.

Zhao, H., Mandich, D., Cartun, R.W., and Ligato, S. (2007). Expression of K homology domain containing protein overexpressed in cancer in pancreatic FNA for diagnosing adenocarcinoma of pancreas. Diagn. Cytopathol. *35*, 700–704.

Zhao, S., Wu, D., Wu, P., Wang, Z., Huang, J., and Gao, J.X. (2015). Serum IL-10 predicts worse outcome in cancer patients: a meta-analysis. PLoS One *10*, 1–15.

Appendix

Abbreviations

APH	Acid phosphatase
BSA	Bovine serum albumin
CCL2	Chemokine ligand 2
CD	Cluster of differentiation
CFSE	Carboxyfluorescein succinimidyl ester
co	Control
CTC	Circulating tumor cells
CXCL9	Chemokine (C-X-C motif) ligand 9
DMEM	Dulbecco's Modified Eagle's Medium
DMSO	Dimethylsulfoxid
dpf	Days post fertilization
dpi	Days post injection
ECAR	Extracellular acidification rate
ECIS	Electric cell-substrate impedance sensing
EDTA	Ethylenediaminetetraacetic acid
EGFP	Enhanced green fluorescent protein
EMT	Epithelial-mesenchymal transition
FCCP	Carbonyl cyanide-4-(trifluoromethoxy)phenylhydrazone
FCS	Fetal calf serum
FSC	Forward scatter
h	Hour
H_2O bidest.	Aqua bidestillata
HCC	hepatocellular carcinoma
hpf	Hours post fertilization
hpi	Hours post injection
HRP	Horseradish peroxidase
HS	Human serum-differentiated
HUVECs	Human umbilical vein endothelial cells
HVA	Homovanillic acid
IFNγ	Interferon γ

IGF2	Insulin-like growth factor 2
IGF2BPs/IMPs	*IGF2* mRNA binding proteins
IL	Interleukin
IP10	Interferon gamma-induced protein 10
IPMN	Intraductal papillary mucinous neoplasms
KH	hnRNP K homology
LPS	Lipopolysaccharide
MFI	Mean fluorescence intensity
min	Minutes
MMP9	Matrix metalloproteinase 9
MOI	Multiplicity of infection
mTORC1	Mechanistic target of rapamycin complex 1
MTT	3-(4,5-dimethylthiazole-2-yl)-2,5 diphenyltetrazolium bromide
MΦ	Macrophage
n.s.	Not significant
NP	Nanoparticle
NSCLC	Non-small cell lung cancer
OCR	Oxygen consumption rate
OXPHOS	Oxidative phosphorylation
PanIN	Pancreatic Intraepithelial Neoplasia
PBS	Phosphate-buffered saline
PDAC	Pancreatic ductal adenocarcinoma
PLGA	Poly(lactic-co-glycolic acid)
PMA	Phorbol 12-myristate 13-acetate
RBPs	RNA binding proteins
REDD1	DNA damage inducible transcript 4
resi	Resistant
RiPP	Ribosomally synthesized and post-translationally modified peptides
ROS	Reactive oxygen species
rpm	Rounds per minute
RPMI	Roswell Park Memorial Institute 1640 Medium

RRM	RNA recognition motifs
SRC	Spare respiratory capacity
SSC	Side scatter
STU	Staurosporin
TAM	Tumor-associated macrophages
TCA	Tricarboxylic acid
TCM	Tumor-conditioned medium
TME	Tumor microenvironment
TNFα	Tumor necrosis factor α
v/v	Volume percent
wt	Wildtype

List of figures

List of tables

Publications

Original publications

Rebets, Yuriy, Suvd Nadmid, Constanze Paulus, **Charlotte Dahlem**, Jennifer Herrmann, Harald Hübner, Christian Rückert, Akexandra K. Kiemer, Peter Gmeiner, Jörn Kalinowski, Rolf Müller, and Andriy Luzhetskyy. 2019. "Perquinolines A-C: Unprecedented bacterial tetrahydroisoquinolines involving an intriguing biosynthesis." *Angewandte Chemie International Edition* 58 (37): 12930–12934. https://doi.org/10.1002/anie.201905538.

Contributions: Biological activity studies of the compounds (see chaper 3.3), description of methods and results. Critical review of the manuscript.

Dahlem, Charlotte, Ahmad Barghash, Philip Puchas, Johannes Haybaeck, and Sonja M. Kessler. 2019. "The insulin-like growth factor 2 mRNA binding protein IMP2/IGF2BP2 is overexpressed and correlates with poor survival in pancreatic cancer." *International Journal of Molecular Sciences* 20 (13): 3204. https://doi.org/10.3390/ijms20133204.

Contributions: GEO dataset analysis, description of methods and results, figure preparations, contributions to the introduction and discussion. Manuscript preparation.

Kiefer, Ruth, Marijas Jurisic, **Charlotte Dahlem**, Marcus Koch, Manfred J. Schmitt, Alexandra K. Kiemer, Marc Schneider, and Frank Breinig. 2019. "Targeted delivery of functionalized PLGA nanoparticles to macrophages by complexation with the yeast *Saccharomyces cerevisiae*." *Biotechnology and Bioengineering* 117 (3): 776-788. https://doi.org/10.1002/bit.27226.

Contributions: NP uptake studies (see chaper 3.4) in macrophages *vs*. tumor cells, description of methods and results, figure preparations. Critical review of the manuscript.

Hoppstädter, Jessica, Anna Dembek, Rebecca Linnenberger, **Charlotte Dahlem**, Ahmad Barghash, Claudia Fecher-Trost, Gregor Fuhrmann, Marcus Koch, Annette Kraegeloh, Hanno Huwer, and Alexandra K. Kiemer. 2019. "Toll-like receptor 2 release by macrophages: An anti-inflammatory program induced by glucocorticoids and lipopolysaccharide." *Frontiers in Immunology* 10: 1634. https://doi.org/10.3389/fimmu.2019.01634.

Contributions: Cell viability studies of THP-1 cells under serum depriviation, description of methods and results, figure preparations. Critical review of the manuscript.

Goes, Adriely, Philipp Lapuhs, Thomas Kuhn, Eilien Schulz, Robert Richter, Fabian Panter, **Charlotte Dahlem**, Marcus Koch, Ronald Garcia, Alexandra K. Kiemer, Rolf Müller, and Gregor Fuhrmann. 2020. "Myxobacteria-derived outer membrane vesicles: Potential applicability against intracellular infections." *Cells* 9 (1): 194. https://doi.org/10.3390/cells9010194.

Contributions: PBMC isolation, description of method. Critical review of the manuscript.

Hoppstädter, Jessica, Jenny V. Valbuena Perez, Rebecca Linnenberger, **Charlotte Dahlem**, Thierry M. Legroux, Anne Hecksteden, William K.F. Tse, Sara Flamini, Anastasia Andreas, Jennifer Herrmann, Christan Herr, Rolf Müller, Tim Meyer, Robert Bals, Carlo Riccardi, Stefan Bruscoli, and Alexandra K. Kiemer. 2020. "The glucocorticoid-induced leucine zipper mediates statin-induced muscle damage." *The FASEB Journal* 34 (3): 4684–4701. https://doi.org/10.1096/fj.201902557RRR.

Contributions: Zebrafish *in vivo* studies of muscle development and function after statin treatment, morpholino construct-mediated *foxo3* knockdown in zebrafish embryos, figure preparations, description of methods and results. Critical review of the manuscript.

Voitsekhovskaia, Irina, Paulus Constanze, **Charlotte Dahlem**, Yuriy Rebets, Suvd Nadmid, Josef Zapp, Denis Axenov-Gribanov, Christan Rückert, Maxim Timofeyev, Jörn Kalinowski, Alexandra K. Kiemer, and Andriy Luzhetskyy 2020. "Baikalomycins A-C, new aquayamycin-type angucyclines isolated from Lake Baikal derived *Streptomyces* sp. IB201691-2A." *Microorganisms* 8 (5): E680. https://doi.org/10.3390/microorganisms8050680.

Contributions: Biological activity studies of the compounds (see chaper 3.3), description of methods and results. Critical review of the manuscript.

Dahlem, Charlotte, Wei X. Siow, Maria Lopatniuk, William K.F. Tse, Sonja M Kessler, Susanne H. Kirsch, Jessica Hoppstädter, Angelika M. Vollmar, Rolf Müller, Andriy Luzhetskyy, and Alexandra K. Kiemer. 2020. "Thioholgamide A, a new anti-proliferative anti-tumor agent, modulates macrophage polarization and metabolism." *Cancers* 12 (5): E1288. https://doi.org/https://doi.org/10.3390/cancers12051288.

Contributions: Study execution, investigation and data analysis (except western blots and RIL175 cell-based data), figure preparations, manuscript writing, submission.

Abuhaliema, Ali, Sonja M. Kessler, **Charlotte Dahlem**, Tarek Kröhler, Ben G.E. Zoller, Susanne H. Kirsch, Stephan Laggai, Rolf Müller, Martin Empting, and Alexandra K. Kiemer. „Discovery of the first small molecules targeting the RNA binding protein IGF2BP2/IMP2 as potential target in cancer therapy." *Submitted*.

Contributions: Zebrafish *in vivo* studies, 3D and migration *in vitro* studies, description of methods and results, figure preparations. Final manuscript and figure preparations and submission.

Conference contributions

Dahlem, Charlotte, Maria Lopatniuk, Jessica Hoppstädter, Sonja M. Kessler, Britta Diesel, Andriy Luzhetskyy, Alexandra K. Kiemer. "Macrophage targeting by the cytotoxic natural product thioholgamide A as an anticancer principle." *Annual Meeting of the European Macrophage and Dendritic Cell Society*, Verona, 2018.

Dahlem, Charlotte, Maria Lopatniuk, William K.F. Tse, Jessica Hoppstädter, Sonja M. Kessler, Andriy Luzhetskyy, Alexandra K. Kiemer. "New natural compound thioholgamide A and its action on cancer cells and tumor-associated macrophages." *Tumor Microenvironment Meeting, British Association for Cancer Research*, Nottingham, 2019.

Dahlem, Charlotte, Maria Lopatniuk, William K.F. Tse, Jessica Hoppstädter, Sonja M. Kessler, Andriy Luzhetskyy, Alexandra K. Kiemer. "New natural compound thioholgamide A and its action on cancer cells and tumor-associated macrophages." *Tumor Metabolism, Keystone Symposia,* Banff, 2019.
Funded by the keystone symposia future of science fund scholarship.
The meeting was cancelled because of the COVID-19 outbreak.

Danksagungen

An dieser Stelle möchte ich mich von Herzen bei Prof. Alexandra K. Kiemer bedanken. Nicht nur für die Möglichkeit meine Doktorarbeit in ihrer Gruppe durchführen zu können, sondern auch für das mir entgegen gebrachte Vertrauen, ihr konstruktives und kritisches Feedback, wissenschaftliche Inspiration und die Unterstützung in den letzten Jahren.

Ein weiterer Dank gilt Prof. Andriy Luzhetskyy, für die Übernahme der Rolle des Wissenschaftlichen Begleiters und die gute Zusammenarbeit in einer Reihe von Projekten.

In diesem Rahmen möchte ich auch allen Co-Autoren, für die erfolgreiche Zusammenarbeit in zahlreichen Projekten, danken.

Ein besonderer Dank gilt dabei Prof. William Ka Fai Tse, der mich in seine Arbeitsgruppe eingeladen hat, um von ihm verschiedene *in vivo* Methoden zu erlernen. Vielen Dank für diese wertvolle Erfahrung während der Kirschblüte in Fukuoka.

Des Weiteren möchte ich Dr. Susanne Kirsch-Dahmen, Dr. Jennifer Herrmann und Prof. Rolf Müller für die Zusammenarbeit und die Bereitstellung von Zebrafischembryonen danken, Dr. Maria Lopatniuk, Lucas Wei Xiong Siow, Dr. Karin Bartel und Prof. Angelika Vollmar für die wertvolle Zusammenarbeit im Thioholgamide A Projekt, sowie Dr. Ruth Kiefer und Dr. Frank Breinig für die interessante Zusammenarbeit im Hefen-Projekt.

Ein herzlicher Dank gilt den Mitgliedern der Arbeitsgruppe Pharmazeutische Biologie. Es war (und ist) eine Freude mit euch zusammen zu arbeiten. Danke für eine schöne und lustige gemeinsame Zeit in und außerhalb des Labors, aus der Freundschaften gewachsen sind. Besonders danken möchte ich dabei Rebecca Linneberger für die zahlreichen gemeinsamen Kaffeepausen, die durch wissenschaftliche, politische und private Diskussionen gefüllt waren, sowie Dr. Jessica Hoppstädter und Prof. Sonja Keßler für all die Aufmunterungen, wissenschaftliche Inspiration und ihre Freundschaft.

Zu Guter Letzt möchte ich mich bei meinen Freunden und Eltern für all ihre Unterstützung bedanken. Ein großer Dank an die Wilde 7, dafür mich an eine Welt außerhalb der Wissenschaft zu erinnern und an Lisa Bindemann und Jan Henrich, ohne die ich es nicht geschafft hätte.